ANALYSIS OF METAL FORMING BY USING ISOGEOMETRIC ELEMENTS

A THESIS SUBMITTED TO
THE GRADUATE SCHOOL OF NATURAL AND APPLIED SCIENCES
OF
MIDDLE EAST TECHNICAL UNIVERSITY

BY

YASİN ÖZDOĞAN

IN PARTIAL FULFILLMENT OF THE REQUIREMENTS
FOR
THE DEGREE OF MASTER OF SCIENCE
IN
MECHANICAL ENGINEERING

JULY 2018

Approval of the thesis:

ANALYSIS OF METAL FORMING BY USING ISOGEOMETRIC ELEMENTS

submitted by **YASİN ÖZDOĞAN** in partial fulfillment of the requirements for the degree of **Master of Science in Mechanical Engineering Department, Middle East Technical University** by,

Prof. Dr. Halil Kalıpçılar
Dean, Graduate School of **Natural and Applied Sciences** _____

Prof. Dr. M. A. Sahir Arıkan
Head of Department, **Mechanical Engineering** _____

Prof. Dr. Haluk Darendeliler
Supervisor, **Mechanical Engineering Dept., METU** _____

Examining Committee Members:

Prof. Dr. Suha Oral
Mechanical Engineering Dept., METU _____

Prof. Dr. Haluk Darendeliler
Mechanical Engineering Dept., METU _____

Prof. Dr. F. Suat Kadıoğlu
Mechanical Engineering Dept., METU _____

Prof. Dr. Can Çoğun
Mechanical Engineering Dept., Cankaya University _____

Asst. Prof. Dr. Ulaş Yaman
Mechanical Engineering Dept., METU _____

Date: July 19th, 2018 _____

I hereby declare that all information in this document has been obtained and presented in accordance with academic rules and ethical conduct. I also declare that, as required by these rules and conduct, I have fully cited and referenced all material and results that are not original to this work.

Name, Last name :   Yasin Özdoğan

Signature   :

ABSTRACT

ANALYSIS OF METAL FORMING BY USING ISOGEOMETRIC ELEMENTS

Özdoğan, Yasin

MSc., Department of Mechanical Engineering

Supervisor: Prof. Dr. Haluk Darendeliler

July 2018, 160 pages

In this thesis, a new numerical analysis method named as isogeometric analysis (IGA), based on usage of non-uniform rational basis spline (NURBS) basis functions is studied in order to examine the behavior of parts in the forming processes. NURBS is a mathematical modeling method used for representing any kind of curves, surfaces and 3-D shapes and it is widely used in computer aided design (CAD) software packages since its favorable and flexible nature makes modelling of complex geometries possible. Isogeometric analysis has emerged with the idea of using same basis functions for both analysis and design stages and it aims to eliminate time consumption during required geometry transformation between these stages. NURBS basis functions have been chosen as common basis function because they enable higher continuity and exact geometry contrary to polynomial based finite element method basis functions. Moreover, due to the recursive nature of NURBS, more general and robust algorithms can be developed for computation procedure. In this study, Matlab codes have been developed to use IGA technique in several linear elasticity problems. Thereafter, isogeometric analysis has been used for plasticity problems; uniaxial loading of a sheet, v-die bending and square deep drawing by using LS-DYNA analysis software. Same analyses were also run by using classical finite

element method with utilizing another commercial analysis software Abaqus. According to obtained results, accuracy and computational efficiency of IGA have been compared with FEA. At the end, isogeometric analysis was evaluated as a suitable technique for analysis of linear elasticity problems and metal forming processes because it gives more accurate results in shorter time compared to finite element analysis.

Keywords: NURBS, Isogeometric Analysis, Finite Element Analysis, Sheet Metal Forming, V-Die Bending, Springback, Square Deep Drawing, Thickness Strain

ÖZ

METAL ŞEKİLLENDİRME SÜRECİNİN İZOGEOMETRİK ELEMANLAR KULLANILARAK ANALİZİ

Özdoğan, Yasin

Yüksek Lisans, Makina Mühendisliği Bölümü

Tez Yöneticisi: Prof. Dr. Haluk Darendeliler

Temmuz 2018, 160 sayfa

Bu tezde, parçaların şekillendirme sürecindeki davranışlarını incelemek amacıyla, NURBS tabanlı fonksiyonların kullanımına dayanan izogeometrik analiz (IGA) yöntemi kullanılmıştır. Düzenli olmayan rasyonel tabanlı eğri, NURBS, her türlü eğrileri, yüzeyleri ve 3 boyutlu şekilleri tanımlamak amacıyla kullanılan bir matematiksel modeldir ve karmaşık geometrilerin modellenmesini mümkün kılan esnek yapısı sayesinde bilgisayar destekli tasarım (CAD) yazılım paketlerinde yaygın olarak kullanılmaktadır. İzogeometrik analiz yöntemi, analiz ve tasarım aşamaları için aynı temel fonksiyonların kullanılması fikri ile ortaya çıkmıştır ve bu aşamalar arasında gerekli olan geometri dönüşümleri sırasında kaybedilen zamanı ortadan kaldırmayı hedeflemektedir. NURBS tabanlı fonksiyonlar, polinom tabanlı sonlu elemanlar yönteminin fonksiyonlarına göre daha yüksek süreklilik ve tam doğru geometri sağlayabildikleri için analiz ve tasarım süreçleri için ortak temel fonksiyon olarak belirlenmiştir. Ayrıca, NURBS'ün tekrarlamalı doğası nedeniyle, hesaplama prosedürü için daha genel ve sağlam algoritmalar geliştirilebilir. Bu çalışmada izogeometrik analiz yöntemi Matlab programı yardımı ile geliştirilen kodlar kullanılarak doğrusal elastisite problemlerine uygulanmış ve yöntemin doğruluğu test edilmiştir. Yöntem daha sonra LS-DYNA analiz yazılımı kullanılarak tek yönlü sac

çekme, v-büküm ve kare şeklindeki sacları derin çekme işlemleri gibi plastisite problemlerine uygulanmıştır. Aynı analizler Abaqus analiz yazılımı yardımı ile klasik sonlu elemanlar yöntemi kullanılarak da gerçekleştirilmiştir. Elde edilen sonuçlara göre izogeometrik analiz yönteminin doğruluk ve hesaplama verimliliği sonlu elemanlar yöntemi ile karşılaştırılmıştır. Sonuçta, izogeometrik analiz yöntemi sonlu elemanlar analizine göre daha kısa analiz süreleri kullanarak daha doğru sonuçlar sağlaması nedeniyle avantajlı görülmüş, doğrusal elastisite ve metal şekillendirme işlemlerinin analizi için uygun bir teknik olarak değerlendirilmiştir.

Anahtar Sözcükler: NURBS, İzogeometrik Analiz, Sonlu Elemanlar Analizi, Sac Metal Şekillendirme, V-Büküm, Geri Yaylanma, Kare Derin Çekme, Kalınlık Gerinimi

To Bright Future of the Universe

ACKNOWLEDGMENTS

"Education breeds confidence. Confidence breeds hope. Hope breeds peace."

Confucius

TABLE OF CONTENTS

LIST OF TABLES

TABLES

LIST OF FIGURES

FIGURES

CHAPTER 1

INTRODUCTION

1.1   Background and Motivation

Human being has been in an incredible development since the tools they have invented using materials such as stone, wood and bone for easy hunting in the hunter-gatherer era. Engineers are the most important contributors to the todays achieved technological developments with new theories and application methods suggested by them for solutions of the worldwide problems. They do not just solve existing problems, they also think about the development of humanity and new problems to make the world a better place to live. However, the increasing number and complexity of the problems made it difficult to find the solutions by using hand calculations. At this point, engineers make use of computers, the most important factor behind the development of mankind over the last fifty years. Computers can perform prescribed mathematical and logical operations at high speed and display the results of these operations while engineers write algorithms to define solution procedure for them by using one of the programming languages. Today, computers are widely used in engineering world for modeling, design and analysis with their cost-effectively developed abilities. Computers allow the engineers to simulate the working conditions of products before the complete system is designed and produced. Therefore, their usage provides saving of time, material and capital. Computer software packages used by engineers generally named in three main groups as Computer Aided Design (CAD), Computer Aided Engineering (CAE) and Computer Aided Manufacturing (CAM). CAD is a computer technology as its name implies used for design of structures and document the design process. Detailed engineering drawings of the parts that contain products on two dimensional diagrams, material information, dimensions and tolerances with specific conventions can be created by using CAD programs and such drawings are main input for the manufacturing process. On the other hand, CAE is

used to conduct engineering analyses such as Structural Analysis, Computational Fluid Dynamics (CFD) and Multibody Dynamics (MBD). Engineering designs are evaluated in terms of their functions. Structures are analyzed under the working conditions with applied forces, pressures or temperatures and so on. Mechanisms are simulated with operation interactions and design constraints. At the end of the analyses if the design functionally operate, production of the system can be started. At the production stage CAM software are utilized to create detailed manufacturing instructions which are generally called as G-Codes for computer numerical control (CNC) machines. In order to obtain high quality manufactured parts CAM programs are widely used in industry.

Various mathematical models are used in the backgrounds of aforementioned computer aided programs. Finite element method is the most known mathematical model which is prevalently used in CAE software for analyses since mid-nineties. Mathematical modelling of CAD programs that will be explained in detail in the following sections also first emerged in the 1970s. As some improvements were made in these mathematical methods, the main parts continued to be used unchanged. In fact, this long-term use can be shown as a proof that analysis and design mathematical models work well throughout years but, these methods only solve the problems that they have developed for and do not process for other problems. Therefore, although design and analysis are interdependent, different solution methods are being used in these two fields and this causes extra time consumption. Models created by using CAD software cannot be directly used by FEA technique. One should make the design model suitable for analysis by transforming the data set performing well-known method called as "meshing". However, this preparation of a CAD model for analysis is the most time consuming part of analysis process. Relative time consumptions during analysis steps were studied in Sandia National Laboratories and results are given in Figure 1.1 [1]. In this study, analysis-suitable geometry creation needs about 50% of overall analysis time while mesh generation takes about 20% and only 4% of overall time is actually devoted to computation. Before running the analysis, it is necessary to make design model as simple as possible by removing fillets, chamfers,

drafts, physical threads and other decorative features. After this operation, geometry decomposition should be performed.
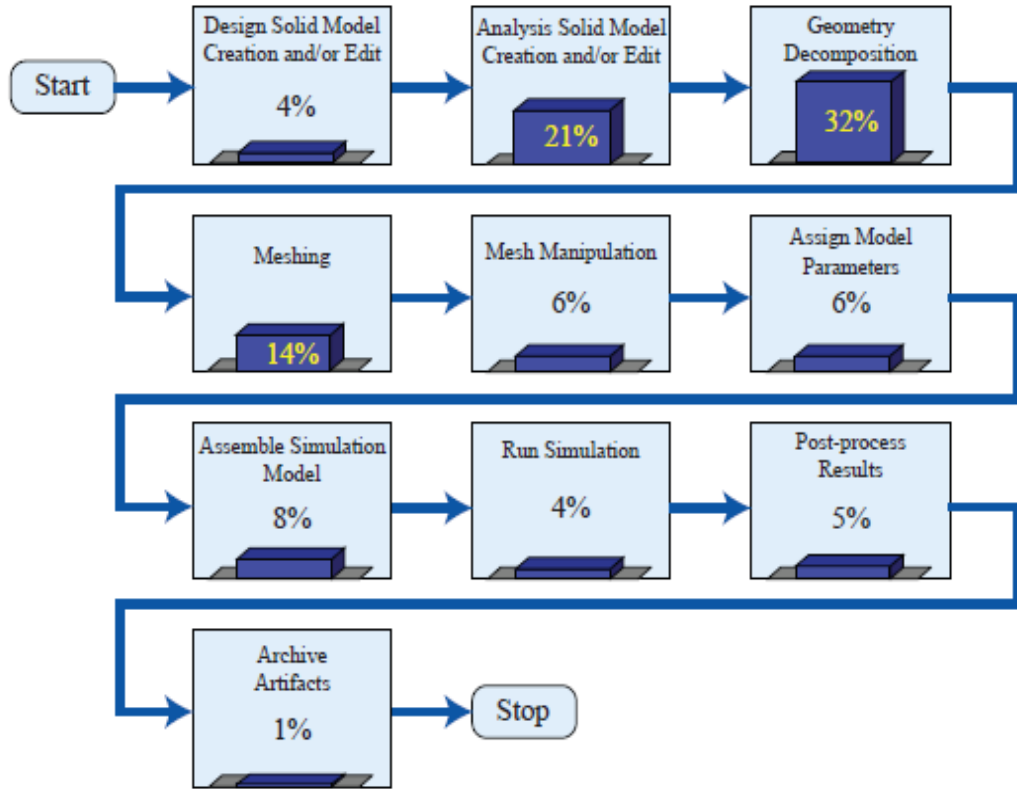
Figure 1.1 Relative time spent during different analysis stages [1]

Besides, designers should carefully construct mating conditions of components in an assembly without allowing any interference. The different requirements and generation methods of the analysis model and the design model also make the communication of designers and analysts more difficult and cause frequent conflicts. On the other hand, it is expected from analysts and designers to be aware of each other's needs and facilitate the solutions of the problems by collaborating. This situation prompted the academy and industry to seek a new solution that could be used jointly for the two main disciplines, design and analysis. Isogeometric analysis emerged in accordance with these conditions. IGA is a recently born analysis method that combines Finite Element Analysis (FEA) and Computer Aided Design (CAD) by providing an appropriate algorithm for computerized solution. The main idea behind

the emergence of isogeometric analysis is utilizing the same basis functions in both design and analysis [2]. It focuses to use one geometric model that can be utilized for analysis directly or can be manipulated for analysis easily and automatically. At this point, isogeometric analysis appeared with the aim of using NURBS geometry, which is commonly preferred by CAD software programs, directly in finite element analysis. In line with these objectives, isogeometric analysis changes classical finite element analysis by using CAD representations and eliminate the data conversion process between design and analysis. [1]

1.1.1 Computer Aided Design (CAD)

In the early 1950s, first commercial computers started to be used in engineering applications, mainly for defense and automotive industries. Since that date, computer technology has been in continuous development and engineers have begun to develop programs to solve engineering problems by taking advantage of the computational power of computers. The first computerized graphical technique was introduced by Ian Edward Sutherland with the name of "Sketchpad" in his thesis [3]. This program was working for 2D drafting operations, but especially automotive and aircraft industries were expecting the developed programs to be able to design 3D surfaces. Under these expectations, companies worked to develop their own design programs. Around 1960, Pierre Bézier, a French engineer, developed a method to define automobile surfaces by using mathematical description of Bernstein polynomials [4]. During construction of these surfaces Bézier used curves mentioned by his name as Bézier curves. At the same time, a French mathematician de Casteljau was also working on Bernstein polynomials. The advantage of their methods was fast and easy definition of part geometries by using linear combinations of control points. By this way, shape modifications were directly applied to the geometry control polygon, without the need to change the properties of the basis functions [5]. After the functionality of the developed method has been proved, a computer algorithm was created for surface modelling by using Bézier curves and program is called as UNISURF and it eventually became an important component of Dassault Systèmes

CAD software CATIA [6]. Although the utilization of Bézier curves made the definition of geometries easier, it has a disadvantage in use. Bézier curves were defined by using only one polynomial and this polynomial had a global effect on the geometry. By this way, it was not possible to obtain local shape changes. In order to overcome this problem, Riesenfeld described a new approach called B-Splines in 1973 [7]. B-Spline is the short form of "basis spline" and it is a superset of Bézier curves and involves its properties. However, it enabled the usage of piecewise polynomials and compact support while defining geometries. Utilization of compact support at the same time provided local geometry changes. After a while, in 1975, Versprille has come up with the method in more generalized form of the B-Splines called as NURBS stands for Non-Uniform Rational B-Splines [8]. NURBS made the usage of rational functions and exact representation of the conic sections possible which is not the case for B-Spline. Today, NURBS is in use by most of the commercial CAD software packages and data exchange standards due to its superior properties.

1.1.2   Computer Aided Engineering (CAE)

The behavior of structures under the working conditions can be analyzed by partial differential equations (PDEs). The solution of such problems can be found analytically for simple geometries and boundary conditions. However, for the complex geometries and boundary conditions it is not possible to obtain analytical solutions with our current mathematical knowledge. In order to reach a solution, instead of applying analytical techniques, some alternative numerical solution techniques such as Finite Element Method (FEM), Boundary Element Method (BEM), Discrete Element Method (DEM), Finite Volume Method (FVM) and Finite Difference Method (FDM) are developed. FEM and BEM are generally used for structural problems, while FVM and FDM are used to solve thermal and fluid flow problems. On the other hand, Discrete Element Method is used for computing large number of small particles as in the case of molecular dynamics. Since this study focuses on structural problems, only FEM will be the numerical method of interest here. The origin of the FEM goes back to study of Richard Courant (1943) [9] where he proposed discretization of the whole

domain into a set of finite triangular subregions in accordance with the philosophy of the finite element method. A few years later, in 1960, Dr. Ray Clough has used the term "finite elements" for the first time in his study [10]. At the same time, since digital computers were invented with capability of making hundreds of operations per second, first commercial FEA programs were began to be developed. In 1963, the first FEA software for structural analysis was improved by MacNeal-Schwendler Corporation (MSC) with the name of SADSAM (Structural Analysis by Digital Simulation of Analog Methods). Milestone of the today's commercial FEA software packages was the enhancement of NASTRAN (NASA Structural Analysis) again by MSC upon request of National Aeronautics and Space Administration (NASA) [11]. Later on, after conducting a lot of structural, acoustic, vibration and thermal analyses, in 1971 company has released commercial version of Nastran named as MSC/Nastran. After that, other commercial software packages such as ANSYS, Marc and Abaqus were released and most of these programs are still in use today because of the advantages they have. The main benefits of finite element analysis are listed below:

- FEA programs decrease the requirement of prototype production with their ability of simulating real conditions. This provides a faster and less expensive design cycle.
- FEA software enables the engineers to easily check the effects of design parameters by successive simulations. Designers can create more effective and accurate designs by taking the effects of parameters into consideration.
- At the end of the design process, engineers can validate their design and its functionality. This helps to reduce the design mistakes to minimum level and increase the quality and performance.

Due to mentioned advantages, computer-aided engineering programs ensure that design decisions can be taken early in the process without prototype production. This provides efficient use of time, money, effort and resources, and creates low-cost success opportunities on projects. Another reason behind the widespread usage of CAE programs is the development of cost effective high performance computers. Early engineering computers were mainframe computers typically came with board-

size floating point options that sold for several thousand dollars. But today, with the advance in personal computers, every engineer can have an individual computer and take advantage of its power of computation in analysis. However, despite the development of computers, solutions are still taking long time during finite element analysis. Mathematicians and engineers continue to work on to enhance existing engineering solution techniques and they are constantly making new contributions to finite element analysis in order to speed up the process. Isogeometric analysis method, the topic of this thesis, is one of these contributions comes from academy to analysis world which is trying to reduce the time, effort and money spent during analysis.

1.2 Research Objective

The main objective of this thesis is to conduct a study about isogeometric analysis (IGA) and its applications to the structural mechanics problems. Isogeometric analysis offers to use NURBS as a basis function in finite element method instead of Lagrange and Hermite polynomials. The main reasons behind the choice of NURBS is listed below:

- NURBS allows exact representation of geometries.
- It is successful in modeling free-form surfaces, conic sections, circular, cylindrical, spherical and ellipsoid shapes with great flexibility and precision.
- With the help of Cox de Boor formulation, efficient and stable algorithms for NURBS can be easily generated or already available algorithms can be found.
- NURBS enables users to easily apply geometry refinement without regeneration of geometry.
- NURBS has non-interpolatory nature and high continuity.

In the classical finite element method approach, the geometric approximation inherent in mesh can cause accuracy problems. Some of the structures as in the case of thin shells are very sensitive to geometric imperfections. Any deficiency in the representation of geometry may change the results tremendously. As can be seen in Figure 1.2, magnitude of allowable buckling load on the cylindrical shell decrease

considerably with the introduced geometrical imperfections. On the other hand, since NURBS can define such cylindrical shapes free from imperfections, these problems can be analyzed with high accuracy. Moreover, isogeometric analysis enables analysts to easily make mesh refinements without communicating and changing the geometry. On the other hand, for classical finite element method application, mesh refinement necessitates the regeneration of geometry and this means a lot of time consumption especially for assemblies with large number of parts.
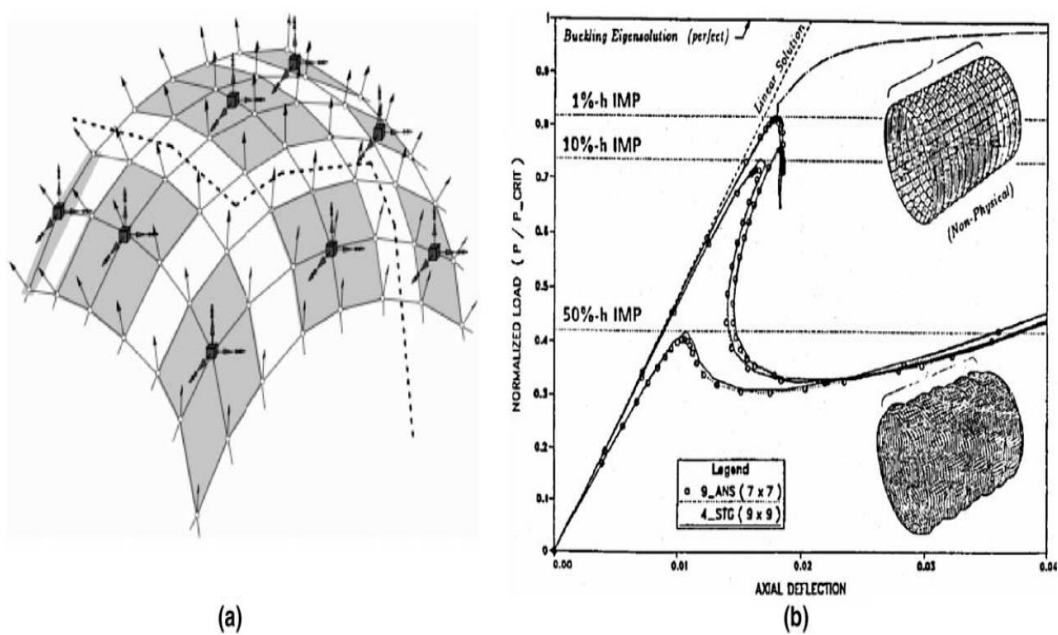
Figure 1.2 Thin shell structures exhibit significant imperfection sensitivity: (a) faceted geometry of typical finite element meshes introduces geometric imperfections and (b) buckling of cylindrical shell with random geometric imperfections [2]

After investigating the advantages of using isogeometric analysis, in this study, it is aimed to apply IGA on linear elasticity and plasticity problems. Specified advantages of NURBS are desired to be utilized on these problems. It is targeted to evaluate the effect of isogeometric analysis method by comparing its results with finite element analysis results.

8

1.3 Scope of the Search

In the present work, the isogeometric analysis is introduced with its theoretical background, numerical applications and experimental verifications. Isogeometric analysis is first applied on the elasticity problems that have exact analytical solutions. Solutions for these problems are obtained in Matlab by developing an algorithm. Same problems are also solved by the classical finite element analysis approach and the results of IGA and FEA are compared. Secondly, basic plasticity problems such as uniaxial loading of a sheet, v-die bending and square deep drawing are considered. Finite element analysis of these problems are performed by using commercial FEA solver Abaqus. Isogeometric analysis of these problems are conducted by the commercial FEA solver LS-DYNA which is adopted for IGA and contains isogeometric NURBS based elements. To better understand the benefits and efficiency of IGA, experiments of the analyzed problems i.e. uniaxial loading of a sheet, v-die bending and square deep drawing are performed. Experimental results are also compared with numerical solutions of IGA and FEA. Experimental tests and numerical simulations are carried by using AISI 304 stainless steel and AA2024-T3 aluminum materials. By conducting these experiments, it is also aimed to bring extensive experimental data to the use in literature.

1.4 Outline of the Thesis

This thesis consists of 6 chapters, and references.

In chapter 1, background and motivation behind the introduction of this work, objectives and scope of the study and outline of the thesis are presented.

In chapter 2, the literature survey that informs about researches and developments in the academic world related with this study is given.

In chapter 3, the theories of mathematical modeling techniques used in geometry creation and also in the development of isogeometric analysis are introduced. Since

this analysis method is a modification of classical finite element method by using introduced basis functions, the theory of FEM is also included.

In chapter 4, application examples of IGA on elasticity problems are investigated. Solutions obtained by using analytical methods and numerical methods are presented. Numerical solutions are obtained with the help of developed Matlab code and Abaqus classical FEA program. Consistency of numerical methods with analytical solution are examined. FEA and IGA techniques are compared by evaluating the results and solution procedure.

In chapter 5, some of the plasticity problems are solved by using isogeometric analysis. During solution process, Abaqus FEA and LS-DYNA programs are utilized for finite element analysis and isogeometric analysis respectively. In order to verify the numerical solutions, experiments are conducted. Finite element analysis and isogeometric analysis results are compared with experimental analysis results in order to observe accuracies for validation of these methods.

In chapter 6, results are summarized and evaluated together, while conclusions are drawn including the recommendations for future work to enhance the method.

CHAPTER 2

LITERATURE SURVEY

In this part, some of the scientific researches reviewed from literature and regarded as important were briefly mentioned. The fundamental topics focused during survey were finite element method, theoretical background of computer aided engineering, isoparametric elements, usage of B-Splines and NURBS for geometric descriptions, isogeometric analysis theory, usage of IGA in structural mechanics problems and other kind of engineering problems and expected future developments in isogeometric analysis with some alternative viewpoints.

Finite element method is beyond argument most widely used numerical method for solving common engineering problems. Therefore, many researchers have been interested in using finite element method to solve their problems without the need for costly and time consuming experimental tests. Although it is difficult to indicate the date of invention for the finite element method, the basis of its development can be dated back to the 1940s. In 1941, Alexander Hrennikoff has improved "Framework Method" for the solution of elasticity problems [12]. The basic idea behind the framework method consists in replacing the continuous material of the elastic structures by a framework of articulated parts arranged into identical definite pattern. The framework was given with boundary conditions and subjected the loads of the real part. Under given conditions stresses were analyzed for articulated parts, and by using these results stresses were also obtained for overall geometry. When the units are infinitesimal in size, the framework of this kind is rigorously equivalent to the whole part with regard to the stresses and deformations [13]. R. Courant has published his work in 1943 with the idea of replacing difficult problem P with simpler problem P_n and its solution S_n. Then by improving the approximation P_n to P, S_n tends to the desired solution S of P [14]. Despite these pioneers used different techniques in their studies, they both highlighted a common point which is discretization of a continuous

domain into a set of sub-domains. These sub-domains have been called as "finite elements" for the first time in the work of Clough (1960) [10]. Clough successfully showed a mathematical approach to minimized potential energy of an assumed potential pattern. In addition to mentioned names; John Argyris, Olgierd C. Zienkiewicz, Ivo Babuška, Bruce Irons, Robert L. Taylor and many other research scientists have contributed to finite element method to make it well-run method. They have centered around numerical perspective of this new technique by enhancing solution approximations and geometrical portrayal to diminish error, convergence and stability problems. In accordance with this purpose, in order to improve the geometrical representation of mechanical analysis models, Ergatoudis et al. [15] have proposed the usage of curved, isoparametric, "quadrilateral" elements for finite element analysis. For the curved shapes, these elements were able to follow the boundaries of the geometry to a good degree of approximation. In this work, parametric coordinates and polynomial shape functions were defined for linear, quadratic and cubic isoparametric elements in 2D. Moreover, stiffness matrix, strain matrix and Jacobian matrix which are necessary for elastic plane stress or plane strain solutions were also defined. Usage of isoparametric elements enabled analysts to use reduced computational effort in their analysis and to decrease the possibility of result errors. Therefore, the popularity of this new approach began to grow in the engineering communities and it is still in use today.

While the finite element method has been improved and its usage became prevalent around engineers and mathematicians, in the meantime, CAD technology was born with the studies of Bézier (1966, 1967 & 1972). In these works, Bezier introduced the use of Bernstein polynomials in creation of curves and surfaces named as "Bézier Curves" and "Bézier Surfaces" respectively [4]. In order to increase the flexibility of design method by using more control points for the same degree, Riesenfield has proposed a new technique in his doctoral thesis with the name of "B-Spline Approximation" [7]. In this thesis, he showed how to create new curves and surfaces by using B-spline basis functions instead of the more classical Bernstein polynomial approximation theory which is a subset of Bézier curves and surfaces. In 1975,

Versprille has come up with the idea of Non-Uniform Rational B-Splines (NURBS) [8]. In this study, he aimed to define different impact to the control points by giving different weights. In this way, NURBS satisfied a great flexibility in geometry creation and today it is most widely used mathematical model of computer aided design programs.

In the 1980s, integration of the FEA and CAD technology has started. Due to the different origins of CAD and FEA technologies, they have always been treated as a completely separate professions handled by distinct engineering departments. Nevertheless, due to various benefits of cooperation of CAD and FEA methods, researchers have focused on the new combined techniques. Accurate geometry description which is vital to avoid approximation errors was the main motivation of the studies in 1990s. S. Arabshahi et al. [16] published a conceptual article that emphasizes the need for integration of design and analysis techniques and gives an overview of a future system which would allow and encourage more automated CAD-FEA transformation. This study discusses the functional components that can be used to achieve fully integrated CAD-FEA system. According to the study, it is indicated that; robust, comprehensive Product Description Systems (PDS) to held geometric data, semi-automated Data Transformation System (DTS) that transforms data held in PDS to analysis suitable finite element model, meshing routines with different meshing strategies, mesh quality and refinement, finite element solvers suitable to new algorithm and range of engineering problems and post-processing components should take a part in the future integrated systems.

Therefore, this study claimed to constitute an analysis process which is in relation with the design requirements. Hence, the study of S. Arabshahi has a special place in literature due to the prediction of future developments by analyzing the needs of industry by the time when it was prepared. The second precursor study about CAD and FEA integration was published by Gontier and Vollmer in 1995 [17]. In this work, large displacement analysis of beams was discussed by using Bezier type geometry definition. Main aim of the study was to benefit from possibility of generating highly flexible beam elements that would accept large distortions from its initial shape. Three

numerical examples were performed in this study. Firstly, clamped-free straight beam under increasing couple at its free end was analyzed. Secondly, clamped-free parabolic beam under increasing load and increasing couple at its free end cases were solved. Finally, a circular arc shaped beam under increasing load system was studied. At the end, it was shown that complex shapes of deformation could be described with fewer elements under favor of utilizing the Bezier representation. On the other hand, main drawback of the Bezier representation due to its global effect was emphasized. Instead of using Bezier representation, in 1998, a new type analysis element called as B-Spline Finite Element (BSFE) has been developed and solution procedure were described and investigated in detail by Kagan et al. [18]. Convergence characteristics and computational effort of the method was compared with classical methods on a linearly elastic Euler-Bernoulli beam model problem. The BSFE solution was found to have prevalent exactness on results with no significant difference in convergence rates, computational effort and implementation complexity. In 2000, Kagan et al. [19] used B-Spline representation to analyze elastic linear plate model by the "Kirchhoff Plate Theory" and it was seen that this method shortens the product analysis duration and decrease the total cost of product development.

In 2005, Hughes et al. [2] have come up with the idea of new NURBS-based finite element method which uses CAD basis functions NURBS also in finite element analysis. They named this method as "Isogeometric Analysis". The main aim of the work was to obtain geometrically exact analysis model independent of discretization. Another aim was to remove the requirement of communication with CAD geometry during mesh refinement process. In the study, theories of B-Splines, NURBS and refinement types were given. Isogeometric analysis was implemented to structural analysis and fluid analysis problems. In structural analysis applications, infinite plate with circular hole under constant in-plane tension; solid circular cylinder subjected to internal pressure loading; solid ''horseshoe'' subjected to equal and opposite in-plane flat edge displacements; thin cylindrical shell with fixed ends subjected to constant internal pressure; Scordelis–Lo roof, pinched hemisphere and pinched cylinder shell

under gravity and concentrated forces respectively; hemispherical shell with a stiffener subjected to gravity loading and external pressure problems were investigated.

Among these problems IGA results were compared with exact analytical solutions for first and second problems. For the remaining problems results were checked with academic studies done on the same problems. For all types of the problems, results were consistent with the compared solutions. Additionally, this compatibility was obtained with coarse discretization and few number of elements. So, the simplicity of mesh refinement was also highlighted in these problems. After the introduction of isogeometric analysis method, lots of researchers from different disciplines have been interested in this new technique. Since then, a number of studies have appeared about refinement, continuity, structural vibrations and so on. After this phase, in 2009 J. Austin Cottrell et al. [1] published the IGA book. This book is the more general form of the paper published in 2005 [2]. In addition to theoretical information and example implementations take a part in previous paper, this book also includes vibrations and wave propagation, time dependent problems, nonlinear problems and incompressible solids for structural analysis and turbulence problems for fluid analysis. Since then, the theory of isogeometric analysis was settled in academic studies and it has been applied to extensive variety of problems to highlight the exact geometry and accuracy properties compared with classic FEA.

Isogeometric analysis has a wide range of application areas from acoustics, structural analysis to electromagnetics. The main interest area of this study is structural analysis and there are a lot of articles in this area focused on different problems. The most basic geometry that has been analyzed with IGA technique was beam model. 3D curved beams were investigated in the study of Guodong Zhang et al. [20] by using isogeometric analysis approach. The behavior of curved structural members described by using the numerical methods based on finite element approximations had still shear locking problems. In the study of Zhang, isogeometric finite element method was formulated for the 3D curved beams in space and by utilizing this formulation, the locking issues were coped with by the help of higher order NURBS interpolations. The validity of the method was examined on the circular balcony problem consists 16

elements with 4th degree basis functions, logarithmic spiral problem having 194 elements with 3rd degree NURBS basis, spiral staircase problem consists of 264 elements with 3rd degree basis functions and S-curved beam analysis carried out using 26 elements with 4th degree NURBS basis. Each problem had specialized end conditions, loads and moments. At the end of the work, it has been concluded that the 3rd and 4th degree NURBS basis usage has minimized the locking problem. Although there were still a few locking problems with cubic NURBS basis, the fourth degree basis totally eliminates locking. Another study about curved space beam analysis by using IGA was done by Ioannis N. Tsiptsis et al. [21]. In this work, complex behaviors of curved beams under the coupled loading conditions of axial load, bending moment and torque were investigated. Static analyses of horizontally curved beams of open or closed cross sections were performed in the light of isogeometric analysis. Although, Thin Tube Theory (TTT) and Generalized Beam Theory (GBT) have been widely used in order to deal with flexural and torsional distortion, IGA approach has been successfully applied to beam with doubly symmetric cross section and monosymmetric cross section. With the use of IGA, distortional effects on curved beams have been analyzed with better accuracy and less computational effort since the geometry curvature which is an actual parameter that affects the results has been better represented. In addition to the aforementioned researches considering the isogeometric beam elements, geometrically nonlinear beam elements including torsion was studied by A.M.Bauer et al. [22]. In this research, a new element formulation by using IGA based on Bernoulli theory was suggested for spatial curved beams under torsion with geometric nonlinearity. As in the case of previously introduced studies, some examples were presented to verify the new element formulation. Firstly, analysis of a quarter circular, clamped at one end and loaded on the free tip was conducted as a membrane-bending interaction problem. Bending-torsion interaction was also investigated for the same quarter circular by changing load condition. Two in-plane examples which are shallow arch clamped at both ends with a single point force applied in the center of the beam and main-spring under pure bending were studied to understand the behavior of geometrical nonlinearities. For all of the examples, it was benefited from the easy implementation of mesh refinement and higher order basis

16

function usage. Different basis orders and element numbers were examined and the accuracy of the method was demonstrated.

In addition to beam analysis, isogeometric analysis method has been successfully used in shell analysis, which is another basic but also common structural analysis subject. IGA has been implemented to Reissner-Mindlin shell formulation by D.J. Benson et al. [23] in order to analyze linear elastic and nonlinear elasto-plastic structures by alleviating shear locking and artificial thinning problems. In his study, one linear elastic and four non-linear elasto-plastic material examples were investigated. Firstly, in order to realize accuracy and convergence of the developed formulation, pinched cylinder linear elastic shell problem was solved. Inward directed point loads were applied to the cylinder surface at the opposite locations. Quadratic to quartic basis functions were used and suitable meshes with these basis consists of 4 to 64 elements were created with the help of h-refinement. Although shear locking problem was still seen for quadratic NURBS basis, increasing the order removed it. In order to examine the sensitivity and robustness of developed shell analysis formulation in the case of distorted elements, nonlinear problems were solved. In the first nonlinear problem, a simply supported plate loaded by a uniform pressure with elastic-perfectly plastic material was analyzed. Meshes with quadratic, cubic and quartic basis that consists 4,16 and 64 elements were employed. Results obtained by using isogeometric elements were compared with the result of analysis done by 64x64 bi-linear Belytschko–Tsay shell elements available for shell analysis in LS-DYNA. The finest mesh solutions were close to the solutions of Belytschko–Tsay shell elements independent from the polynomial order. Therefore, the effect of element number dominates the basis order effect. For the second nonlinear problem, a roof formed from 120° cylindrical panel under velocity impulse was studied. As in the previous case, quadratic, cubic and quartic isogeometric elements were used for calculations. Shear locking was experienced for quadratic basis functions with less number of elements while the increasing number of elements deals with this problem. Another implementation was performed on an isotropic linearly elastic-linearly plastic cylindrical tube under buckling loading. Buckling mode of the tube was captured by

using 1440 IGA elements. The critical pressure has been found as 3.04 MPa while in the experimental study it was found as 2.83 MPa. Final example in this study for nonlinear analysis was analysis of square tube buckling into an accordion mode which is one of the most sensitive cases for element distortions. An isotropic elastic-plastic material with linear plastic hardening was used. Quadratic and quartic polynomial orders with 640 elements were used. A geometric imperfection was introduced to specified location of the structure in order to initiate buckling deformation. Same problem was solved by using surface contact algorithm. At the end, a good agreement between the results was attained. Therefore, isogeometric analysis method was seen suitable for Reissner-Mindlin shell theory, and well-suited for linear and nonlinear applications even for large deformations with element distortions. D.J. Benson et al. [24] have also introduced the rotation free isogeometric shell elements to be used in several problems. In this work by Benson, large deformations were analyzed by utilizing NURBS based isogeometric shell elements which were developed without rotational degrees of freedom contrary to conventional finite element formulations. Since usage of rotational degrees of freedom increases stiffness matrix size, computational effort and probability of encountering convergence problems are higher than rotation free formulations. Therefore, shell formulations with only translational degrees of freedom is more practical. Two nonlinear elastic-plastic problems have also been solved by using the provided formulations. In the first problem, a roof loaded by velocity impulse analysis was performed by using 450 isogeometric elements and same displacement results were found by using 4656 Belytschko-Tsay elements. CPU time required for solution in IGA is the half of time required in reference analysis. For the second problem, metal stamping procedure for S-rail was examined on aluminum 6111-T4 metal sheet. Hill anisotropic yield function was used for definition of material behavior in plastic region. Simulations were carried out with 240, 1092, 3840 and 7680 quadratic isogeometric elements for metal blank. On the other hand, same analysis was done by Alcoa with using 11550 elements to create analysis model of blank in LS-DYNA. Although no wrinkles were seen with the analysis done by using 240 elements, for the other mentioned mesh numbers, wrinkles were captured. On the other hand, maximum plastic strain value of the process was found as 0.291 with the

reference analysis and this result could only be obtained by using 3840 and 7680 elements. Thus, usage of isogeometric rotation-free elements decreased the necessary element number from 11550 to 3840. Reissner-Mindlin shear deformable theory uses C^0 continuous basis functions as in the case of most structural elements in finite element analysis. However, Kirchhoff-Love shell theory requires C^1 continuity of the displacement field which is hard to get for free-form geometries and this theory is generally used for thin shell structures where shear deformations are neglected. Nguyen et al. [25] presented a study that provides extended isogeometric element type for analysis of the cracks in thin shell bodies along the thickness. C^1 continuity was obtained without using additional rotational degrees of freedom. The absence of rotational degrees of freedom has diminished the complexity of the enrichment strategy and computational cost. By using plate and cylinder examples that carry variously settled cracks on them with tensile, shear and inner pressure loadings, the agreement and accuracy of the method with analytical and extended finite element method (XFEM) solutions was aimed to be shown besides its computational performance.

In addition to the isogeometric analysis studies conducted on beam, shell and plates by using general material models, another common area of usage of IGA is composite materials. Xuan Wang et al. [26] investigated buckling analysis of laminated composite beams. In their work, cross-ply and angle-ply composite beams with symmetry and anti-symmetry were examined as a numerical example to compare the IGA with other available solutions. It was aimed to consider critical buckling load of the beams. Additionally, effects of the slenderness ratio, stacking sequence, modulus ratio and fiber angles were evaluated. Clamped-clamped, simply supported and clamped-free boundary conditions were applied to problems. The critical buckling analyses of cross-ply laminated beams were conducted by using symmetric [0/90/0] and anti-symmetric [0/90] cross-ply laminated composite beams for two different modulus ratios E1/E2=10; 40 and also for two different slenderness ratios L/h=5; 20. Quadratic isogeometric elements with 10, 20, 100 and 200 control points were used. Thereafter, the free vibration analyzes of an anti-symmetric composite beam with

[45/-45/45/-45] sequence stack for fully clamped and simply supported boundary conditions were run to show the impact of including the poisson effect to the results in the analysis of angle ply laminated composite beams. Finally, symmetric angle-ply beams with stacking sequences [θ/-θ/θ] and [θ/-θ/-θ/θ] and an anti-symmetric two-layer angle-ply laminated composite beam with lay-up [θ/-θ] were investigated to observe the effects of the fiber orientations on the critical buckling loads where the θ grows from 0 to 90 by fifteens. At the end of the work it was concluded that, boundary conditions have a profound influence on the critical buckling loads, and the beam subjected to clamped-clamped boundary condition i.e. more fixed degrees of freedom has largest buckling load limit for all lay-up configurations. Although symmetric lay-up provides the largest critical buckling load in cross ply laminated beams, anti-symmetric stacking sequences provide the largest critical buckling load for angle-ply laminated composite beams with the same modulus ratios and slenderness ratios. The critical buckling loads decrease with the increase of the fiber angle for each set of boundary conditions. Laminated composite beams with large modulus ratios and low slenderness ratios have also higher critical buckling loads for the same ply sequence and orientation. Poisson effect included numerical results are in very excellent agreement with the analytical solutions while the results with neglected poisson effect have significant errors for angle-ply composite beam and therefore, poisson effect should be included in the analysis of angle-ply composite beams.

Besides the examination of buckling analysis of straight beams, bending and buckling behaviors of curved beams with varying stack-up and curvature values were also studied by Anh-Tuan Luu et al. [27] with the isogeometric approach. A number of numerical examples were presented for bending and buckling analyses of laminated composite curved beams with arc length L, span length l and rise f. As a first example bending analysis was conducted on cantilever circular curved beam with anti-symmetric cross-ply [0/90] lamination subjected to uniform normal load was considered where slenderness ratio was equal to 20 and the deepness ratio, which is ratio of length to radius, was 1. Meshes consist of two elements with quadratic to quintic orders were used to model the circular curved beam. By conducting

h-refinement and k-refinement, element numbers have been increased up to 64 in order to increase the accuracy. When the results obtained by using h-refinement and k-refinement were compared, it was seen that for higher order of basis functions they both gave the same value while for lower orders k-refinement results were more accurate. For verification purpose, the numerical results of the general differential quadrature (GDQ) analysis and finite element analysis were also given. In order to investigate more examples for the sake of validity of IGA, maximum deflections of cantilever composite beams with circular curved shapes, symmetric $[0/90]_s$ and antisymmetric cross-ply $[0/90]$ laminations were analyzed for different deepness ratios. With the increased deepness ratio, deformations of the beams were decreased. Around analyzed beam models symmetric one has experienced the least deformation while antisymmetric cross-ply has become most deformed one. Another deformation type that was analyzed in Anh-Tuan Luu's study was buckling of circular curved beams and parabolic curved beams under uniform compression. For both of these problems $[0/90/0]$, $[0/90]$, $[45/-45]$ and $[0/45/-45/90]$ lay-up sequences were used with different deepness ratios under clamped-clamped and hinged-hinged boundary conditions. Uttermost critical buckling load value was obtained for $[0/90/0]$ configuration where the second highest value was obtained for $[0/45/-45/90]$ and lowest value was found for $[45/-45]$ lay-up. Other common conclusion drawn from the results was greater critical buckling load for clamped-clamped end condition and for higher deepness ratio. In addition to beam problems mentioned above, isogeometric analysis was also used for composite plate analyses. Reissner-Mindlin theory with isogeometric approach mentioned before for shell analyses, was also used to investigate bending behavior of laminated and sandwich composite plates in the work of Abha Gupta and Anup Ghosh [28]. The common conclusions drawn in other studies about the accurate results with less number of elements, computational performance and flexible usage of IGA were also drawn from this study. Additional remarks about the decreased shear deformation of the sandwich structures with increasing span to thickness ratio has been expressed. As in the works conducted on beams with different boundary conditions, the deformation reducing effect of clamped boundary condition was re-experienced. Nonlinear geometries of composite plates

21

were analyzed by using NURBS isogeometric elements in the study of Hitesh Kapoor and R.K. Kapania [29]. First order shear deformable theory was also utilized with isogeometric analysis for analyses of isotropic, orthotropic and laminated composite thin plates for various boundary conditions, different length to thickness ratios and ply-angles. Center deflection of the plates were evaluated and compared with the results of Urthaler and Reddy study [30]. Geometrically nonlinear thin plates prone to suffer from shear locking problem due to the high length to thickness ratios of elements. K-refined quadratic isogeometric elements can be a remedy for this problem. Besides usage of FSDT, higher order shear deformation theory on composite plates with IGA was also studied in Loc V.Tran et al. publication [31]. Cubic approximation functions were utilized to satisfy the C^1 continuity across inter-element boundaries without any additional variables. Shear locking problem was eliminated.

In addition to structural analysis, IGA has another application area which is contact problems. In contact formulations, with the usage of conventional finite element geometry discretization, representation of faceted surfaces can cause jumps and oscillations in traction responses. Since the IGA provides an opportunity to create smooth contact surfaces, it makes achievement of physically accurate contact stresses possible [32-36].

IGA has been preferred to traditional methods in optimization problems due to the tight interaction with CAD geometries which makes it an attractive choice for industrial applications to represent actual geometry. In the studies [37-39], structural shape optimization, its application to vibrating membranes and analytical sensitivities of optimization with IGA were discussed respectively. Additionally, sizing and shape optimization of beam structures were studied in [40] while stacking sequence optimization of laminated composite beams were investigated for maximum strength in the work [41]. In isogeometric shape optimization, since the geometric properties of design were embedded in NURBS basis functions, the change of design parameterization is much easier than that in finite element based method without sub-sequent communications with CAD description.

Another application area of IGA is structural vibration problems [42-45]. Timoshenko beams and complex spatial beams, curvilinear stiffened shells and composite laminated Reissner-Mindlin plates were examined under free vibration. Finally, usage of higher order mass matrices in isogeometric structural vibration analysis has been evaluated. It was shown that the quadratic and cubic higher order mass matrices have 6th and 8th orders of accuracy, which are two orders higher than those of their corresponding in finite element analysis despite the usage of low order mass formulations.

Utilization of NURBS basis functions is a good preference for analysis of fluid mechanics and fluid-structure interaction problems due to the smooth geometry supply. Navier-Stokes-Korteweg equations were solved and Navier-Stokes flow was discretized by conducting isogeometric approach [46-47]. Flow behavior around a cylinder, turbulent flow and unsaturated flow problems were also investigated [48-50]. Theory and computation of the fluid-structure interaction problems were developed in the study [51] while an application of this theory was also performed on thoracic aortic blood flow [52].

Isogeometric analysis concerns with the solutions of thermal analysis and thermomechanical coupling problems. In study of Zbigniew Kacprzyk and Katarzyna Ostapska-Luczkowska [53], steady state thermal analysis of a simple geometry was conducted. By using h-refinement technique different mesh sizes were experienced. In the publication [54], an isogeometric shape sensitivity analysis method was developed for heat conduction problems using the adjoint variable method. Moreover, thermomechanical coupling problems, thermal buckling analysis of functionally graded materials [55] and fracture of inhomogeneous cracked solids under thermal loading [56] were studied by using isogeometric analysis**.**

Thereafter concerning thermal problems, acoustic problems can also be solved by IGA. Interior acoustic problems were analyzed by using IGA [57]. Novel isogeometric boundary elements were developed in frequency domain by using indirect variational BEM which is better for open boundary containing 3D acoustic problems [58]. In

order to simulate acoustic fluid-structure interaction problems, a beam coupled to rectangular fluid cavity, a Kirchhoff plate coupled to a cuboidal cavity, a circular plate coupled to a doubly curved barrel shaped cavity and a car interior cavity in two dimension coupled to a beam cases were analyzed by using isogeometric analysis [59]. At the end, IGA found 500 non-zero natural frequencies with error less than 5% while FEM results were erroneous up to 25% at the higher modes for both weak and strong coupling in 2D.

Together with increasing industrial applications, isogeometric method has been also widely used to solve mathematical problems. Since it is easy to construct high order continuous basis functions in IGA, it is possible to get great success in solving PDEs that include fourth order or higher derivatives of the field variable, such as the Hill-Cahnard equation [60], explicit gradient damage models [61] and gradient elasticity [62]. Moreover, singular integrals were evaluated by using isogeometric boundary element method [63].

For most of the studies and publications mentioned above, in order to benefit from calculation ability of the computers, computational implementations were performed. However, the usage of IGA is limited mostly within academic community. The absence of automated, bug-free commercial programming framework is the main reason that prevents spread of IGA usage in entire industry. Up to now, none of the written software are industrialized, but some of the implementations are open-source to facilitate the research burden of other researchers. To be used in 2D scalar PDEs an open source IGA Matlab code was described in [64]. More useful free software tool with the name of GeoPDEs which was also developed in Matlab to focus discretization and solution of partial differential equations was given in the study of [65]. Another program developed by using isogeometric analysis is PetIGA which focuses mainly the solutions of nonlinear partial differential equations [66]. Therefore, PetIGA was applied to challenging solid and fluid mechanics problems such as hyperelasticity [67]. In addition to the open source newly developed software tools, in some researches industrial software packages were used with additional subroutines. Abaqus user element was defined in [68] to solve higher order strain gradient elasticity problems.

In another survey [69], again isogeometric analysis method was implemented into Abaqus by taking advantage of user-defined elements to analyze industrial problems such as thermal residual stresses and bond line failures. LS-DYNA commercial program was managed to consider both elastic and plastic deformations of parts [23]. Another software used for IGA was AbqNURBS which was developed in Lyon, France [70]. Among the all introduced programs, it was decided that the most stable and powerful software is LS-DYNA and so, as a commercial software LS-DYNA was used in plasticity part of this study. On the other hand, for elasticity problems of this study, developed Matlab codes were used.

Isogeometric analysis based on NURBS but, it exhibits some shortcomings from both computational and analysis point of view. The major disadvantage of NURBS is its global refinement nature causes from tensor product structure. For this reason, fine meshes were constructed in the areas of geometry which are not desired to be finely meshed. This leads to inefficient error estimation and time consumption. T-Splines were accepted from both the computational geometry and analysis communities as a solution technique to overcome the limitations of NURBS while retaining the familiar structure of NURBS algorithms. T-Splines enable the usage of local refined meshes and make it easy to create and edit freeform models. In some researches, IGA formulations were developed by using T-Splines and T-splines can be incorporated efficiently into existing FE codes [71-73]. Usage of T-Splines can be a good future work for this study.

CHAPTER 3

ISOGEOMETRIC ANALYSIS USING NURBS

In this chapter, a brief discussion about the theories of B-splines and NURBS which are necessary to use isogeometric analysis approach are presented. Some basic concepts, commonly used notations and B-spline curves and surfaces are introduced. Thereafter, element and space definitions and their implementations are discussed. Further, comparison between isogeometric analysis and classical finite element analysis is reported.

3.1 B-Splines

Non-Uniform Rational B-Splines (NURBS) are used as basis functions of isogeometric analysis. NURBS are a superset of B-Splines and many features of these two are common. B-splines are built from piecewise polynomial functions that are defined by knot vectors on non-overlapping connected intervals. Within these intervals B-splines are smooth, differentiable and continuous while at the boundaries of these intervals they are still continuous but not necessarily differentiable. Although, in classical finite element method, the parameter space is local to individual elements, the B-spline parameter space is local to the entire patch since internal knots partition the patches into elements. In other words, in FEA, each element has its own mapping from the reference element while a single B-spline map takes the patch from the parameter space to the physical space. Therefore, in IGA the mapping is global to the whole patch, rather than to the elements themselves. The term patch is used to specify the parametric space partitions or subdomains within which element types and material models are assumed to be uniform.

3.1.1 Knot Vectors

In order to define B-Splines, partition of the parameter domain should be applied by

one dimensional vector that comprise of non-decreasing coordinates in parameter space. This vector is called as "knot vector" and written as follows

$$\Xi = \{\xi_1, \xi_2, \ldots, \xi_{n+p+1}\}$$

where $\xi_i \in \mathbb{R}$ is the ith knot, $i = 1, 2, \ldots, n+p+1$, is the knot index, p is the polynomial order, and n is the number of basis functions used to constitute B-Spline curve. Generally, knot values are normalized in the range between 0 and 1. The knots partition the parameter space into elements, usually referred as "knot spans". Element boundaries in the physical space are simply the images of knot lines under the B-spline mapping.

Knot vectors can be classified as uniform or non-uniform and open or periodic knot vectors. If knot values in the knot vector are equally spaced in the parameter space such as [0 1 2 3 4] or [0 0,1 0,2 0,3 0,4], then knot vector is called as uniform. Otherwise it is named as non-uniform knot vector. A knot vector can be defined as open if its first and last knot values appear $p+1$ times. B-Spline basis that are constructed from open knot vectors interpolate to the control points at the ends of the parameter space interval, $[\xi_1, \xi_{n+p+1}]$, for one dimension. On the other hand, for multiple dimensions, they interpolate at the corners of patches. However, in general they are not interpolatory at interior knots. This is a distinctive property between knots in isogeometric analysis and nodes in finite element analysis.

In the parametric space more than one knot can be located at the same coordinate and thus, knot values can repeat in knot vector. The number of repetitive knots is called as knot multiplicity and this case has essential effects on the properties of basis functions. Knot repetition can decrease the continuity of the basis function to C^{p-m} where m is the number of multiplication. When the number of multiplication is equal to polynomial degree p, the basis will be C^0 continuous at the multiplied knot value [74]. This makes the basis function non-differentiable at that knot. This property makes it possible to create sharp corners in the spline curve by controlling the continuity to the associated basis functions.

3.1.2 Basis Functions

Definition of B-Spline basis functions has a recursive nature which begins with zero polynomial degree $(p = 0)$

$$N_{i,0}(\xi) = \begin{cases} 1 & if \ \xi_i \leq \xi < \xi_{i+1} \\ 0 & otherwise \end{cases} \tag{3.1}$$

For the polynomial degrees greater than zero $(p \geq 1)$ piecewise definition of the basis functions follows the formula given as;

$$N_{i,p}(\xi) = \frac{\xi - \xi_i}{\xi_{i+p} - \xi_i} N_{i,p-1}(\xi) + \frac{\xi_{i+p+1} - \xi}{\xi_{i+p+1} - \xi_{i+1}} N_{i+1,p-1}(\xi) \tag{3.2}$$

This piecewise mathematical definition is referred as Cox-de Boor recursion formula [75-76]. While working with open knot vectors or repeated knots, it is very crucial to take into account that one might encounter with zero denominator. This problem was solved by defining the result of such equations equal to zero.

During the calculation of basis functions, due to the recursive nature of formulation, results of higher order polynomials require the results of lower orders. This dependency is shown in Figure 3.1.
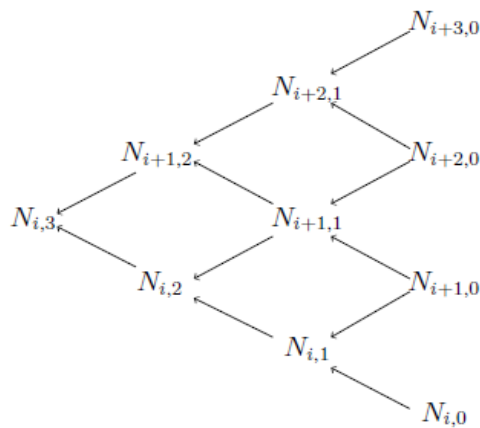
Figure 3.1 Dependencies between results of basis functions for computing a cubic basis function [74]

For constant and linear basis functions with a uniform knot vector $\Xi = \{0,1,2,3,4,5\}$ the results are represented in the Figure 3.2. Looking at the figure shown, it can be said dynamic programming code is necessary to improve the efficiency of this recursive formula. Otherwise, the same values will be calculated several times. It should be noted that for $p = 0$ and $p = 1$, B-Spline basis functions have the same values as constant and linear shape functions of classical finite element method. However, by increasing the order, B-Spline basis functions differentiate from their finite element counterparts. This difference can be observed in Figure 3.3 where the graphs of quadratic B-Spline basis functions and quadratic finite element shape functions are drawn. Quadratic B-spline basis functions are exactly same but shifted relative to each other with varying knot values. As we continue to higher-order basis functions this "homogeneous" pattern continues for the B-spline basis functions. On the other hand, quadratic finite element shape function differs according to the corresponding node position. This is a distinguishing feature between B-Spline basis and FEM shape functions that makes IGA superior to FEA.
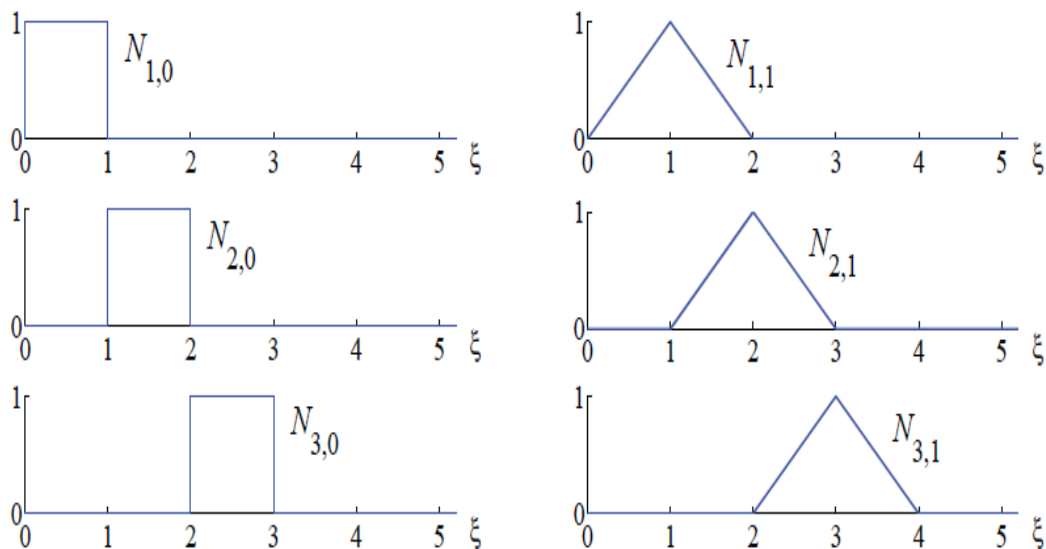
Figure 3.2 Basis functions for order 0 and 1 for uniform knot vector
$\Xi = \{0,1,2,3,4,5\}$ [1]
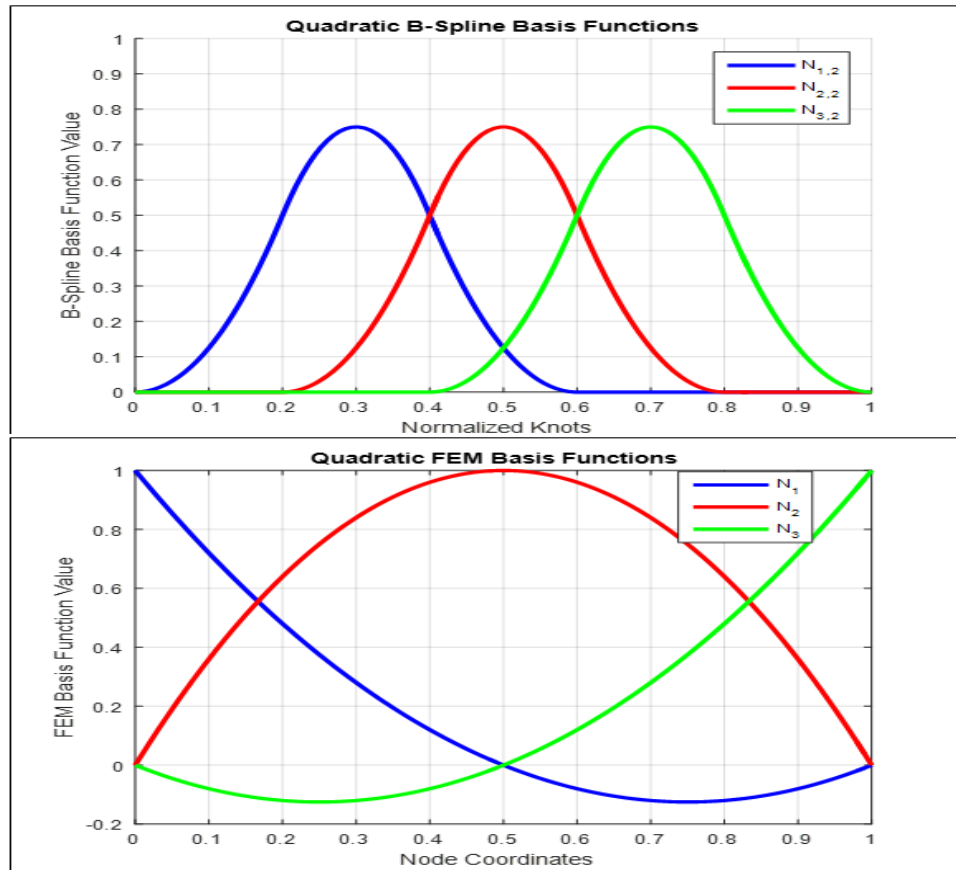
Figure 3.3 Comparison of quadratic finite element shape functions and B-spline basis functions

In addition to mentioned homogeneity, B-Spline basis functions have several important properties as explained below:

- B-Spline basis functions constitute a partition of unity $\sum_{i=1}^{n} N_{i,p}(\xi) = 1$
- Each basis function is non-negative over the entire domain $N_{i,p}(\xi) \geq 0, \forall \xi$
- B-Spline basis functions are linearly independent $\sum_{i=1}^{n} \alpha_i N_i(\xi) = 0$ only for $\alpha_i = 0, i = 1,2, \dots, n$
- The support of a B-Spline basis function of order p is $p+1$. $N_{i,p}$ is non-zero over $[\xi_i, \xi_{i+p+1}]$
- Basis functions of order p have $p-m_i$ continuous derivatives across knot ξ_i where m_i is the multiplicity of knot ξ_i.
- Scaling or translating the knot vector does not alter the basis functions.

- B-Spline basis are generally only approximate to control points and not interpolate. Therefore, they do not satisfy the Kronecker delta property $N_{i,p}(\xi) \neq \delta_{ij}$. Only in the case $m_i = p$, then $N_{i,p}(\xi) = 1$.

Non-uniform knot vectors should be preferred to obtain richer behavior for basis functions rather than uniform knot vectors. An example created by using an open non-uniform knot vector $\Xi = [0\ 0\ 0\ 0.2\ 0.4\ 0.4\ 0.6\ 0.8\ 1\ 1\ 1]$ is shown in Figure 3.4. Basis functions are interpolatory at the end points and additionally at the repeated knots where multiplicity is equal to polynomial degree p. At this repeated knot, only C^0 continuity is attained. Elsewhere the functions have C^1 continuity. When the multiplicity is $p+1$, the basis becomes discontinuous and the patch boundary is formed.
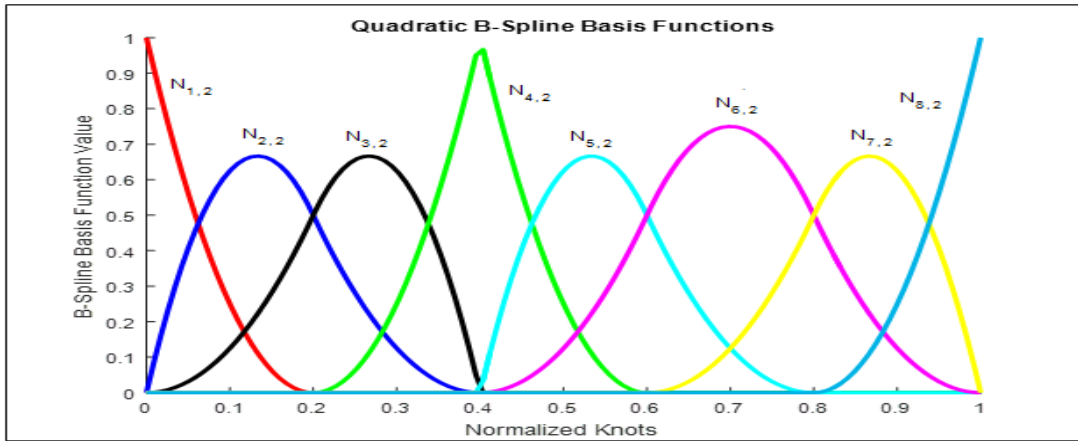
Figure 3.4 Quadratic basis functions drawn for non-uniform open knot vector
$\Xi = [0\ 0\ 0\ 0.2\ 0.4\ 0.4\ 0.6\ 0.8\ 1\ 1\ 1]$

3.1.2.1   Derivatives of B-Spline Basis Functions

The derivatives of B-Spline basis functions are properly formulated by utilizing lower order basis due to their recursive nature. For a given polynomial order p and knot vector Ξ, the derivative of the ith basis function is defined as follows

$$\frac{d}{d\xi}N_{i,p}(\xi) = \frac{p}{\xi_{i+p} - \xi_i}N_{i,p-1}(\xi) - \frac{p}{\xi_{i+p+1} - \xi_{i+1}}N_{i+1,p-1}(\xi) \qquad (3.3)$$

For the higher order derivatives above formula can be generalized by simply taking the derivatives of each side to get

$$\frac{d^k}{d^k\xi} N_{i,p}(\xi) = \frac{p}{\xi_{i+p} - \xi_i}\left(\frac{d^{k-1}}{d^{k-1}\xi} N_{i,p-1}(\xi)\right)$$
$$- \frac{p}{\xi_{i+p+1} - \xi_{i+1}}\left(\frac{d^{k-1}}{d^{k-1}\xi} N_{i+1,p-1}(\xi)\right)$$

(3.4)

Expanding (3.4) by means of (3.3) results in an expression purely in terms of lower order basis functions, $N_{i,p-k}, \ldots, N_{i+k,p-k}$, are given below;

$$\frac{d^k}{d^k\xi} N_{i,p}(\xi) = \frac{p!}{(p-k)!} \sum_{j=0}^{k} \alpha_{k,j} N_{i+j,p-k}(\xi)$$

(3.5)

with

$$\alpha_{0,0} = 1,$$

$$\alpha_{k,0} = \frac{\alpha_{k-1,0}}{\xi_{i+p-k+1} - \xi_i},$$

$$\alpha_{k,j} = \frac{\alpha_{k-1,j} - \alpha_{k-1,j-1}}{\xi_{i+p+j-k+1} - \xi_{i+j}} \quad \text{where } j = 1, \ldots, k-1,$$

$$\alpha_{k,k} = \frac{-\alpha_{k-1,k-1}}{\xi_{i+p+1} - \xi_{i+k}}.$$

(3.6)

Efficient algorithms for these calculations can be found in Piegl and Tiller, 1997 [74].

3.1.3 B- Spline Curves

B-Spline curves in $\mathbb{R}^d$ are created by taking linear combination of multiplication of B-Spline basis functions with coefficients called as "control points". When the control points are linearly interpolated, the resultant polygon is referred as "control polygon". Given n basis functions $N_{i,p}$ with specific order p, where $i = 1,2,\ldots,n$, and corresponding control points $\boldsymbol{B}_i \in \mathbb{R}^d, i = 1,2,\ldots,n$, then B-Spline curve is defined by

$$C(\xi) = \sum_{i=1}^{n} N_{i,p}(\xi)\, \boldsymbol{B}_i \qquad\qquad (3.7)$$

The resulting B-Spline curve does not necessarily interpolate the control points. Nevertheless, when the interpolation is desired, by using the properties stated in the previous part, curve can interpolate to specific control points.

A B-Spline curve example is shown in Figure 3.5 which is constructed by using quadratic basis functions given in Figure 3.4 created from specified knot vector $\Xi = [0\ 0\ 0\ 0.2\ 0.4\ 0.4\ 0.6\ 0.8\ 1\ 1\ 1]$. The control points and control polygon is also seen in the figure. Since the curve built from an open knot vector, it interpolates to first and last control points. Moreover, curve is also interpolatory at the forth control point due to the repetition of knot $\xi = 0.4$ as much as polynomial order. B-Spline curves carry many properties of their basis functions. For instance, in the absence of repeated knots or control points, B-Spline curves of degree p have $p\text{-}1$ continuous derivatives. In the light of this information, sample curve is $C^{p-1} = C^1$ continuous everywhere except at the location of the repeated knot, $\xi = 0.4$, where it is $C^{p-2} = C^0$ continuous.
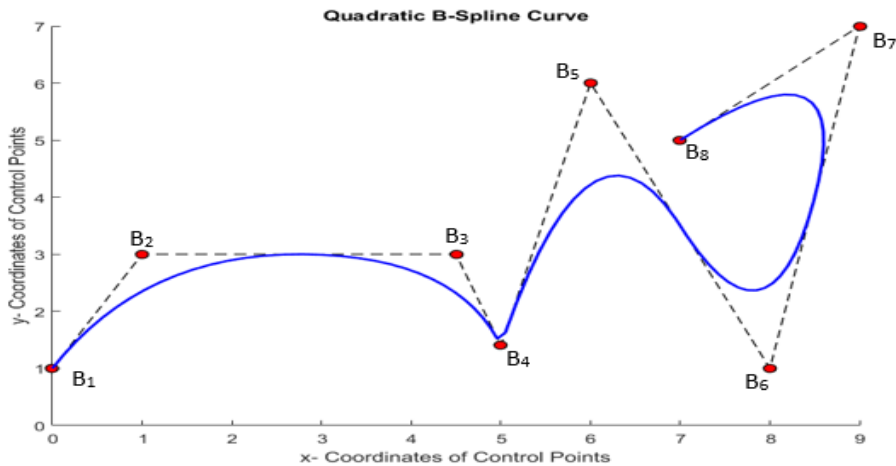
Figure 3.5 A Quadratic B-Spline curve example

Another property the curves inherit from their basis is "locality". Due to the compact support of the B-spline basis functions, moving a single control point can affect the geometry of curve by affecting $p + 1$ elements of the curve.

3.1.4   B-Spline Surfaces

In order to obtain a B-spline surface, it is necessary to take a bidirectional net of control points, $\{B_{i,j}\}$, $i = 1, 2, \ldots, n$, and $j = 1, 2, \ldots, m$ and two knot vectors $\Xi = \{\xi_1, \xi_2, \ldots, \xi_{n+p+1}\}$, $\mathcal{H} = \{\eta_1, \eta_2, \ldots, \eta_{m+q+1}\}$ where p and q are polynomial orders. Calculation is done by the combination of the tensor products of corresponding univariate B-spline functions defined as follows:

$$S(\xi, \eta) = \sum_{i=1}^{n} \sum_{j=1}^{m} N_{i,p}(\xi) M_{j,q}(\eta) B_{i,j} \tag{3.8}$$

An example for the B-Spline surface is considered by using following knot vectors $\Xi = \{0,0,0,0.5,1,1,1\}$ of degree $q = 2$ and $\mathcal{H} = \{0,0,0,0.25,0.5,0.75,1,1,1\}$ of degree $p = 2$. Basis functions for these knot vectors are given in Figure 3.6 and the created surface is shown in Figure 3.7.
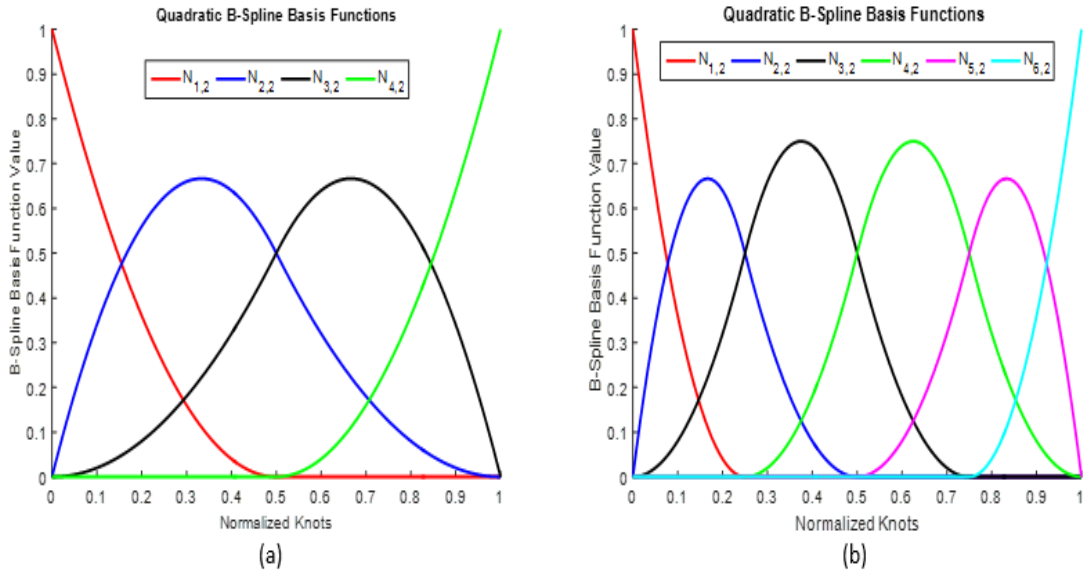
Figure 3.6 Basis functions of knot vectors (a) $\Xi = \{0,0,0,0.5,1,1,1\}$ and (b) H = $\{0,0,0,0.25,0.5,0.75,1,1,1\}$

Coordinates of the utilized control net on the surface is given in Table 3.1 [77].
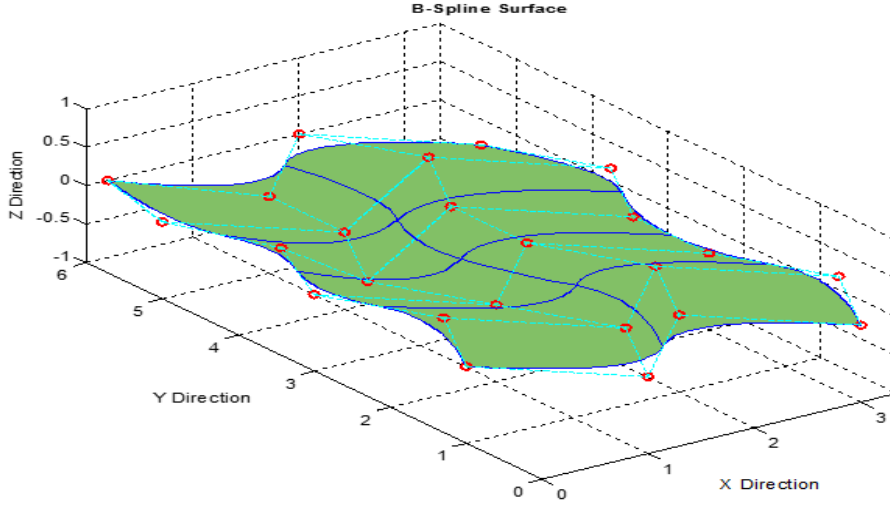
Figure 3.7 An Example B-Spline surface [77]

Table 3.1 Control net $B_{i,j}$ [77]

(i,j)	1	2	3	4	5	6
1	(0,1)	(0.5,2)	(0,3)	(0.4,4)	(0,5)	(0.2,6)
2	(1,0)	(1.5,1)	(1,2)	(0.5,3)	(1,4)	(1,5)
3	(2,1)	(2.5,2)	(2,3)	(2,4)	(2.5,5)	(2,6)
4	(3,0)	(3.5,1)	(3,2)	(3,3)	(3.5,4)	(3,5)

3.1.5   B-Spline Solids

B-spline solids are produced by using control lattice, $\{B_{i,j,k}\}$, $i = 1,2,\ldots,n$; $j = 1,2,\ldots,m$ and $k = 1,2,\ldots,l$ knot vectors are $\Xi = \{\xi_1, \xi_2, \ldots, \xi_{n+p+1}\}$, $\mathcal{H} = \{\eta_1, \eta_2, \ldots, \eta_{m+q+1}\}$ and $\mathcal{L} = \{\zeta_1, \zeta_2, \ldots, \zeta_{l+r+1}\}$ where p, q and r are polynomial orders. Construction formulation for the B-Spline solids is given by

$$S(\xi, \eta) = \sum_{i=1}^{n}\sum_{j=1}^{m}\sum_{k=1}^{l} N_{i,p}(\xi)M_{j,q}(\eta)L_{k,r}(\zeta)\,\boldsymbol{B}_{i,j,k} \tag{3.9}$$

An example of B-Spline solid is represented in Figure 3.8.

36

3.1.6 Refinement Techniques

In classical finite element method approach, in order to get more accurate results, basis enriched by using two common refinement techniques: h-refinement and p-refinement. The former method, h-refinement, increases the number of elements by decreasing the element size to get higher resolutions. On the other hand, the latter one, p-refinement, increases the polynomial degree of basis functions.
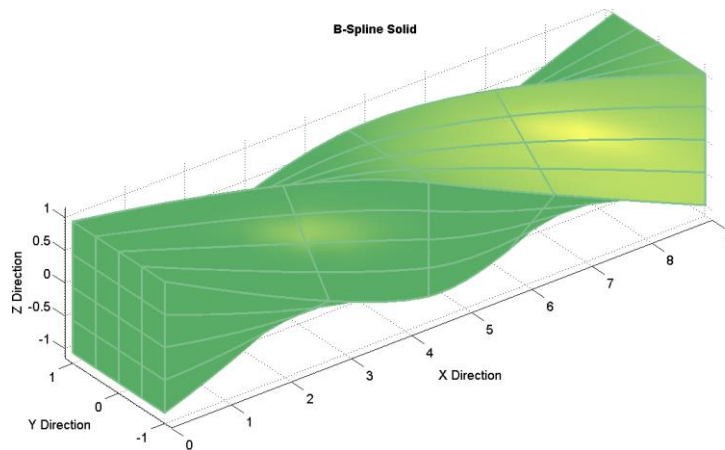
Figure 3.8 An Example B-Spline solid

These refinement techniques in isogeometric analysis are named as knot insertion which is similar to h-refinement and order elevation similar to p-refinement. Contrary to the finite element methods, the geometry remains unchanged under each refinement and the continuity across each element is more controllable in isogeometric analysis. Moreover, IGA has one more refinement technique superior to FEM. It is the combination of order elevation and knot insertion respectively and called as "k-refinement" that brings many benefits to analysis world. Details of these refinement techniques are given in the succeeding parts.

3.1.6.1 Knot Insertion (h-refinement)

In isogeometric analysis first technique used to enhance basis is knot insertion which is analogous to h-refinement in FEA. During the application of knot insertion, new knots are inserted into already existing knot vector without changing the geometry.

For a given knot vector $\Xi = \{\xi_1, \xi_2, \ldots, \xi_{n+p+1}\}$, a new knot vector can be obtained by inserting additional knots as $\bar{\Xi} = \{\bar{\xi}_1, \bar{\xi}_2, \ldots, \bar{\xi}_{n+m+p+1}\}$ such that $\bar{\xi}_1 = \xi_1$ and $\bar{\xi}_{n+m+p+1} = \xi_{n+p+1}$ and thus, $\Xi \subset \bar{\Xi}$. New $n+m$ basis functions should be calculated by using equations 3.1 and 3.2. The novel $n+m$ control points, $\bar{\mathcal{B}} = \{\bar{B}_1, \bar{B}_2, \ldots, \bar{B}_{n+m}\}^T$, are generated from linear combinations of the original control points, $\mathcal{B} = \{B_1, B_2, \ldots, B_n\}^T$, as defined by,

$$\bar{B}_i = \alpha_i B_i + (1 - \alpha_i) B_{i-1} \tag{3.10}$$

where,

$$\alpha_1 = \begin{cases} 1 & if & 1 \le i \le k - p \\ \dfrac{\bar{\xi} - \xi_i}{\xi_{i+p} - \xi_i} & if & k - p + 1 \le i \le k \\ 0 & if & k + 1 \le i \le n + p + 2 \end{cases} \tag{3.11}$$

Insertion of the already existing knot value causes a repetition and decreases the continuity of the basis functions. In order to preserve the continuity, equations 3.10 and 3.11 are developed for the choice of proper control points.

An example of knot insertion procedure for a simple, one-element, quadratic B-spline curve is given in the Figure 3.9. A new knot is inserted at $\bar{\bar{\xi}} = 0.5$ to the existing knot vector $\Xi = \{0, 0, 0, 1, 1, 1\}$, which is used to create the original curve. The newly created curve is geometrically and parametrically identical to the original curve. However, control points have been changed, the mesh has partitioned, and the basis functions have been enriched. In the new case, the number of control points, elements and basis functions, all increased by one. This process may be repeated to enrich the solution space by adding more basis functions of the same order until the desired sensitivity is reached.

Knot insertion refinement method is similar to the h-refinement technique of finite element method. As can be understood from the above mentioned procedure, knot insertion creates new knot spans i.e. new elements in the knot vector. Similarly, in

finite element method, h-refinement increases the element number, creates a finer mesh of the same type of element to improve the results. However, IGA and FEA differ in the number of new basis functions and in the continuity of the basis across the novel element boundaries. To perfectly replicate h-refinement, one would need to insert each of the new knot values p times so that the functions will be C^0 continuity.
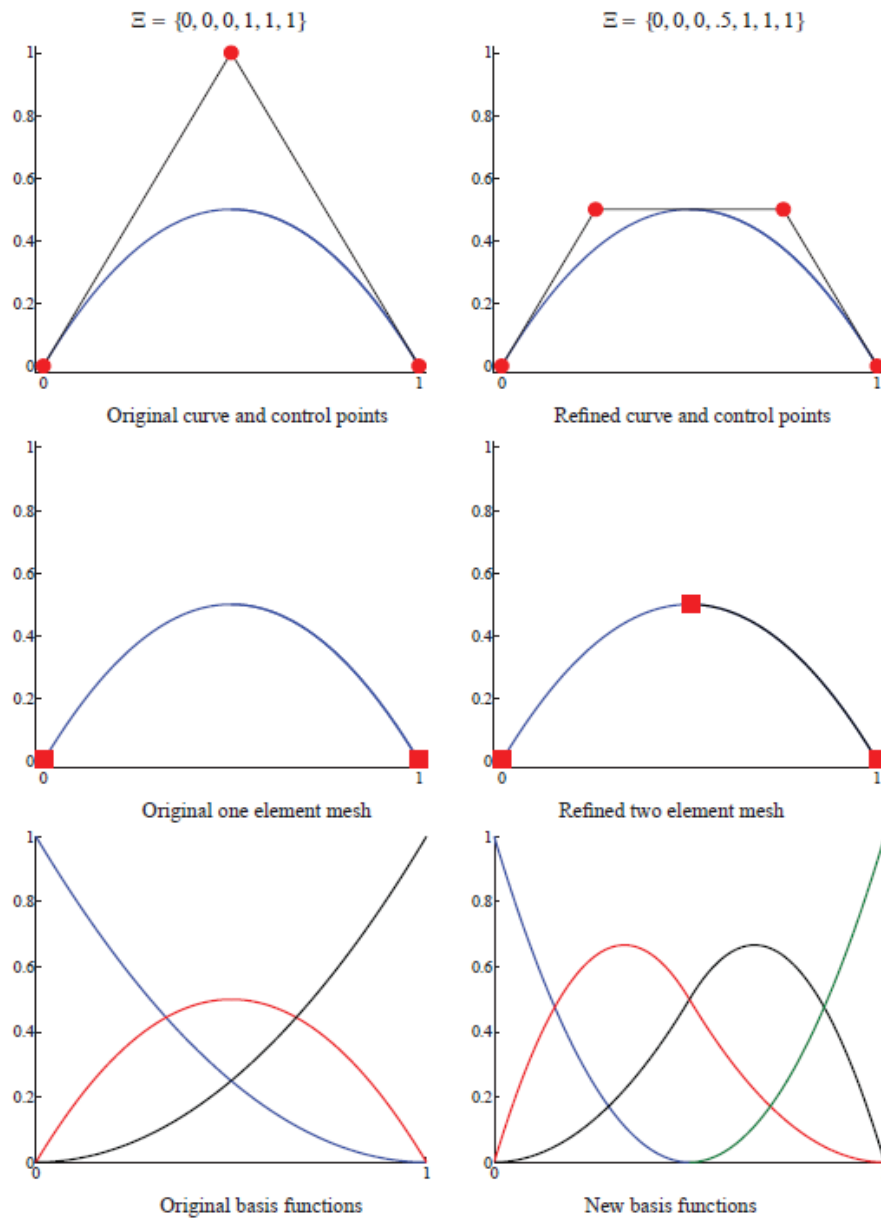
Figure 3.9 Knot insertion refinement technique [1]

3.1.6.2 Order Elevation (p-refinement)

Another basis improvement method which B-Spline theory enables the users is order elevation also called as degree elevation since the degree and order terms are used interchangeably in B-Spline theory. In this technique, polynomial order of the basis functions is increased. Since the basis functions have p-m_i continuous derivatives across element boundaries, if the continuity is desired to be preserved, it is obvious that when the order p is increased, multiplicity m must also be increased by the same amount of degree. Therefore, during order elevation process, the multiplicity of each knot value is increased. As in the case of knot insertion, geometry and parameterization remains unchanged.

Order elevation begins by replicating existing knots by the same amount as the increase in polynomial order. Thereafter, the order of polynomial is increased. Several efficient algorithms for the application of order elevation procedure can be found in Piegl and Tiller, 1997 [74]

An example for the order elevation procedure from quadratic to cubic order is represented in Figure 3.10. The original control points, mesh, and quadratic basis functions are shown on the left. Each knot value in knot vector has been increased by one but no new knot values were added. For this example, number of control points and basis functions increased from 8 to 13. The new control points calculation procedure is again given in Piegl and Tiller, 1997. Although the locations of the control points change, the order elevated curve is geometrically and parametrically identical to the original curve. Additionally, multiplicities of the knots have been increased but the element number is preserved.

Order elevation process is analogues to p-refinement technique in finite element analysis. Both of the strategies increases the order of basis functions. The most critical distinction between these two is that p-refinement always begins with a basis that is C^0 everywhere, while order elevation is compatible with any combination of continuities.

$$\Xi = \{0, 0, 0, 1, 2, 3, 4, 4, 5, 5, 5\}$$

$$\bar{\bar{\Xi}} = \{0, 0, 0, 0, 1, 1, 2, 2,$$
$$3, 3, 4, 4, 4, 5, 5, 5, 5\}$$

Original curve and control points

Refined curve and control points

Original five element mesh

Refined five element mesh

Original basis functions

New basis functions
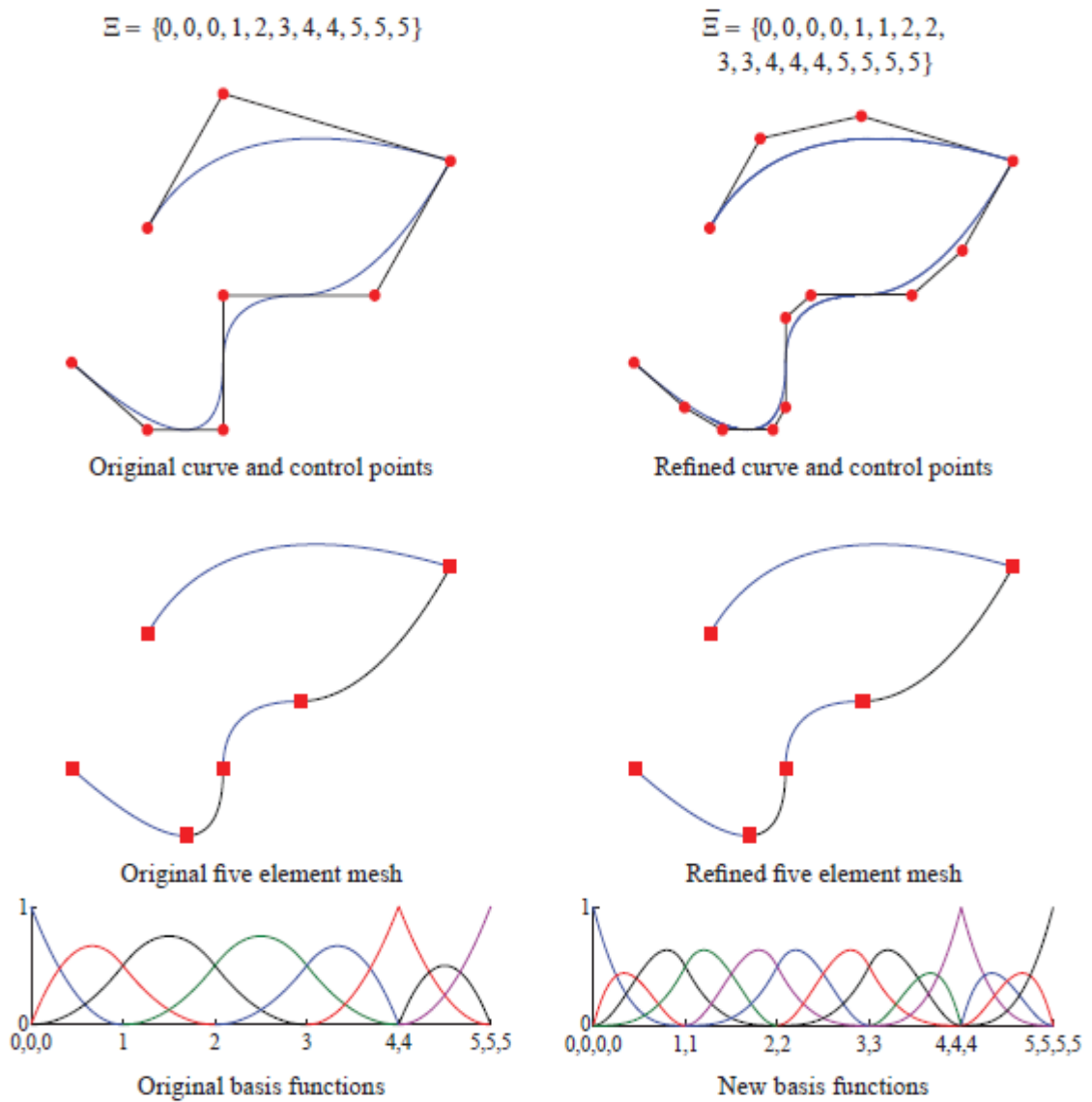
Figure 3.10 Order elevation refinement technique [1]

3.1.6.3 K-refinement

As mentioned in the previous parts, when a new knot values with multiplicities equal to one are inserted, functions across the boundaries will have C^{p-1} continuity. It is possible to lower the continuity by increasing the multiplicity as well. This shows knot insertion is a more flexible process than simple *h*-refinement. Likewise, order elevation technique is also more flexible than *p*-refinement technique. The stated

41

flexibilities of knot insertion and order elevation techniques force us to develop another refinement technique which is unique in the field.

In a curve of order p, if a unique knot value, $\bar{\xi}$, is inserted between two distinct knots, the number of continuous derivatives of the basis functions at $\bar{\bar{\xi}}$ is *p-1*. After knot insertion, even though the order is elevated, the basis still has *p-1* continuous derivatives at $\bar{\bar{\xi}}$. However, if we change the sequence i.e. if the order of the original curve elevated to order q first and then a unique knot value is inserted, the basis will have *q-1* continuous derivatives at $\bar{\bar{\xi}}$. Thus an alternative order elevation method which has significant advantages over standard order elevation emerges. This procedure is called k-refinement. There is no analogous refinement technique in finite element method similar with k-refinement. The concept of k-refinement is important and potentially a superior approach to high-precision analysis than p-refinement. In traditional p-refinement there is an inhomogeneous structure to arrays due to the different basis functions associated with surface, edge, vertex and interior nodes. In k-refinement, there is a homogeneous structure within patches and growth in the number of control variables is limited.

In order to make it more clear, two different sequences of refinement processes are compared with an example in Figure 3.11. Initial domain consists of one element and *p+1* basis functions. On the left side of the figure, firstly, knot is inserted until getting *n-p* elements and *n* basis functions and then order is elevated. In this process, to maintain the continuity at the *p-1* level each distinct knot value is replicated and the total number of basis functions is increased by *2n-p*. After a total of *r* order elevations of this type, we have *(r + 1)(n)-(r)(p)* basis functions, where *p* is still the order of our original basis functions. On the right side of figure, beginning with the same element domain this time order elevation is applied primarily, and then knot insertion is proceeded which is suitable to k-refinement procedure. In this case for each order elevated *r* times, total number of basis functions increases by only one for each refinement. Then domain can be h-refined until having *n-p* elements. The final number of basis functions is *n+r*, each having *r + p -1* continuity. This amounts to an enormous

42

savings in the number of basis functions as $n + r$ is considerably smaller than $(r + 1)(n)-(r)(p)$. Moreover, this technique enables the arrangement of continuity of basis contrast to p-refinement.
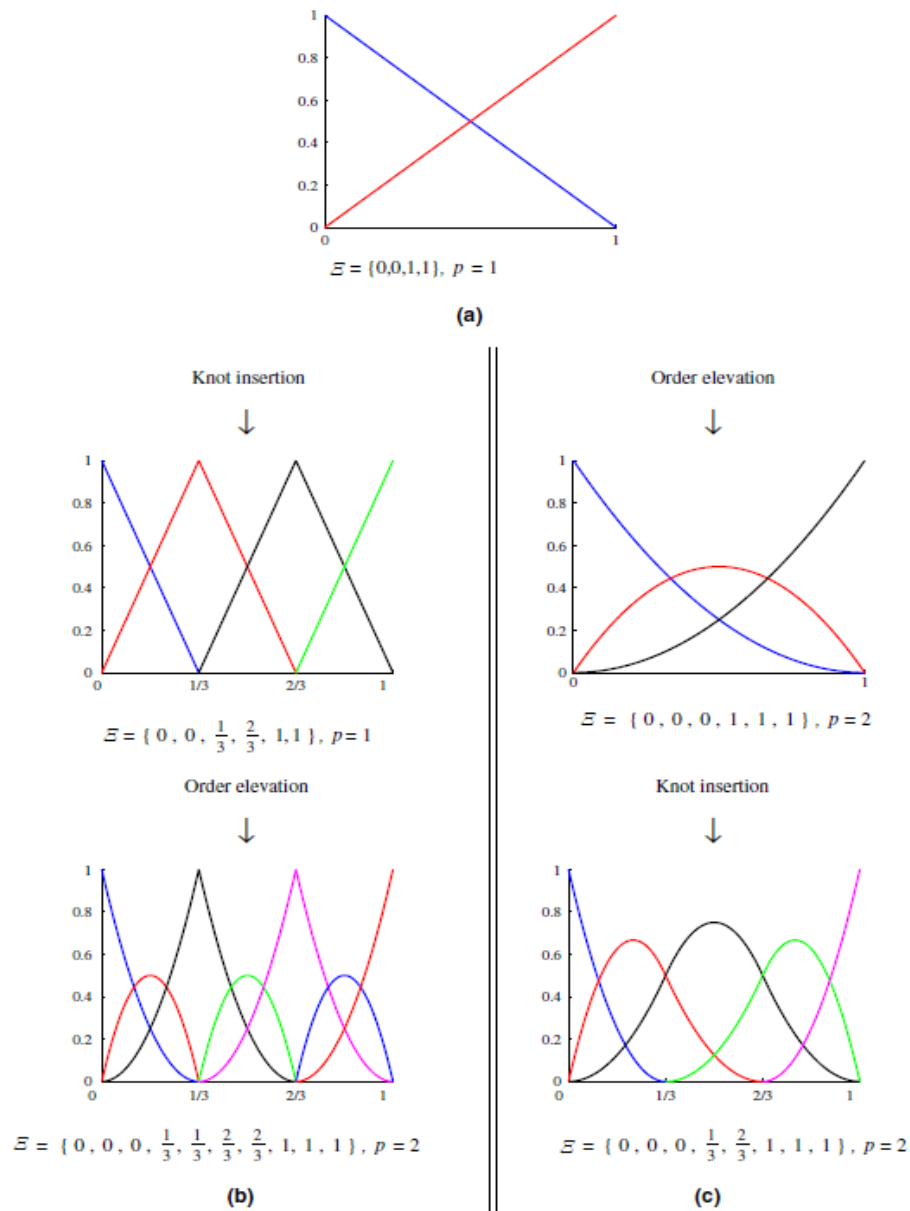
Figure 3.11 k-refinement sequence comparison (a) Base case of one linear element. (b) Classic p-refinement approach: knot insertion followed by order elevation results in seven piecewise quadratic basis functions that are C^0 at internal knots (c) New k-refinement approach: order elevation followed by knot insertion results in five piecewise quadratic basis functions that are C^1 at internal knots. [2]

43

3.2 Non-Uniform Rational B-Splines (NURBS)

Although the B-Splines are convenient for free-form modeling and provide some advantages in geometry definition which were mentioned in the previous sections, they have still deficiencies in exact representation of some simple shapes such as circles and ellipsoids. In order to overcome this lack of ability, NURBS, a superset of B-Splines with its rational nature, is preferred. Today, NURBS is accepted as a de facto standard in CAD technology. Therefore, this section was devoted to discussion of NURBS concept and aims to show how they are constructed, what their advantages are and what separates them from B-splines.

As its name implies, NURBS are piecewise rational polynomials built from B-Splines and inherit all the favorable properties of them. The *rational* term refers to the fact that NURBS are a combination of B-splines basis functions multiplied by a weighting factor. If all the weights are equal to one, then NURBS will be equal to B-splines. On the other hand, *non-uniform* term is used to define non-uniform knot vector. Therefore, in addition to the polynomial degree, knot vector values and multiplicity parameters, one more parameter weight is introduced to obtain more flexible design with desired properties.

NURBS are constructed in $\mathbb{R}^d$ by the projective transformation of B-Splines defined in $\mathbb{R}^{d+1}$. To illustrate, a circle in $\mathbb{R}^2$ constructed by the projective transformation of a piecewise quadratic B-spline defined using homogenous coordinates in $\mathbb{R}^3$ is shown in Figure 3.12.

In this figure, $C^w(\xi)$ is a B-spline curve in $\mathbb{R}^3$ which is created by $\{B_i^w\}$ set of control points. These control points are defined utilizing homogenous coordinates. Terminologically, this curve is called as "projective curve" and its associated control points are called as "projective control points", B_i^w, while the terms "curve" and "control points" are used to describe NURBS curve $C(\xi)$ and its control points B_i respectively.
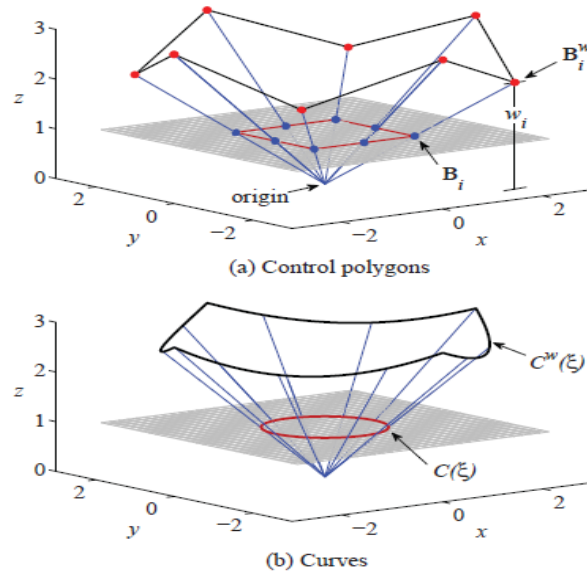
Figure 3.12 An Example of projective transformation of (a) Control points
(b) Curves [2]

The projected control points for the NURBS curve are obtained by the following relations:

$$(B_i)_j = \frac{(B_i^w)_j}{w_i} \qquad j = 1, \ldots, d \tag{3.12}$$

$$w_i = (B_i^w)_{d+1} \tag{3.13}$$

Here, $(B_i)_j$ is the jth component of the vector $\mathbf{B}_i$ and w_i is the ith weight. In $\mathbb{R}^{d+1}$, the weights correspond to the $(d + 1)^{th}$ component of the homogenous coordinates of B-spline curve. For example, in Figure 3.12, weights are taken as z-components of projective curves. Dividing the B-Spline control point by its corresponding weight is thus named as a projective transformation. The same transformations need to be exploited on every point on the curve by the definition of weighting function:

$$W(\xi) = \sum_{i=1}^{n} N_{i,p}(\xi)w_i \tag{3.14}$$

Now the NURBS curve can be defined as

45

$$\left(C(\xi)\right)_j = \frac{\left(C^w(\xi)\right)_j}{W(\xi)}, \qquad j = 1, \ldots, d \tag{3.15}$$

The curve $C(\xi)$ is a piecewise rational function since each element of it is found by division of $C^w(\xi)$ to $W(\xi)$ which are both piecewise polynomial functions. Since this projective transformation seems intimidating, it is rarely used in practice. The main reason behind the explanation of projective transformation is to understand the underlying nature of NURBS and recognize that everything that have been discussed thus far for B-splines still holds true for NURBS.

3.2.1 NURBS Basis Functions and Derivatives

In order to define the construction and manipulation of NURBS geometries it is necessary to introduce a basis function as in the case of B-Splines. NURBS basis function can be defined as follows:

$$R_i^p(\xi) = \frac{N_{i,p}(\xi)w_i}{W(\xi)} = \frac{N_{i,p}(\xi)w_i}{\sum_{\hat{i}=1}^{n} N_{\hat{i},p}(\xi)w_{\hat{i}}} \tag{3.16}$$

Thereafter, NURBS curve defined in equation 3.17 by

$$C(\xi) = \sum_{i=1}^{n} R_i^p(\xi)\boldsymbol{B}_i \tag{3.17}$$

One should note that, the weighting function in equation 3.14 is developed for the projection of B-Spline curve from $\mathbb{R}^{d+1}$ into $\mathbb{R}^d$. Since it is embedded into basis function definition, we can built geometries and meshes in $\mathbb{R}^d$ without regarding the projective geometry behind the scenes. For this reason, equation 3.17 is generally preferred to Eqn. 3.15 due to the usage of practical basis function although they are equivalent.

Rational basis functions are also defined analogously for the generation of rational surfaces and solids in Eqn. 3.18 and 3.19 respectively as follows

$$R_{i,j}^{p,q}(\xi,\eta) = \frac{N_{i,p}(\xi)M_{j,q}(\eta)w_{i,j}}{\sum_{\hat{i}=1}^{n}\sum_{\hat{j}=1}^{m}N_{\hat{i},p}(\xi)M_{\hat{j},q}(\eta)w_{\hat{i},\hat{j}}} \qquad (3.18)$$

$$R_{i,j,k}^{p,q,r}(\xi,\eta,\zeta) = \frac{N_{i,p}(\xi)M_{j,q}(\eta)L_{k,r}(\zeta)w_{i,j,k}}{\sum_{\hat{i}=1}^{n}\sum_{\hat{j}=1}^{m}\sum_{\hat{k}=1}^{l}N_{\hat{i},p}(\xi)M_{\hat{j},q}(\eta)L_{\hat{k},r}(\zeta)w_{\hat{i},\hat{j},\hat{k}}} \qquad (3.19)$$

Related NURBS surfaces and solids are defined respectively by

$$S(\xi,\eta) = \sum_{i=1}^{n}\sum_{j=1}^{m}R_{i,j}^{p,q}(\xi,\eta)\,\boldsymbol{B}_{i,j} \qquad (3.20)$$

$$V(\xi,\eta,\zeta) = \sum_{i=1}^{n}\sum_{j=1}^{m}\sum_{k=1}^{l}R_{i,j,k}^{p,q,r}(\xi,\eta,\zeta)\,\boldsymbol{B}_{i,j,k} \qquad (3.21)$$

The derivatives of NURBS basis functions get by using quotient rule and their non-rational similitudes

$$\frac{d}{d\xi}R_i^p(\xi) = w_i\frac{W(\xi)N_{i,p}'(\xi) - W'(\xi)N_{i,p}(\xi)}{(W(\xi))^2} \qquad (3.22)$$

Finally, an example of a NURBS surface represents a torus geometry which is difficult to create by using B-Splines is given in Figure 3.13.
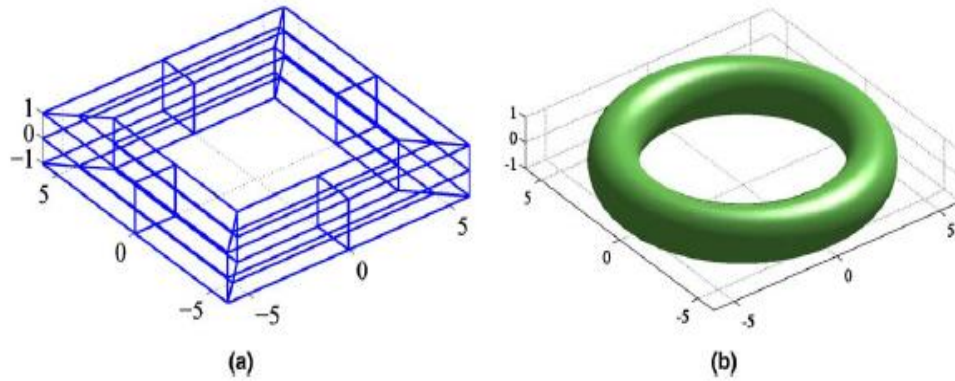
Figure 3.13 An Example for NURBS surface (a) Control net for toroidal surface (b) Toroidal surface [2]

3.3 Isogeometric Analysis (IGA) Formulation

In the previous section, NURBS theory and properties were introduced. The objective of this section is explaining the usage of NURBS as an analysis tool. Important processes for the formulation such as spaces, mappings and numerical integration will be declared.

3.3.1 Relevant Spaces and Mappings

In this section, the relevant spaces used in isogeometric analysis and relations between them are explained to be familiar with the concepts. In order to facilitate the understanding of the subject, it is better to begin with well-known finite element analysis spaces. In classical FEA, we have mesh, elements and the parent element specified in physical and parent spaces respectively. Geometry is represented with mesh which is built by the usage of non-overlapping elements. On the other hand, elements are constructed by the nodal coordinates, and the degrees of freedom at the nodes. The parent element is used to perform Gaussian quadrature integration. All elements are mapped to the same parent element, and we can apply the inverse mapping to return to the physical element after the integration is done.

Isogeometric analysis have different spaces from the finite element method. IGA uses the control mesh, physical elements and parent element defined in index, parameter, physical and parent spaces as shown in Figure 3.14.

3.3.1.1 Index Space

Index space is formed through the specified knot vectors by giving each knot value a distinct coordinate, regardless of whether the knot is repeated or not. As an example, consider a NURBS patch defined through bivariate NURBS basis functions with knot vectors $\Xi = \{0,0,0,1,2,3,3,3\}$ and $\mathcal{H} = \{0,0,1,1\}$. The formed index space is given in Figure 3.15 where the presence of repeated knots leads to several regions of zero parametric area. During implementations, index space is often used by considering the non-zero parametric area.
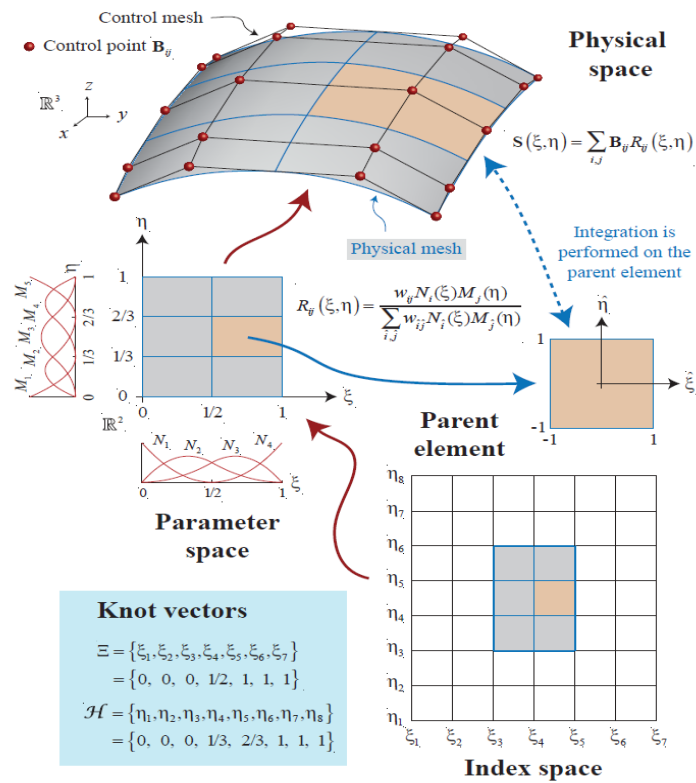
Figure 3.14 Different spaces of isogeometric analysis and relation between them [1]
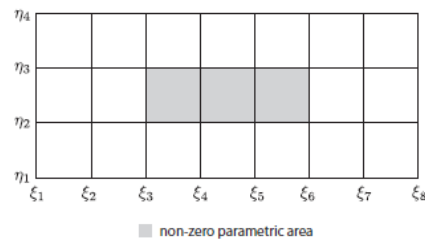
Figure 3.15 Index space created by knot vectors $\Xi=\{0,0,0,1,2,3,3,3\}$ and $H=\{0,0,1,1\}$

3.3.1.2 Parameter Space

Parameter space is constituted by regarding only non-zero knot spans. For the knot vectors given in previous section, parameter space is shown in Figure 3.16. In the same figure both normalized and un-normalized parameter spaces are given. All parametric spaces can be reduced to a unit interval by utilizing normalization. Each element in the physical space is an image of the corresponding element in the parameter space

49

[17]. The mapping from the parameter space to the physical space is applied by using NURBS basis functions to create physical elements.
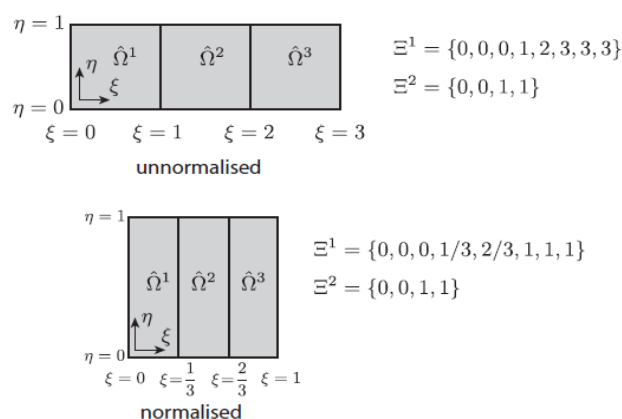
Figure 3.16 Parameter space definition for knot vectors Ξ={0,0,0,1,2,3,3,3} and H={0,0,1,1} both un-normalized and normalized

3.3.1.3 Parent Space

In order to perform Gaussian quadrature integration, parent space definition is required. The parent element is defined on a constant area $\widetilde{\Omega} = [-1,1]^{d_p}$ where d_p is the problem dimension. Parent space coordinates are denoted as $\hat{\boldsymbol{\xi}} = (\hat{\xi}, \hat{\eta}, \hat{\zeta})$ corresponding to the specified dimension. We can map $\hat{\xi}$ and $\hat{\eta}$ in the parent element to ξ and η in the parameter space. This mapping operation is defined in section 3.3.1.5.

3.3.1.4 Physical Space

The physical space is where the actual geometry is represented by a linear combination of the basis functions and the control points. The physical mesh is a decomposition of the geometry and created from physical elements. Figure 3.17 illustrates a NURBS mapping for the parametric space defined in Figure 3.16. Control mesh, control points and elements are defined in Figure 3.17.
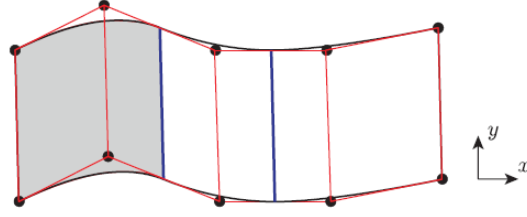
Figure 3.17 A 2D NURBS surface defined for knot vectors Ξ={0,0,0,1,2,3,3,3} and H={0,0,1,1}. The control mesh is shown in red with control points denoted by black circles. Knot lines shown in blue indicate element boundaries.

3.3.1.5 Mappings

While utilizing isogeometric analysis three mapping is required; first mapping from index space to parameter space, one between parent space and parameter space and the other is from parameter space to physical space. Mapping between index and parameter space is easy and done by just considering non-zero knot spans. In other respects, the mapping from parent space to parameter space is given in equation 3.23.

$$\xi(\hat{\xi}) = \frac{(\xi_{i+1} - \xi_i)\hat{\xi} + (\xi_{i+1} + \xi_i)}{2}$$

$$\eta(\hat{\eta}) = \frac{(\eta_{j+1} - \eta_j)\hat{\eta} + (\eta_{j+1} + \eta_j)}{2}$$

(3.23)

Associated Jacobian determinant of this transformation which is necessary for computations is defined by

$$\left| J_{\hat{\xi}} \right| = \frac{(\xi_{i+1} - \xi_i)(\eta_{j+1} - \eta_j)}{4}$$

(3.24)

Similarly, the mapping from parametric domain to the physical domain is given in more general form as

$$x = \sum_{i=1}^{n} N(\xi) \boldsymbol{B}_i$$

(3.25)

51

where the shape function $N(\boldsymbol{\xi})$ refers to univariate NURBS basis function for curve, bivariate NURBS basis function for surface and triple variable NURBS basis for solids. $\boldsymbol{B}_i$ denotes control points and the number of control points is given by n. Variable vector $\boldsymbol{\xi}$ is used for definition of parametric coordinates. Therefore, in one dimension $\boldsymbol{\xi} = (\xi)$, for two dimensions $\boldsymbol{\xi} = (\xi, \eta)$ and for three dimensions $\boldsymbol{\xi} = (\xi, \eta, \zeta)$. Jacobian of the transformation for this mapping is represented by the matrix

$$\boldsymbol{J}_\xi = \begin{bmatrix} \dfrac{\partial x}{\partial \xi} & \dfrac{\partial x}{\partial \eta} \\ \dfrac{\partial y}{\partial \xi} & \dfrac{\partial y}{\partial \eta} \end{bmatrix} = \begin{bmatrix} x_{,\xi} & x_{,\eta} \\ y_{,\xi} & y_{,\eta} \end{bmatrix} \tag{3.26}$$

with the components calculated as

$$\frac{\partial x_i}{\partial \xi_j} = \frac{\partial N_i}{\partial \xi_j} B_{i,I} \tag{3.27}$$

where $B_{i,I}$ is the ith coordinate of control point I. The Jacobian is defined as the determinant of the Jacobian matrix, $|J_\xi|$. The Jacobian represents the transformation from the physical space to the parameter space, and consequently the inverse represents the transformation from the parameter space back to the physical space. In the light of this information, finally, spatial derivatives of basis functions with respect to physical domain coordinate required for element assembly algorithms can be written as follows

$$\begin{bmatrix} N_{i,x} & N_{i,y} \end{bmatrix} = \begin{bmatrix} N_{i,\xi} & N_{i,\eta} \end{bmatrix} \begin{bmatrix} \xi_{,x} & \xi_{,y} \\ \eta_{,x} & \eta_{,y} \end{bmatrix} = \begin{bmatrix} N_{i,\xi} & N_{i,\eta} \end{bmatrix} \boldsymbol{J}_\xi^{-1} \tag{3.28}$$

3.3.1.6 *Numerical Integration*

By completing the mapping operation between three different spaces and introducing Jacobians, a numerical integration for the elements is developed. Integrals over the entire geometry, or physical domain Ω, are split into element integrals with domain

designated by Ω_e. These integrals are calculated in parent domain to perform standard Gauss-Legendre quadrature. Specially, a *(p+1)×(q+1)* Gaussian quadrature is adopted for two dimensional elements with *p* and *q* denoting the orders of the NURBS basis in the ξ and η directions. An integration of a function with variables x and y is given below

$$\int_\Omega f(x,y)d\Omega = \sum_{e=1}^{n} \int_{\Omega_e} f(x,y)d\Omega_e$$

$$= \sum_{e=1}^{n} \int_{\widehat{\Omega}_e} f(x(\xi),y(\eta))|J_\xi|d\widehat{\Omega}_e \qquad (3.29)$$

$$= \sum_{e=1}^{n} \int_{\widetilde{\Omega}_e} f(\bar{\xi},\bar{\eta})|J_\xi|d\widetilde{\Omega}_e$$

where $\Omega_e, \widehat{\Omega}_e, \widetilde{\Omega}_e$ are used to indicate physical, parameter and parent spaces respectively. Since in parent space problem domain is changing from -1 to 1, integration can be written as such

$$\sum_{e=1}^{n} \int_{\widetilde{\Omega}_e} f(\bar{\xi},\bar{\eta})|J_\xi|d\widetilde{\Omega}_e = \sum_{e=1}^{n} \int_{-1}^{1}\int_{-1}^{1} f(\bar{\xi},\bar{\eta})|J_\xi|d\bar{\xi}\,d\bar{\eta} \qquad (3.30)$$

Integral on the right side of equation 3.30 can be replaced by summation of multiplication of function value at specified Gauss points and weights of these points. This relation is shown below

$$\int_{-1}^{1}\int_{-1}^{1} f(\bar{\xi},\bar{\eta})\,d\bar{\xi}d\bar{\eta} = \sum_{i=1}^{p}\sum_{j=1}^{r} W_i\,W_j f(\bar{\xi}_i,\bar{\eta}_j) \qquad (3.31)$$

where $\bar{\xi}_i$ and W_i are Gaussian quadrature points and related weights of these points in ξ direction while $\bar{\eta}_j$ and W_j are Gaussian quadrature points and related weights of these points in η direction.

3.3.2 Galerkin's Method

Although there are several numerical methods applicable to isogeometric analysis, since Galerkin's method is the most widely used finite element numerical method, in this study it has been chosen as a solution method. In this section, application of Galerkin's method in isogeometric analysis will be explained briefly by using an example of Poisson problem stated as follows [78].

$$\nabla^2 u(x, y) + f(x, y) = 0 \tag{3.32}$$

with boundary conditions;

$$
\begin{aligned}
u(x, y) &= g & on\ \Gamma_D, \\
\nabla u(x, y) \cdot \boldsymbol{n} &= h & on\ \Gamma_N, \\
\beta u + \nabla u(x, y) \cdot \boldsymbol{n} &= r & on\ \Gamma_R
\end{aligned}
\tag{3.33}
$$

The problem is defined on two dimensional domain Ω with boundary conditions $\Gamma_D \cup \Gamma_N \cup \Gamma_R = \Gamma = \partial\Omega$ and $\Gamma_D \cap \Gamma_N \cap \Gamma_R = \emptyset$ and $\boldsymbol{n}$ is the unit outward normal vector on $\partial\Omega$. $\Gamma_D, \Gamma_N\ and\ \Gamma_R$ represent the Dirichlet, Neuman and Robin boundary conditions respectively and all of them are defined in real value domain. β is also stated as a real valued constant. Equation 3.32 is a strong form boundary value problem which is specifically named as "poisson problem".

3.3.2.1 Weak Form of the Problem

In order to solve equation 3.32 under the specified conditions given in equation 3.33, given strong form of the equation will be transformed to weak formulation as suitable to instruction of Galerkin's method. For this purpose, both sides of equation 3.32 will be multiplied by a test function which is defined as NURBS basis function and integrated over the defined domain Ω,

$$\int_\Omega \nabla^2 u N d\Omega = -\int_\Omega f N d\Omega \tag{3.34}$$

Since the result of the basis function is equal to zero for Drichlet boundary condition, the resultant weak form of the equation is obtained as follows

$$\int_\Omega \nabla u \cdot \nabla N d\Omega + \beta \int_{\Gamma_R} u N d\Gamma = -\int_\Omega f N d\Omega + \int_{\Gamma_N} h N d\Gamma + \int_{\Gamma_R} r N dS \quad (3.35)$$

The solution for this equation is called as weak solution and under appropriate assumptions weak solution and strong solution of the equation 3.32 are identical.

Since in equation 3.35 unknown field variable u is placed on the left hand side of the equation while the all known data are contained on the right side of the equation, this weak form can be rewritten as

$$a(u, N) = L(N) \quad (3.36)$$

where

$$a(u, N) = \int_\Omega \nabla u \cdot \nabla N d\Omega + \beta \int_{\Gamma_R} u N d\Gamma \quad (3.37)$$

and

$$L(N) = -\int_\Omega f N d\Omega + \int_{\Gamma_N} h N d\Gamma + \int_{\Gamma_R} r N dS \quad (3.38)$$

One should note the some important properties of a and L functions. Function a is symmetric and bilinear while L is linear.

$$a(N, u) = a(u, N) \quad (3.39)$$

$$a(C_1 u + C_2 v, w) = C_1 a(u, w) + C_2 a(v, w), \quad (3.40)$$

$$L(C_1 u + C_2 v) = C_1 L(u) + C_2 L(v). \quad (3.41)$$

Once the finite-dimensional approximation space in which we are going to search for the trial solution u and test function N have been chosen, we can proceed with the matrix representation of the weak form. This procedure is quite familiar for people acquainted with the FEM. We write the solution on the form

$$u_h = \sum_{i=1}^{n} u_h^i N_i \qquad\qquad (3.42)$$

when equation 3.42 is inserted into 3.36 it gives

$$\sum_{i=1}^{n} a(N_i, N_j) u_h^i = L(N_j) \quad \forall N_j \in S_n, \qquad\qquad (3.43)$$

We immediately recognize equation 3.43 as a system of linear equations, and thus formulate it as

$$\boldsymbol{Ku} = \boldsymbol{F} \qquad\qquad (3.44)$$

where elements of the stiffness matrix $\boldsymbol{K}$ are $K_{ij} = a(N_i, N_j)$ and the elements of the force vector $\boldsymbol{F}$ are $f_j = L(N_j)$. Moreover, $\boldsymbol{u}$ represents the field variable vector which is displacement vector.

3.3.3 Isogeometric Linear Elasticity Formulation

All the required mathematical definitions necessary for generation of linear elasticity formulation with isogeometric method is given in previous sections. Therefore, in this section, basic linear elasticity formulation will be derived by using IGA concepts.

Let the total number of basis functions in a 2D problem domain is denoted by n_{np} and the corresponding total number of control points are given with its components as $\boldsymbol{B}^{cp} = \begin{bmatrix} \boldsymbol{B}_x^{cp} & \boldsymbol{B}_y^{cp} \end{bmatrix}$. Basis functions are represented by $\boldsymbol{N}$. The mapping is given by

$$x = \begin{bmatrix} x \\ y \end{bmatrix} = \begin{bmatrix} \displaystyle\sum_{i=1}^{n_{np}} N_i(\xi, \eta) B_{x_i}^{cp} \\ \displaystyle\sum_{i=1}^{n_{np}} N_i(\xi, \eta) B_{y_i}^{cp} \end{bmatrix} \qquad\qquad (3.45)$$

The trial solution $\boldsymbol{u}(x,y)$, the weight functions $\boldsymbol{w}(x,y)$, and the body force $\boldsymbol{b}(x,y)$ are stated as;

$$\boldsymbol{u}(x,y) = \boldsymbol{N}(\xi,\eta)\boldsymbol{u} \qquad (x,y) \in \ \Omega,$$

$$\boldsymbol{w}(x,y) = \boldsymbol{N}(\xi,\eta)\boldsymbol{w} \qquad (x,y) \in \ \Omega, \qquad (3.46)$$

$$\boldsymbol{b}(x,y) = \boldsymbol{N}(\xi,\eta)\boldsymbol{b} \qquad (x,y) \in \ \Omega,$$

and

$$\boldsymbol{u} = [\, u_{x_1} \ \ u_{y_1} \ \ u_{x_2} \ \ u_{y_2} \ \ \cdot \cdot \cdot \ \ u_{n_{np}} \ \ u_{n_{np}} \,]^T$$

$$\boldsymbol{w} = [\, w_{x_1} \ \ w_{y_1} \ \ w_{x_2} \ \ w_{y_2} \ \ \cdot \cdot \cdot \ \ w_{n_{np}} \ \ w_{n_{np}} \,]^T \qquad (3.47)$$

$$\boldsymbol{b} = [\, b_{x_1} \ \ b_{y_1} \ \ b_{x_2} \ \ b_{y_2} \ \ \cdot \cdot \cdot \ \ b_{n_{np}} \ \ b_{n_{np}} \,]^T$$

where $\boldsymbol{u}$ vector contains displacements at the control points and $\boldsymbol{w}$ represents the values of the weight functions at the control points while $\boldsymbol{b}$ gives body forces acting on control points. Here, two degrees of freedom one for x-direction and the other for y-direction are assigned for each control point.

In the weak form we compute the integral over the domain Ω as a sum of integrals computed over each element domain Ω^e;

$$\sum_{e=1}^{n} \left\{ \int_{\Omega^e} (\nabla \boldsymbol{w}^e)^T \boldsymbol{C}^e \nabla \boldsymbol{u}^e \, d\Omega - \int_{\Gamma_{te}} \boldsymbol{w}^{e^T} \bar{\boldsymbol{t}} d\Gamma - \int_{\Omega^e} \boldsymbol{w}^{e^T} \boldsymbol{b} d\Omega \right\} = 0 \qquad (3.48)$$

Now, equations 3.45 and 3.46 will be written in element domain.

$$\boldsymbol{u}^e(x,y) = \boldsymbol{N}^e(\xi,\eta)\boldsymbol{u}^{\ e} \qquad (x,y) \in \ \Omega,$$

$$\boldsymbol{w}^e(x,y) = \boldsymbol{N}^e(\xi,\eta)\boldsymbol{w}^e \qquad (x,y) \in \ \Omega, \qquad (3.49)$$

$$\boldsymbol{b}^e(x,y) = \boldsymbol{N}^e(\xi,\eta)\boldsymbol{b}^e \qquad (x,y) \in \ \Omega,$$

where

$$\boldsymbol{u}^e = [\, u^e_{x_1} \quad u^e_{y_1} \quad u^e_{x_2} \quad u^e_{y_2} \quad \cdots \quad u^e_{x_{nen}} \quad u^e_{y_{nen}} \,]^T$$

$$\boldsymbol{w}^e = [\, w^e_{x_1} \quad w^e_{y_1} \quad u^e_{x_2} \quad u^e_{y_2} \quad \cdots \quad w^e_{x_{nen}} \quad w^e_{y_{nen}} \,]^T \tag{3.50}$$

$$\boldsymbol{b}^e = [\, b^e_{x_1} \quad b^e_{y_1} \quad b^e_{x_2} \quad u^e_{y_2} \quad \cdots \quad b^e_{x_{nen}} \quad b^e_{y_{nen}} \,]^T$$

This time x_1 represents the x-component of element local control point while y_1 represents y-component of it and n_{en} defines the basis function number in the element. The basis function of the element is given by

$$N^e = \begin{bmatrix} N^e_1 & 0 & N^e_2 & 0 & \cdots & N^e_{n_{en}} & 0 \\ 0 & N^e_1 & 0 & N^e_2 & \cdots & 0 & N^e_{n_{en}} \end{bmatrix} \tag{3.51}$$

Then, the element strain and stress matrices can be expressed as follows

$$\epsilon^e = \begin{bmatrix} \epsilon^e_{xx} \\ \epsilon^e_{yy} \\ \gamma^e_{xy} \end{bmatrix} = \nabla \boldsymbol{u}^e = \nabla N^e \boldsymbol{u}^e = \boldsymbol{B}^e \boldsymbol{u}^e \tag{3.52}$$

$$\sigma^e = \boldsymbol{C}^e \epsilon^e$$

where $\boldsymbol{C}^e$ is constitutive relation and in two dimension it is defined by 3x3 matrix as given below

$$\boldsymbol{C}^e = \frac{E}{1 - v^2} \begin{bmatrix} 1 & v & 0 \\ v & 1 & 0 \\ 0 & 0 & (1 - 2v)/2 \end{bmatrix} \tag{3.53}$$

and $\boldsymbol{B}^e$ in equation 3.52 is calculated in the following way

$$\boldsymbol{B}^e = \nabla N^e = \begin{bmatrix} \dfrac{\partial N^e_1}{\partial x} & 0 & \dfrac{\partial N^e_2}{\partial x} & 0 & \cdots & \dfrac{\partial N^e_{n_{en}}}{\partial x} & 0 \\ 0 & \dfrac{\partial N^e_1}{\partial y} & 0 & \dfrac{\partial N^e_2}{\partial y} & \cdots & 0 & \dfrac{\partial N^e_{n_{en}}}{\partial y} \\ \dfrac{\partial N^e_1}{\partial y} & \dfrac{\partial N^e_1}{\partial x} & \dfrac{\partial N^e_1}{\partial y} & \dfrac{\partial N^e_1}{\partial x} & \cdots & \dfrac{\partial N^e_{n_{en}}}{\partial y} & \dfrac{\partial N^e_{n_{en}}}{\partial x} \end{bmatrix} \tag{3.54}$$

Inserting the 3.52 and 3.54 into equation 3.48

$$\sum_{e=1}^{n} \left\{ \int_{\Omega^e} \boldsymbol{w}^{e^T} \boldsymbol{B}^{e^T} \boldsymbol{C}^e \boldsymbol{B}^e \boldsymbol{u}^e \, d\Omega - \int_{\Gamma_{te}} \boldsymbol{w}^{e^T} \boldsymbol{N}^{e^T} \bar{\boldsymbol{t}} d\Gamma \right. $$
$$\left. - \int_{\Omega^e} \boldsymbol{w}^{e^T} \boldsymbol{N}^{e^T} \boldsymbol{N}^e \boldsymbol{b}^e \, d\Omega \right\} = 0 \tag{3.55}$$

If we take the element stiffness matrix as below

$$\boldsymbol{K}^e = \int_{\Omega^e} \boldsymbol{B}^{e^T} \boldsymbol{C}^e \boldsymbol{B}^e \, d\Omega = \int_{-1}^{1} \int_{-1}^{1} \boldsymbol{B}^{e^T} \boldsymbol{C}^e \boldsymbol{B}^e \left| J_\xi^e \right| d\tilde{\xi} d\tilde{\eta}$$

$$= \sum_{i=1}^{n_{gp}} \sum_{j=1}^{n_{gp}} \boldsymbol{B}^{e^T}(\xi(\tilde{\xi}_i), \eta(\tilde{\eta}_j)) \boldsymbol{C}^e \boldsymbol{B}^e(\xi(\tilde{\xi}_i), \eta(\tilde{\eta}_j)) \left| J_\xi^e(\tilde{\xi}_i, \tilde{\eta}_j) \right| w_i w_j \tag{3.56}$$

where n_{gp} is the number of gauss points and $w_i \; and \; w_j$ are corresponding weights.

Then, external force matrix can be obtained

$$\boldsymbol{f}^e = \int_{\Gamma_{te}} \boldsymbol{N}^{e^T} \bar{\boldsymbol{t}} d\Gamma + \int_{\Omega^e} \boldsymbol{N}^{e^T} \boldsymbol{N}^e \boldsymbol{b}^e \, d\Omega \tag{3.57}$$

Element body force and prescribed traction at the boundary can be calculated respectively as follows

$$\boldsymbol{f}_\Omega^e = \int_{\Omega^e} \boldsymbol{N}^{e^T} \boldsymbol{N}^e \boldsymbol{b}^e \, d\Omega = \int_{-1}^{1} \int_{-1}^{1} \boldsymbol{N}^{e^T} \boldsymbol{N}^e \boldsymbol{b}^e \left| J_\xi^e \right| d\tilde{\xi} d\tilde{\eta}$$

$$= \sum_{i=1}^{n_{gp}} \sum_{j=1}^{n_{gp}} \boldsymbol{N}^{e^T} \left(\xi(\tilde{\xi}_i), \eta(\tilde{\eta}_j) \right) \boldsymbol{N}^e \left(\xi(\tilde{\xi}_i), \eta(\tilde{\eta}_j) \right) \boldsymbol{b}^e \left| J_\xi^e(\tilde{\xi}_i, \tilde{\eta}_j) \right| w_i w_j$$

$$\boldsymbol{f}_\Gamma^e = \int_{\Gamma_{te}} \boldsymbol{N}^{e^T} \bar{\boldsymbol{t}} d\Gamma = \int_{-1}^{1} \boldsymbol{N}^{e^T} \left(\xi(\tilde{\xi} = a), \eta(\tilde{\eta}) \right) \bar{\boldsymbol{t}} \left| J_\xi^e \right| d\tilde{\eta} \tag{3.58}$$

$$= \sum_{j=1}^{n_{gp}} \boldsymbol{N}^{e^T} \left(\xi(\tilde{\xi} = a), \eta(\tilde{\eta}_j) \right) \bar{\boldsymbol{t}} \left| J_\xi^e(\tilde{\xi} = a, \tilde{\eta}_j) \right| w_j$$

$$f_\Gamma^e = \int_{\Gamma_{te}} N^{e^T} \bar{t} d\Gamma = \int_{-1}^{1} N^{e^T} \left(\xi(\tilde{\xi}), \eta(\tilde{\eta} = b) \right) \bar{t} |J_{\tilde{\xi}}^e| d\tilde{\xi}$$

$$= \sum_{j=1}^{n_{gp}} N^{e^T} \left(\xi(\tilde{\xi}_i), \eta((\tilde{\eta} = b)) \right) \bar{t} |J_{\tilde{\xi}}^e(\tilde{\xi}_i, \tilde{\eta} = b)| w_i$$

where a and b are constant values for $\tilde{\xi}$ and $\tilde{\eta}$ respectively.

Finally, equation 3.55 turns into

$$\sum_{e=1}^{nel} w^{e^T} \{K^e u^e - f^e\} = 0 \qquad (3.59)$$

By solving the discrete problem $K^e u^e - f^e$, displacement values for each element can be evaluated. Thereafter, by using the equation 3.52 strain and stress values for these elements also can be found. Utilizing the assembly process for these equations, one can obtain global stiffness and global force matrices and corresponding strain and stress values.

3.4 Comparison of Isogeometric Analysis and Finite Element Analysis

In this section, isogeometric analysis is compared with classical finite element analysis. The differences and similarities between these two methods are explained. The most important distinction that brings the IGA one step forward is handling the basis functions used to represent exact geometry for solution field at the same time. Conversely, in classical FEA, basis functions that are chosen to approximate the unknown solution field are also used to approximate the already known geometry. This geometric exactness of IGA provides a great advantage in obtaining precise and accurate results. Second important difference between IGA and FEA is non-interpolating nature of isogeometric analysis contrary to finite element analysis. While the basis functions interpolate nodes in FEA, in IGA basis functions does not necessarily interpolate control points. Therefore, the node concept is different in isogeometric analysis. In FEA, the degrees of freedom are located at the nodes, while

in IGA they are located at the control points. Another difference that separate NURBS basis from the polynomial finite element basis is their non-negative nature. NURBS basis functions take only positive values while classical finite element basis functions can be positive or negative. All the differences between isogeometric analysis and finite element analysis are listed in Table 3.2.

Isogeometric analysis and FEA share some common properties also as stated in Table 3.3. Both of the methods employ Galerkin's method with isoparametric approach and solution for the weak form of the problems are obtained by using linear combination of coefficients and basis functions that have compact support. NURBS basis and polynomial basis both have partition of unity property. Finally, the code architecture for finite element analysis and the single patch isogeometric analysis is same.

Table 3.2 Differences between isogeometric analysis and finite element analysis

Isogeometric Analysis	Finite Element Analysis
NURBS basis	Polynomial basis
Exact Geometry	Approximate geometry
Control Points	Nodal points
Control Variables	Nodal variables
Basis does not interpolate control points	Basis interpolates nodal points
hpk-refinement space	*hp*-refinement space
Pointwise positive basis	Basis not necessarily positive
Convex hull property	No convex hull property
Variation diminishing in the presence of discontinues data	Oscillatory in the presence of discontinues data

Table 3.3 Similarities between isogeometric analysis and finite element analysis

Isogeometric Analysis and Finite Element Analysis
Isoparametric concept
Galerkin's method
Code architecture
Compactly supported basis
Bandwidth of matrices
Partition of unity

Since both methods are numerical solution techniques, it is necessary to implement them on the problems of interest by using the computational programs. Therefore, an algorithm for the application should be created by using a code architecture. The code architecture of the IGA and FEA is same and given in Figure 3.18. The program starts with reading the input data usually composed of boundary values, elements and overall geometry data. Thereafter, connectivity is built by allocating the global arrays. Once these preprocessing periods are finished, element stiffness matrix and element force vector begin to be calculated by a loop turns through the quadrature points in the code. At each quadrature point, a routine is called to evaluate all of the basis functions and any necessary derivatives. By using these calculations, local stiffness matrix and force vector are generated for each element and with the help of connectivity information they are imported to the corresponding elements of global stiffness and force matrices. Same operations are conducted for each element till local values are calculated for all elements and global matrices are completed by assembling the local values. Then the solution for whole system is calculated, results can be exported to a file and other post-processing steps such as visual illustrations can be performed. Although, the code architecture is same for IGA and FEA, there are some differences in the content of routines. In Figure 3.18, routines are illustrated with blue color differ from their counterparts in finite element method. In FEA, input data is given as nodal points and mesh structure to construct the geometry. However, in isogeometric analysis control points, their corresponding weight values and knot vectors are given as input. The connectivity array that links the local basis function numbering to a global basis function numbering is also different. In isogeometric analysis, the connectivity array is calculated automatically from knot vectors and their polynomial orders. Since the main difference between methods is usage of different basis functions, evaluating procedure of these basis and their derivatives are also different.
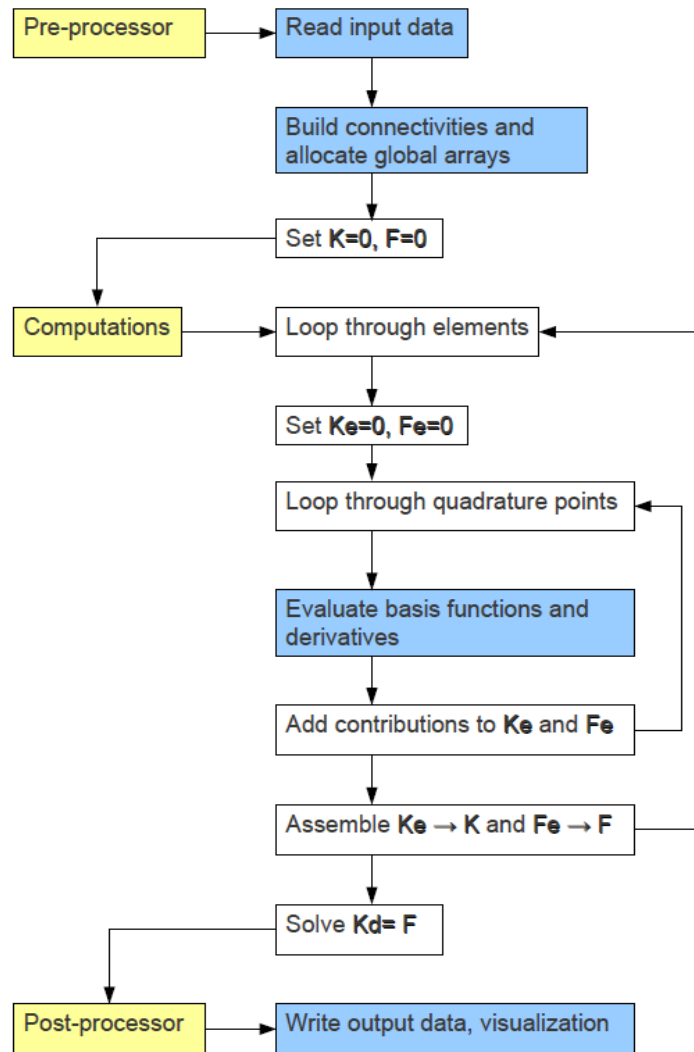
Figure 3.18 Code architecture for classical finite element and isogeometric analysis. The routines in blue color different for each method

CHAPTER 4

APPLICATION OF ISOGEOMETRIC ANALYSIS TO LINEAR ELASTICITY PROBLEMS

In this part of the thesis, the structures made of isotropic materials which obey Hooke's law will be considered for small deformations.

4.1   1D Isogeometric Analysis

In this part, isogeometric analysis method is applied to one dimensional problems. Bars under axial loading and beams under transverse loadings with different boundary conditions were evaluated. IGA results were obtained by using Matlab code. During development of algorithms it has been benefited from the study conducted by Nguyen at al. [79]. On the other hand, results were also obtained by using finite element method approach again by using Matlab code. Finally, IGA results were compared with both analytical results and finite element analysis results.

4.1.1   *Axial Force Members: Rods and Bars*

Consider the equilibrium equation of an infinitesimal section of the bar shown in Figure 4.1
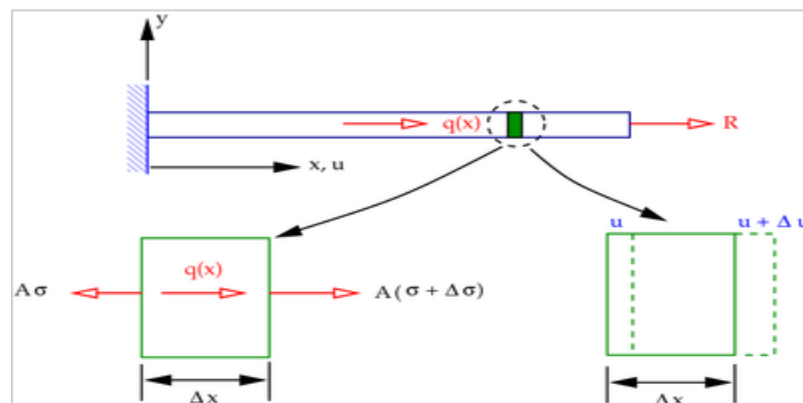
Figure 4.1 Representation of the axially loaded bar with fixed end

$$A\sigma_{xx} = q(x)\Delta x + A(\sigma_{xx} + \Delta\sigma_{xx})$$

$$A\left(\frac{(\sigma_{xx} + \Delta\sigma_{xx}) - \sigma_{xx}}{\Delta x}\right) + q(x) = 0 \tag{4.1}$$

As Δx approaches to zero; the following equation is obtained

$$A\frac{d\sigma_{xx}}{dx} + q(x) = 0 \tag{4.2}$$

Using Hooke's law

$$AE\frac{d\epsilon_{xx}}{dx} + q(x) = 0 \tag{4.3}$$

By using the relation between strain components and and taking $q(x) = ax$, equation 4.3 can be written as

$$AE\frac{d^2u_x}{dx^2} + ax = 0 \tag{4.4}$$

In this problem, one essential or Dirichlet boundary condition and one natural or Neumann boundary condition can be stated.

$$at\ x = 0, \quad u = 0$$

$$at\ x = L, \quad f = R \tag{4.5}$$

The analytical solution for this "strong form" of the problem can be easily get by integrating the equation 4.6 twice.

$$AE\frac{d^2u_x}{dx^2} = -ax \tag{4.6}$$

Result is given in equation 4.7.

$$u(x) = \frac{-ax^3 + 6C_1x + 6C_2}{6AE} \qquad (4.7)$$

With the application of given boundary conditions given in equation 4.5 the general form of the solution set can be obtained as below

$$u(x) = \frac{-ax^3 + (6R + 3aL^2)x}{6AE}$$

$$\varepsilon(x) = \frac{-ax^2 + 2R + aL^2}{2AE} \qquad (4.8)$$

$$\sigma(x) = \frac{-ax^2 + 2R + aL^2}{2A}$$

In order to develop finite element equations, strong form of the problem that contains partial differential equations should be rewritten in integral form which is called as "*weak form*". Weak form can be sometimes called also as "*principle of virtual work*". Weak forms of the equation 4.4 and natural boundary condition given in equation 4.5 are obtained by multiplying these equations with an arbitrary function *w(x)* and integrating the main equation over the domain of interest which is length of the bar in this case.

$$\int_0^L w(x)\left[\frac{d}{dx}\left(AE\frac{du}{dx}\right) + q(x)\right]dx = 0 \qquad (4.9)$$

$$w(x)\left(AE\frac{du}{dx} - R\right) = 0 \quad at\ x = L \qquad (4.10)$$

One should note that, the displacement boundary condition at the fixed wall end of the bar is not multiplied by weighting function. It is due to the fact that; it is easy to satisfy this displacement boundary condition by trial solutions.

Finite element method can be developed by using equations given in 4.9. However, since the equation contains second derivative of the u, very smooth trial solutions are needed which are generally difficult to obtain. Additionally, since the integral is not symmetric in terms of *w(x)* and *u(x),* the resultant stiffness matrix also will not be symmetric. Therefore, the equation should be transformed into a form that contains only first derivatives. This condition will allow the usage of less smooth trial solutions and obtaining symmetric stiffness matrix.

Using integration by parts and putting the boundary values into obtained equations, resultant form can be written as

$$\int_0^L \frac{dw}{dx} AE \frac{du}{dx} dx = (wR)_{x=L} + \int_0^L wq(x)\, dx \quad \forall\, w \text{ with } w(0) = 0 \quad (4.11)$$

By using the Galerkin's method approximate solution for the above equation, it can be written as follows

$$u_h(x) = u_1\phi_1(x) + u_2\phi_2(x) + \ldots + u_n\phi_n(x) = \sum_{i=1}^n u_i\phi_i(x) \qquad (4.12)$$

Here ϕ_i are basis functions. Another important property of Galerkin's method is usage of same functions for both approximate solution and weighting function. However, arbitrary coefficients can be used in weighting functions. The expression written to specify weighting function is given in equation 4.13.

$$w(x) = b_1\phi_1(x) + b_2\phi_2(x) + \ldots + b_n\phi_n(x) = \sum_{j=1}^n b_j\phi_j(x) \qquad (4.13)$$

If the obtained approximate solution and weighting functions are put into weak form formulation, then below equation is obtained

$$\int_0^L AE \left(\sum_{i=1}^n u_i \frac{d\phi_i}{dx} \right) \left(\sum_{j=1}^n b_j \frac{d\phi_j}{dx} \right) dx$$

$$= R \left(\sum_{j=1}^n b_j \phi_j(x) \right)_{x=L} + \int_0^L q(x) \left(\sum_{j=1}^n b_j \phi_j(x) \right) dx \tag{4.14}$$

This equation can be rewritten as

$$\sum_{j=1}^n b_j \left[\int_0^L AE \left(\sum_{i=1}^n u_i \frac{d\phi_i}{dx} \frac{d\phi_j}{dx} \right) dx \right]$$

$$= \sum_{j=1}^n b_j \left[\int_0^L q(x) \phi_j dx + \left(R\phi_j \right)_{x=L} \right] \tag{4.15}$$

Since the coefficients b_j are arbitrary they can be cancelled from both sides and equation 4.15 can be rewritten as

$$\sum_{i=1}^n \left[\int_0^L \frac{d\phi_j}{dx} AE \frac{d\phi_i}{dx} dx \right] u_i = \int_0^L q(x) \phi_j dx + \left(R\phi_j \right)_{x=L} \quad j = 1, \ldots, n \tag{4.16}$$

Equation 4.16 is a system of n equations that can be solved for the unknown coefficients u_i named as displacements in structural mechanics approach. When these unknown coefficients are obtained, approximate solution given in 4.12 can be computed. Additionally, equation 4.16 can be written in matrix form which makes the writing of computer algorithms easier.

$$\boldsymbol{Ku} = \boldsymbol{f} \tag{4.17}$$

$$K_{ji} u_i = f_j \tag{4.18}$$

where

$$K_{ji} = \int_0^L \frac{d\phi_j}{dx} AE \frac{d\phi_i}{dx} dx \qquad (4.19)$$

$$f_j = \int_0^L q(x)\phi_j dx + \left(R\phi_j\right)_{x=L} \qquad (4.20)$$

The main problem in the formulation steps given above for Galerkin method is determining ϕ_i basis functions for complex cases. However, isogeometric approach makes it easy with the already defined basis function calculation procedure given in 3.2.1.

As the first step of finite element method is discretization of the domain, bar is divided into 3 elements using 4 nodes as shown in Figure 4.2. The relation between displacement values of these nodes is given by basis functions. Moreover, for isoparametric formulation geometric relation between these nodes is also expressed by these basis functions. Although it is defined as ϕ_i in derivations given above, basis functions are generally denoted by N_i in finite element formulations. Basis functions can also be called as shape functions or interpolation functions. For linear elements with 2 nodes, shape functions for nodes of an element e can be formulated as such

$$N_1^e(x) = \frac{x_2 - x}{h_e} ; \quad N_2^e(x) = \frac{x - x_1}{h_e} \qquad (4.21)$$

where h_e is the length of the element. After writing the shape functions, element stiffness matrix components can be easily calculated.

$$K_{11}^e = \int_{x_1}^{x_2} \frac{dN_1^e}{dx} AE \frac{dN_1^e}{dx} dx = \int_{x_1}^{x_2} \left(-\frac{1}{h_e}\right) AE \left(-\frac{1}{h_e}\right) dx = \frac{AE}{h_e}$$

$$K_{12}^e = \int_{x_1}^{x_2} \frac{dN_1^e}{dx} AE \frac{dN_2^e}{dx} dx = \int_{x_1}^{x_2} \left(-\frac{1}{h_e}\right) AE \left(\frac{1}{h_e}\right) dx = -\frac{AE}{h_e} \qquad (4.22)$$

$$K_{22}^e = \int_{x_1}^{x_2} \frac{dN_2^e}{dx} AE \frac{dN_2^e}{dx} dx = \int_{x_1}^{x_2} \left(\frac{1}{h_e}\right) AE \left(\frac{1}{h_e}\right) dx = \frac{AE}{h_e}$$
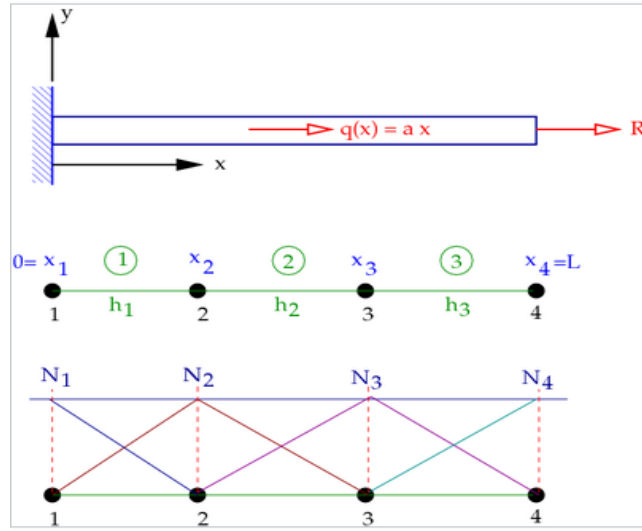
Figure 4.2 Finite element discretization and basis functions for axially loaded bar

Since the element stiffness matrix is symmetric there is no need to calculate K_{21}^e. Then, element stiffness matrix is written below

$$\boldsymbol{K}^e = \frac{AE}{h_e}\begin{bmatrix} 1 & -1 \\ -1 & 1 \end{bmatrix} \tag{4.23}$$

On the other hand, the global stiffness matrix can be written by considering the contributions of each element through assembling

$$\boldsymbol{K} = AE\begin{bmatrix} 1/h_1 & -1/h_1 & 0 & 0 \\ -1/h_1 & 1/h_1 + 1/h_2 & -1/h_2 & 0 \\ 0 & -1/h_2 & 1/h_2 + 1/h_3 & -1/h_3 \\ 0 & 0 & -1/h_3 s & 1/h_3 \end{bmatrix} \tag{4.24}$$

Same calculations can be done for the load vector $\boldsymbol{f}$.

$$f_j = \int_0^L N_j q(x)dx + (N_j R)_{x=L}$$

$$= \int_{\Omega_1} N_j q(x)dx + \int_{\Omega_2} N_j q(x)dx + \int_{\Omega_3} N_j q(x)dx + (N_j R)_{x=L} \tag{4.25}$$

By considering the basis function values at each element and boundaries, global load vector components can be obtained as follows

71

$$f_1 = \int_{\Omega_1} N_1 q(x) dx + (N_1 R)_{x=L} = f_1^1$$

$$f_2 = \int_{\Omega_1} N_2 q(x) dx + \int_{\Omega_2} N_2 q(x) dx + (N_2 R)_{x=L} = f_2^1 + f_1^2$$

$$f_3 = \int_{\Omega_2} N_3 q(x) dx + \int_{\Omega_3} N_3 q(x) dx + (N_3 R)_{x=L} = f_2^2 + f_1^3$$

(4.26)

$$f_4 = \int_{\Omega_3} N_4 q(x) dx + (N_4 R)_{x=L} = f_2^3 + R$$

Using the linear basis functions introduced previously and taking $q = ax$ element load vector components can be obtained

$$f_1^e = \int_{x_1}^{x_2} N_1^e ax\,dx = \int_{x_1}^{x_2} \left(\frac{x_2 - x}{h_e}\right) ax\,dx = \frac{a}{h_e}\left(\frac{x_2(x_2^2 - x_1^2)}{2} - \frac{x_2^3 - x_1^3}{3}\right)$$

$$f_2^e = \int_{x_1}^{x_2} N_2^e ax\,dx = \int_{x_1}^{x_2} \left(\frac{x - x_1}{h_e}\right) ax\,dx = -\frac{a}{h_e}\left(\frac{x_1(x_2^2 - x_1^2)}{2} - \frac{x_2^3 - x_1^3}{3}\right)$$

(4.27)

By regarding the values of equation 4.27 for each element, global force vector components can be evaluated.

After all, taking the lengths of all elements are equal and value of h, finite element method system of equations is obtained as given below

$$\frac{AE}{h}\begin{bmatrix} 1 & -1 & 0 & 0 \\ -1 & 2 & -1 & 0 \\ 0 & -1 & 2 & -1 \\ 0 & 0 & -1 & 1 \end{bmatrix}\begin{bmatrix} u_1 \\ u_2 \\ u_3 \\ u_4 \end{bmatrix}$$

$$= \frac{a}{h}\begin{bmatrix} \dfrac{x_2(x_2^2 - x_1^2)}{2} - \dfrac{x_2^3 - x_1^3}{3} \\[2mm] \left(\dfrac{x_2^3 - x_1^3}{3} - \dfrac{x_1(x_2^2 - x_1^2)}{2}\right) + \left(\dfrac{x_3(x_3^2 - x_2^2)}{2} - \dfrac{x_3^3 - x_2^3}{3}\right) \\[2mm] \left(\dfrac{x_3^3 - x_2^3}{3} - \dfrac{x_2(x_3^2 - x_2^2)}{2}\right) + \left(\dfrac{x_4(x_4^2 - x_3^2)}{2} - \dfrac{x_4^3 - x_3^3}{3}\right) \\[2mm] \left(\dfrac{x_4^3 - x_3^3}{3} - \dfrac{x_3(x_4^2 - x_3^2)}{2}\right) + R\dfrac{h}{a} \end{bmatrix}$$

(4.28)

Then by considering the essential boundary condition $u = 0$ at $x = 0$, this system of equations is reduced to following

$$\frac{AE}{h}\begin{bmatrix} 2 & -1 & 0 \\ -1 & 2 & -1 \\ 0 & -1 & 1 \end{bmatrix}\begin{bmatrix} u_2 \\ u_3 \\ u_4 \end{bmatrix}$$

$$= \frac{a}{h}\begin{bmatrix} \left(\frac{x_2^3 - x_1^3}{3} - \frac{x_1(x_2^2 - x_1^2)}{2}\right) + \left(\frac{x_3(x_3^2 - x_2^2)}{2} - \frac{x_3^3 - x_2^3}{3}\right) \\ \left(\frac{x_3^3 - x_2^3}{3} - \frac{x_2(x_3^2 - x_2^2)}{2}\right) + \left(\frac{x_4(x_4^2 - x_3^2)}{2} - \frac{x_4^3 - x_3^3}{3}\right) \\ \left(\frac{x_4^3 - x_3^3}{3} - \frac{x_3(x_4^2 - x_3^2)}{2}\right) + R\frac{h}{a} \end{bmatrix} \qquad (4.29)$$

Assuming all material property constants, dimensions and applied force values equal to one for the sake of simplicity, in other words A, E, L, a and R are all equal to one and h_1, h_2 and h_3 are all equal to $1/3$, system of equation in 4.29 can be solved and nodal displacement values are obtained.

$$\begin{bmatrix} 2 & -1 & 0 \\ -1 & 2 & -1 \\ 0 & -1 & 1 \end{bmatrix}\begin{bmatrix} u_2 \\ u_3 \\ u_4 \end{bmatrix} = \begin{bmatrix} 0.037 \\ 0.074 \\ 0.383 \end{bmatrix} \implies \begin{bmatrix} u_1 \\ u_2 \\ u_3 \\ u_4 \end{bmatrix} = \begin{bmatrix} 0 \\ 0.4938 \\ 0.9506 \\ 1.3333 \end{bmatrix} \qquad (4.30)$$

After getting nodal displacement values, one can easily calculate element strain and stress values.

$$\boldsymbol{u^e} = u_1^e N_1^e(x) + u_2^e N_2^e(x)$$

$$\boldsymbol{\varepsilon^e} = \frac{\partial \boldsymbol{u^e}}{\partial x} = u_1^e \frac{\partial N_1^e}{\partial x} + u_2^e \frac{\partial N_2^e}{\partial x}$$

$$\boldsymbol{\varepsilon^e} = \boldsymbol{B^e u^e} = \begin{bmatrix} \frac{\partial N_1^e}{\partial x} & \frac{\partial N_2^e}{\partial x} \end{bmatrix}\begin{bmatrix} u_1^e \\ u_2^e \end{bmatrix} = \begin{bmatrix} -\frac{1}{h} & \frac{1}{h} \end{bmatrix}\begin{bmatrix} u_1^e \\ u_2^e \end{bmatrix} \qquad (4.31)$$

$$\boldsymbol{\sigma^e} = E\boldsymbol{\varepsilon^e}$$

Putting found nodal displacement values into given relations in equation 4.31, values of stresses for three elements were obtained and given below. Units are taken in

newtons (N) for forces and millimeters (mm) for dimensions. Therefore, obtained stress values are in MPa while strain values are unitless.

$$\begin{bmatrix} \sigma_1 \\ \sigma_2 \\ \sigma_3 \end{bmatrix} = \begin{bmatrix} 1.4815 \\ 1.3704 \\ 1.1481 \end{bmatrix} \tag{4.32}$$

In equation 4.8 exact analytical solution of the problem was given. Again by using unit constants for A, E, L, a and R values and equally spaced nodes, exact results for displacement values at nodes and stress values at midpoints of elements were computed.

$$\begin{bmatrix} u_1 \ at \ x = 0 \\ u_2 \ at \ x = 1/3 \\ u_3 \ at \ x = 2/3 \\ u_4 \ at \ x = 1 \end{bmatrix} = \begin{bmatrix} 0 \\ 0.4938 \\ 0.9506 \\ 1.3333 \end{bmatrix} \tag{4.33}$$

$$\begin{bmatrix} \sigma_1 \ at \ x = 1/6 \\ \sigma_2 \ at \ x = 1/2 \\ \sigma_3 \ at \ x = 5/6 \end{bmatrix} = \begin{bmatrix} 1.4861 \\ 1.375 \\ 1.1528 \end{bmatrix} \tag{4.34}$$

As seen from the results of equation 4.30, exact displacement values were obtained in finite element method by utilizing three elements. When stress values were regarded, again quite close results were obtained. Graphs drawn to compare exact and FEM results are given in Figure 4.3 and 4.4.
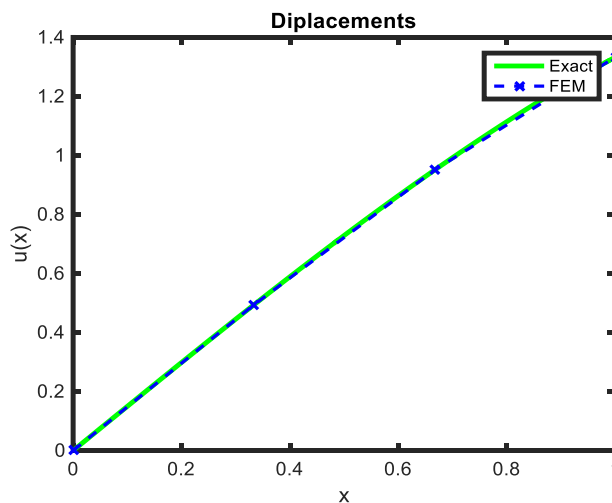
Figure 4.3 Displacement values for exact and FEM solutions
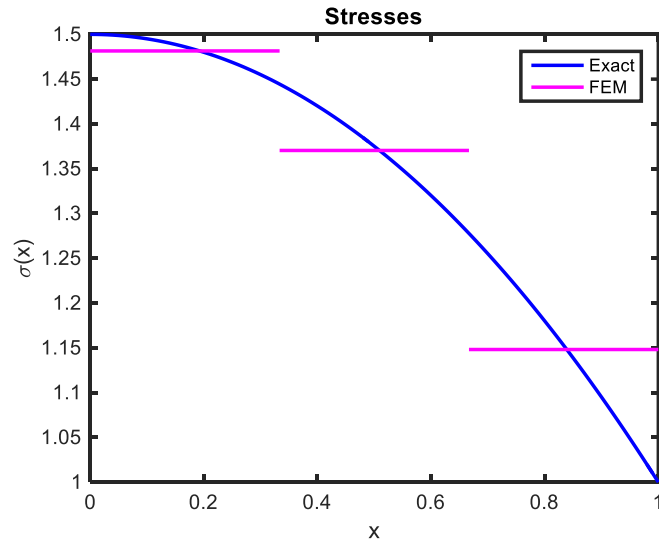
Figure 4.4 Stress values for exact and FEM solutions

It was aimed to solve same axially loaded bar problem by using isogeometric analysis method. All the procedures passed during application of finite element method was clearly stated above step by step. Isogeometric analysis uses same steps except geometry data and basis functions. Only these differences for the isogeometric analysis will be declared for the application of IGA onto axially loaded bar and since the remaining procedure is same, they will not be repeated.

In order to simulate the similar case with finite element method, again three equally spaced linear elements will be taken in IGA. For this purpose, knot vector is taken as $\Xi = [0 \ 0 \ \frac{1}{3} \ \frac{2}{3} \ 1 \ 1]$. Control points and their corresponding weights are given in Table 4.1. Representation of the problem is same with Figure 4.2.

Table 4.1 Control points coordinates and corresponding weights

	X coordinate	Y coordinate	Weight
Point 1	0	0	1
Point 2	1/3	0	1
Point 3	2/3	0	1
Point 4	1	0	1

Since the problem is one dimensional, y-components of the control points are all zero. Since the bar is straight and all control points are on it, weights are also taken as unity. Elements are first order linear elements. Under these conditions main goal is to find shape function derivatives for elements and calculate element stiffness matrix and force vector. Finally, found values will be assembled to get overall results. Since all weights are equal to one, NURBS basis functions and their derivatives are equal to B-Spline basis functions. Therefore, equations 3.1 to 3.3 can be used for basis function calculations. However, firstly the parameter coordinates should be determined since all the calculations are done according to this parameter coordinates. Parameter coordinates are defined according to equation 3.23 by using element coordinates

$$\xi = \frac{(\xi_{i+1} - \xi_i)c_i + (\xi_{i+1} + \xi_i)}{2} \tag{4.35}$$

where i is the element number, ξ_{i+1} and ξ_i are corresponding element knot values and c_i is the Gauss quadrature point. For the first element with one quadrature point where $c = 0$ and weight $w = 2$, result of equation 4.35 is found as $\xi = 0.1667$. Using this parametric coordinate, related basis derivative with respect to parametric space is calculated below

$$\frac{d}{d\xi} N_{1,1}(0.1667) = \frac{1}{\xi_2 - \xi_1} N_{1,0}(0.1667) - \frac{1}{\xi_3 - \xi_2} N_{2,0}(0.1667) \tag{4.36}$$

In order to find the result of equation 4.36, values for $N_{1,0}$ and $N_{2,0}$ are required. These values can be found by using equation 3.1 as $N_{1,0} = 0$ and $N_{2,0} = 1$. Put these values and stated knot values in above equation

$$\frac{d}{d\xi} N_{1,1}(0.1667) = \frac{1}{0 - 0} 0 - \frac{1}{\frac{1}{3} - 0} 1 = -3 \tag{4.37}$$

One should note that, in Cox de Boor iteration, $0/0 = 0$.

Similarly, derivative of basis function at second control point is given below

$$\frac{d}{d\xi} N_{2,1}(0.1667) = \frac{1}{\xi_3 - \xi_2} N_{2,0}(0.1667) - \frac{1}{\xi_4 - \xi_3} N_{3,0}(0.1667) \quad (4.38)$$

Now, $N_{2,0}$ and $N_{3,0}$ values are necessary. Again by using equation 3.1 for $\xi = 0.1667$, $N_{2,0} = 1$ and $N_{3,0} = 0$ values are obtained. By putting these values and stated knot values in equation 4.38

$$\frac{d}{d\xi} N_{2,1}(0.1667) = \frac{1}{1/3 - 0} 1 - \frac{1}{2/3 - 1/3} 0 = 3 \quad (4.39)$$

In order to find the components of element stiffness matrix, equation 4.22 can be used. However, in this equation derivatives of basis functions with respect to physical space instead of parametric space should be used. This transformation can be obtained by using inverse of Jacobian matrices obtained both for parametric and parent space transformations. These matrices for one dimension are given below

$$J_\xi = \left[\frac{\partial x}{\partial \xi}\right] \quad (4.40)$$

$$J_{\hat{\xi}} = \left[\frac{\partial \xi}{\partial \hat{\xi}}\right] \quad (4.41)$$

Here, ξ is used to define parametric space where $\hat{\xi}$ is used to define parent space. Since gauss quadrature integration is performed in parent space, it is required to transform results founded in parametric space to parent space. In order to calculate jacobian matrix between physical space and parametric space, for element one, x can be written in terms of element node coordinates as follows

$$x = \sum_{i=1}^{2} N_{i,1} x_i = N_{1,1} x_1 + N_{2,1} x_2 \quad (4.42)$$

And derivative of x in parameter space can be found by using results found in 4.37 and 4.39

$$J_\xi = \left[\frac{\partial x}{\partial \xi}\right] = \frac{\partial N_{1,1}}{\partial \xi} x_1 + \frac{\partial N_{2,1}}{\partial \xi} x_2 = (-3)(0) + (3)\left(\frac{1}{3}\right) = 1 \quad (4.43)$$

77

Therefore, the value of jacobian between physical space and parametric space is found as 1. Inverse of jacobian is also 1. For this reason, jacobian between physical space and parametric space and its inverse do not affect the results. However, they will continue to be included in the following solution steps for clarity. Jacobian between parametric space and parent space is also necessary for calculations. Mapping between coordinates of these two spaces is given in equation 3.23. For investigated element, element knot values are 0 and 1/3. By using these values equation 3.23 turns into below form

$$\xi(\hat{\xi}) = \frac{(1/3 - 0)\hat{\xi} + (1/3 + 0)}{2}$$

$$J_{\hat{\xi}} = \left[\frac{\partial \xi}{\partial \hat{\xi}}\right] = \frac{1}{6}$$

(4.44)

Jacobian between parameter space and parent space is found as 1/6.

After all necessary calculations are performed, element stiffness components can be evaluated by using Gauss quadrature integration.

$$K_{11}^e = \int_{x_1}^{x_2} \frac{dN_{1,1}}{dx} AE \frac{dN_{1,1}}{dx} dx = \int_{-1}^{1} \left(\frac{dN_{1,1}}{d\xi}\frac{d\xi}{dx}\right) AE \left(\frac{dN_{1,1}}{d\xi}\frac{d\xi}{dx}\right) J_\xi J_{\hat{\xi}} d\hat{\xi}$$

$$= \sum_{i=1}^{1} w \left(\frac{dN_{1,1}}{d\xi}\frac{d\xi}{dx}\right) AE \left(\frac{dN_{1,1}}{d\xi}\frac{d\xi}{dx}\right) J_\xi J_{\hat{\xi}}$$

$$= 2(-3)(1)AE(-3)(1)(1)(\tfrac{1}{6}) = 3AE$$

$$K_{12}^e = \int_{x_1}^{x_2} \frac{dN_{1,1}}{dx} AE \frac{dN_{2,1}}{dx} dx = \int_{-1}^{1} \left(\frac{dN_{1,1}}{d\xi}\frac{d\xi}{dx}\right) AE \left(\frac{dN_{2,1}}{d\xi}\frac{d\xi}{dx}\right) J_\xi J_{\hat{\xi}} d\hat{\xi} \quad (4.45)$$

$$= \sum_{i=1}^{1} w \left(\frac{dN_{1,1}}{d\xi}\frac{d\xi}{dx}\right) AE \left(\frac{dN_{2,1}}{d\xi}\frac{d\xi}{dx}\right) J_\xi J_{\hat{\xi}}$$

$$= 2(-3)(1)AE(3)(1)(1)(\tfrac{1}{6}) = -3AE$$

$$K_{22}^e = \int_{x_1}^{x_2} \frac{dN_{2,1}}{dx} AE \frac{dN_{2,1}}{dx} dx = \int_{-1}^{1} \left(\frac{dN_{2,1}}{d\xi} \frac{d\xi}{dx} \right) AE \left(\frac{dN_{2,1}}{d\xi} \frac{d\xi}{dx} \right) J_\xi J_{\hat{\xi}} d\hat{\xi}$$

$$= \sum_{i=1}^{1} w \left(\frac{dN_2^1}{d\xi} \frac{d\xi}{dx} \right) AE \left(\frac{dN_2^1}{d\xi} \frac{d\xi}{dx} \right) J_\xi J_{\hat{\xi}}$$

$$= 2(-3)(1)AE(-3)(1)(1)(\tfrac{1}{6}) = 3AE$$

After putting these values into results of equation 4.51, symmetric element stiffness matrix can be written as follows

$$\boldsymbol{K}^e = AE \begin{bmatrix} 3 & -3 \\ -3 & 3 \end{bmatrix} \tag{4.46}$$

Global stiffness matrix can be written by considering the contributions of each elements through assembling

$$\boldsymbol{K} = AE \begin{bmatrix} 3 & -3 & 0 & 0 \\ -3 & 6 & -3 & 0 \\ 0 & -3 & 6 & -3 \\ 0 & 0 & -3 & 3 \end{bmatrix} \tag{4.47}$$

Assume the area A and elastic modulus E values are constant and equal to one as in the finite element method application. Load vector for the element one can be calculated by using the formulation given in equation 4.27. This time solution will be found with the help of gauss quadrature since solution of the integral cannot be calculated for complex basis functions. However, firstly, it is necessary to calculate the values of $N_{1,1}$ and $N_{2,1}$ by using equation 3.2. Using equation 3.1 for $\xi = 0.1667$, $N_{1,0} = 0, N_{2,0} = 1$ and $N_{3,0} = 0$ values are obtained and putting these values into equation 3.2

$$N_{1,1}(0.1667) = \frac{0.1667 - 0}{0 - 0}(0) + \frac{\tfrac{1}{3} - 0.1667}{\tfrac{1}{3} - 0}(1) = 0.5 \tag{4.48}$$

$$N_{2,1}(0.1667) = \frac{0.1667 - 0}{\frac{1}{3} - 0}(1) + \frac{\frac{2}{3} - 0.1667}{\frac{2}{3} - \frac{1}{3}}(0) = 0.5$$

Then, for element one, load vector components can be calculated by using below process and taking $a = 1$.

$$f_1^1 = \int_{x_1}^{x_2} N_{1,1}xdx = \int_{-1}^{1}(N_{1,1})((N_{1,1})(x_1) + (N_{2,1})(x_2))J_\xi J_{\hat{\xi}}d\hat{\xi}$$

$$= \sum_{i=1}^{1} w(N_{1,1})((N_{1,1})(x_1) + (N_{2,1})(x_2))J_\xi J_{\hat{\xi}}$$

$$= (2)(0.5)((0.5)(0) + (0.5)(1/3))(1)(1/6) = 0.0278$$

$$f_2^1 = \int_{x_1}^{x_2} N_{2,1}xdx = \int_{-1}^{1}(N_{2,1})((N_{1,1})(x_1) + (N_{2,1})(x_2))J_{\hat{\xi}}d\hat{\xi}$$

$$= \sum_{i=1}^{1} w(N_{2,1})\left((N_{1,1})(x_1) + (N_{2,1})(x_2)\right)J_\xi J_{\hat{\xi}}$$

$$= (2)(0.5)((0.5)(0) + (0.5)(1/3))(1)(1/6) = 0.0278$$

(4.49)

By considering the other load components coming from element two and element three, matrix assembly process should be applied. For the sake of convenience, these steps have been skipped and final force vector is directly given below.

$$\mathbf{f} = \begin{bmatrix} 0.0278 \\ 0.1111 \\ 0.2222 \\ 1.1389 \end{bmatrix} \tag{4.50}$$

Finally, system of linear equations can be written in matrix form in equation 4.51.

$$\begin{bmatrix} 3 & -3 & 0 & 0 \\ -3 & 6 & -3 & 0 \\ 0 & -3 & 6 & -3 \\ 0 & 0 & -3 & 3 \end{bmatrix} \begin{bmatrix} u_1 \\ u_2 \\ u_3 \\ u_4 \end{bmatrix} = \begin{bmatrix} 0.0278 \\ 0.1111 \\ 0.2222 \\ 1.1389 \end{bmatrix} \tag{4.51}$$

When the equation 4.51 is solved with the application of boundary conditions, resultant displacements are found and given below.

$$\boldsymbol{u} = \begin{bmatrix} u_1 \\ u_2 \\ u_3 \\ u_4 \end{bmatrix} = \begin{bmatrix} 0 \\ 0.4907 \\ 0.9444 \\ 1.3241 \end{bmatrix} \tag{4.52}$$

This result is slightly different than what is found in equation 4.30 for finite element application. This difference can be attributed to application of quadrature for the evaluation of force vector. Since it is stated in literature as *2n-1* quadrature points satisfy enough accuracy for the results where *n* is the order of function, one quadrature point was used during calculations. If number of gauss points is increased to two, IGA better converges to exact solution. Research about the effect of quadrature rule on the results of isogeometric analysis was conducted in [80] and a new numerical integration called as "half-point rule" is suggested to be used in isogeometric analysis to get optimal results. However, in this study classical gauss quadrature integration was utilized for numerical integration.

After finding out nodal displacements, element strain and stress values can be found with the application of equation 4.31. Stress results are shared in equation 4.53 and graphs are given in Figure 4.5 and Figure 4.6.

$$\begin{bmatrix} \sigma_1 \\ \sigma_2 \\ \sigma_3 \end{bmatrix} = \begin{bmatrix} 1.4722 \\ 1.3611 \\ 1.1389 \end{bmatrix} \tag{4.53}$$
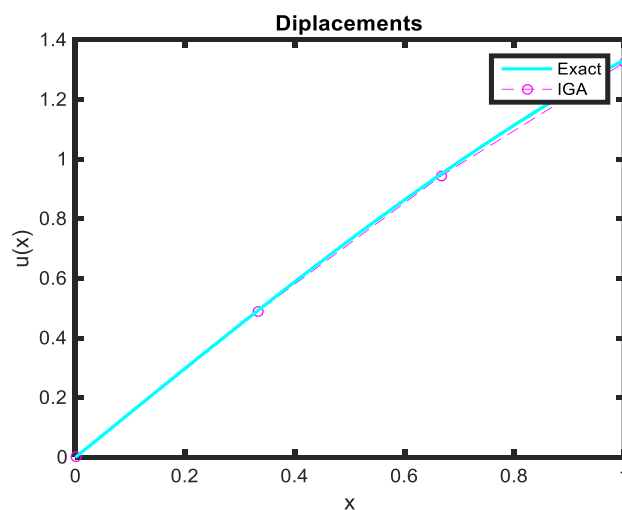
Figure 4.5 Displacement values for exact and IGA solutions
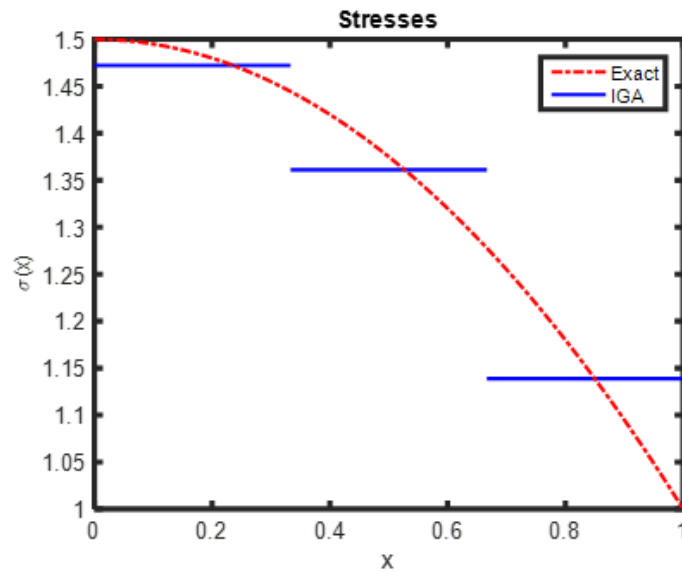
Figure 4.6 Stress values for exact and IGA solutions

Since the results of mentioned numerical techniques are close to the exact solution, it can be concluded that usage of first order linear elements is enough for bar problems. For first order elements, finite element basis functions are same with NURBS basis functions and difference between the two methods disappears. This can be drawn from the same stiffness matrices. As mentioned previously, difference between results of FEA and IGA caused from calculation of force vector. In isogeometric analysis application, force vector was calculated by using gauss quadrature method and only one quadrature point was used during estimation of force vector components. Additionally, solution process in finite element analysis lasted for 0.223 seconds while it took 0.194 seconds in isogeometric analysis despite latter analysis code includes extra lines for geometry definition and element stiffness calculation.

4.1.2 Bending of Euler – Bernoulli Beams

In this section Euler-Bernoulli beam problem is analyzed by using isogeometric analysis. As in the previous section, finite element solution for the same problem is also introduced and a comparison between these two numerical methods is conducted. Since all steps beginning from equilibrium equations to obtaining element stiffness

matrix has been explained in the previous section they were not mentioned in this section.

The Euler–Bernoulli beam theory assumes that the plane cross-sections, which are normal to the undeformed centroidal axis, remain plane after bending and remain normal to the deformed axis [81]. A section of a beam with incremental length is given in Figure 4.7.
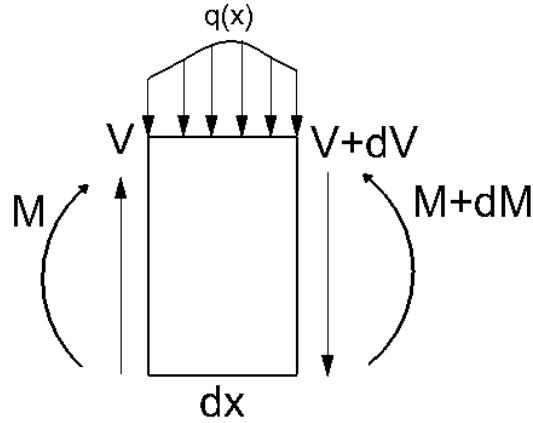
Figure 4.7 Beam section with length dx and forces on it

Equilibrium equations give the strong form of the beam bending problem as follows

$$\frac{d^2}{dx^2}\left(EI\frac{d^2u}{dx^2}\right) - q = 0, \qquad 0 < x < L \tag{4.54}$$

Then, weak form of the solution is given below,

$$\int_0^L \left(EI\frac{d^2v}{dx^2}\frac{d^2u}{dx^2} - vq\right)dx - v(0)Q_1^e - \left(-\frac{dv}{dx}\right)\bigg|_0 Q_2^e - v(L)Q_3^e$$
$$- \left(-\frac{dv}{dx}\right)\bigg|_L Q_4^e = 0 \tag{4.55}$$

where 0 and L are nodal coordinates and v is test function and Q_i^e are described in equation 4.56.

$$Q_1^e = \left[\frac{d}{dx}\left(EI\frac{d^2u}{dx^2}\right)\right]\Big|_0 = -V(0)$$

$$Q_2^e = \left(EI\frac{d^2u}{dx^2}\right)\Big|_0 = -M(0)$$

$$Q_3^e = -\left[\frac{d}{dx}\left(EI\frac{d^2u}{dx^2}\right)\right]\Big|_L = V(L)$$ (4.56)

$$Q_4^e = -\left(EI\frac{d^2u}{dx^2}\right)\Big|_L = M(L)$$

In order to apply Galerkin's finite element approximation, required trial solution and weight functions are given below

$$u(x) = \sum_{i=1}^{n} u_i N_i(x)$$ (4.57)

and

$$v(x) = \sum_{j=1}^{n} b_j N_j(x)$$ (4.58)

In above equations u_i are used to define unknown nodal transverse displacements and b_j are arbitrarily chosen points and n is the number of points. Additionally, $N(x)$ represents NURBS basis functions. In accordance with the Galerkin's method same basis functions are used in description of both approximate solution and weighting function. When equations 4.57 and 4.58 are put into 4.55, equation 4.55 is reduced to classical equation $\boldsymbol{Ku} = \boldsymbol{f}$ in matrix form. Stiffness matrix and force vector of this equation can be obtained as follows

$$\boldsymbol{K_{ji}} = \int_0^L EI\frac{d^2N_j}{dx^2}\frac{d^2N_i}{dx^2}dx$$

$$\boldsymbol{f_i} = \int_0^L qN_i dx$$ (4.59)

After deriving the stiffness matrix and force vector, problem case which is a simply supported slender beam under uniformly distributed load was introduced. The most important advantage to be mentioned here about isogeometric analysis is its rotation free formulation for deformation due to high order continuity of NURBS. Therefore, in deformation analysis of Euler-Bernoulli beam by IGA, only transverse degrees of freedoms are assigned to control points. However, if stress values are desired to be obtained, then rotation values should be calculated.

Consider the slender beam with rectangular cross section shown in Figure 4.8. Uniformly distributed load is applied along the beam. Beam is simply supported and dimensions and material properties of the beam are given in Table 4.2.

Table 4.2 Values of parameters for beam bending problem

Elastic Modulus (E) [GPa]	70
Height x width x length of the beam (h x w x L) [mm]	10 x 8 x 1000
Load per unit length (q_0) [N/m]	30
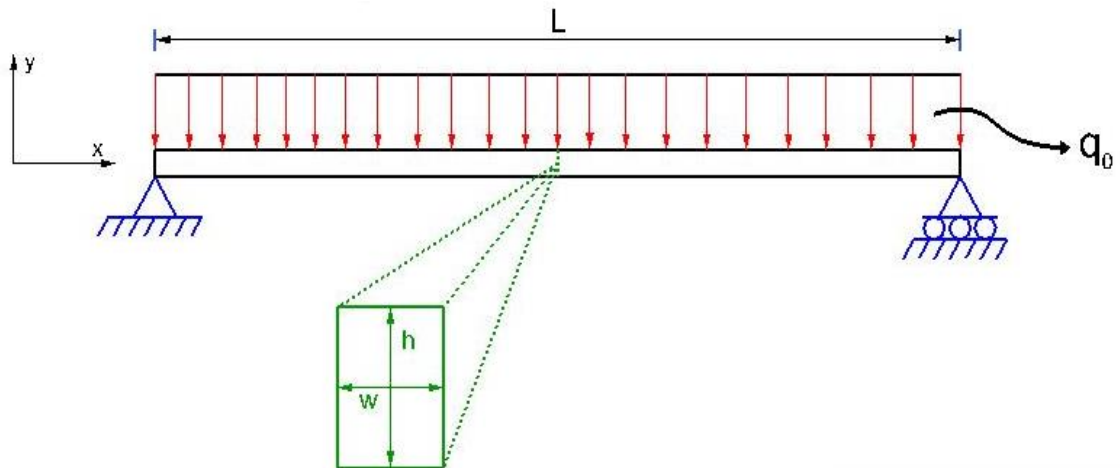
Figure 4.8 Simply supported beam under uniform distributed load

Problem begins by taking the knot vector as $\Xi = [0\ 0\ 0\ 0\ 1\ 1\ 1\ 1]$ and control points are stated in Table 4.3 since beams are already defined using cubic basis functions in finite element analysis.

Table 4.3 Beam control points and corresponding weights

	X coordinate	Y coordinate	Weight
Point 1	0	0	1
Point 2	0.3	0	1
Point 3	0.6	0	1
Point 4	1	0	1

Cubic NURBS basis functions have been used during solution. Moreover, four quadrature points were used for numerical integration. In order to obtain exact results, two knot insertion operations (h-refinement) were performed. After these refinements, four elements were obtained and resultant knot vector turned into $\Xi = [0\ 0\ 0\ 0\ 0.25\ 0.5\ 0.75\ 1\ 1\ 1\ 1]$ and control points are given in Table 4.4.

Table 4.4 Beam control points and corresponding weights after refinements

	X coordinate	Y coordinate	Weight
Point 1	0	0	1
Point 2	0.075	0	1
Point 3	0.225	0	1
Point 4	0.4594	0	1
Point 5	0.7125	0	1
Point 6	0.9	0	1
Point 7	1	0	1

Exact solution of displacement and stress values on a simply supported beam under distributed uniform load are given as follows,

$$u(x) = \frac{qx(L^3 - 2x^2L + x^3)}{24EI} \tag{4.60}$$

$$\sigma(x) = -\frac{qx(L - x)h}{4I} \tag{4.61}$$

Isogeometric analysis of Euler-Bernoulli beam under defined conditions conducted by four cubic elements produces consistent results with exact solution. Same analysis was also conducted by using classical finite element method. These results are given in Figure 4.9 and Figure 4.10.
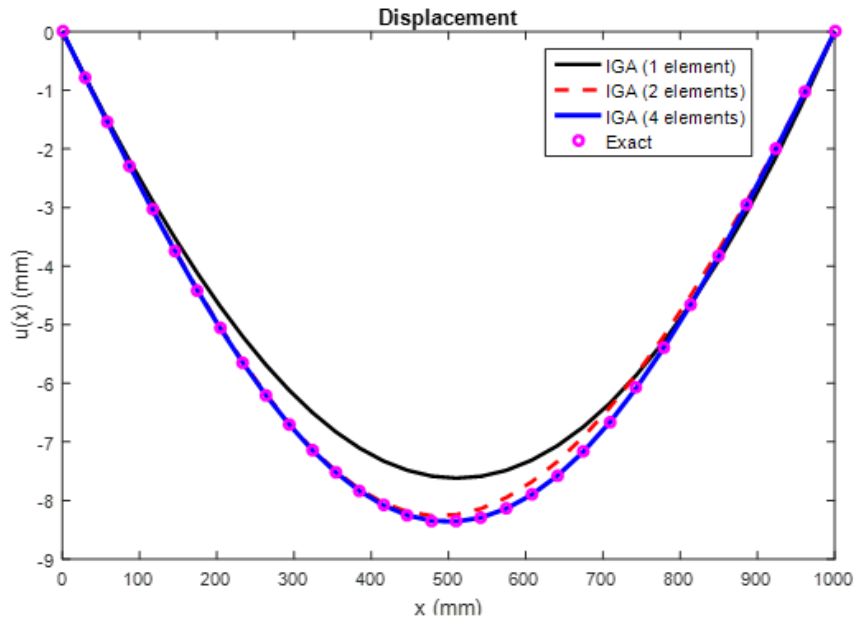
Figure 4.9 Displacement curves for exact and IGA results
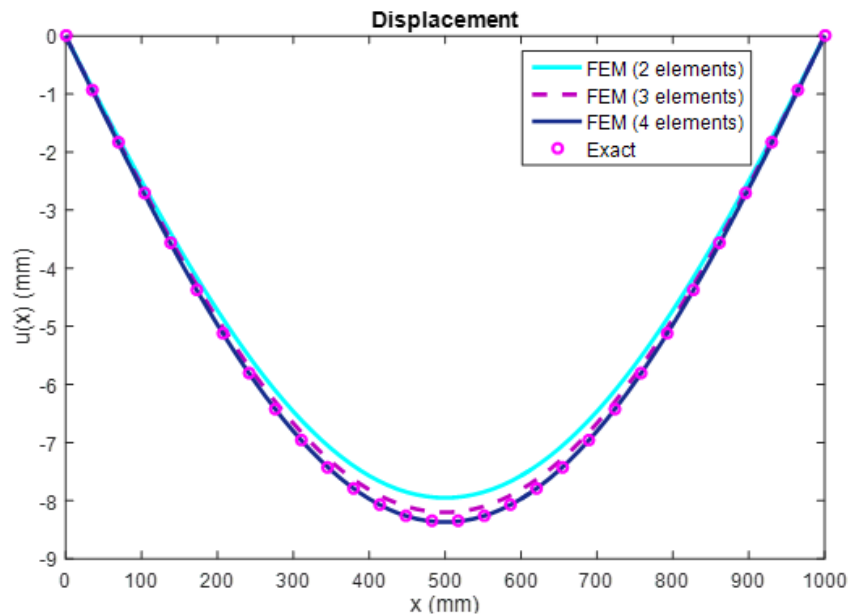
Figure 4.10 Displacement curves for exact and FEM results

In Figure 4.9, for four element IGA solution maximum displacement value was obtained as 8.4 mm at the mid-length of the beam. Same value can be obtained from analytical solution by using equation 4.60. Moreover, at every point IGA catches a good matching with exact results. On the other hand, in Figure 4.10, FEM also captures the exact result by using 4 elements with 2 nodes for each. Therefore, since both IGA and FEM beam elements have cubic order, both numerical methods converge to exact result with same number of elements. However, using the same computer conditions and similar code architecture isogeometric analysis performs the operation in shorter time. The computation time for finite element analysis has taken as 0.623 seconds while, IGA solved the problem in 0.438 seconds. Additionally, if the order of IGA solution has been increased to quartic order, then exact solution can be obtained with only one element usage in 0.386 seconds. Result of this case is given in Figure 4.11. Although the order of IGA is increased, the time required for the solution was decreased since required control point number and basis function calculation is less for quartic degree one element than cubic degree four elements.
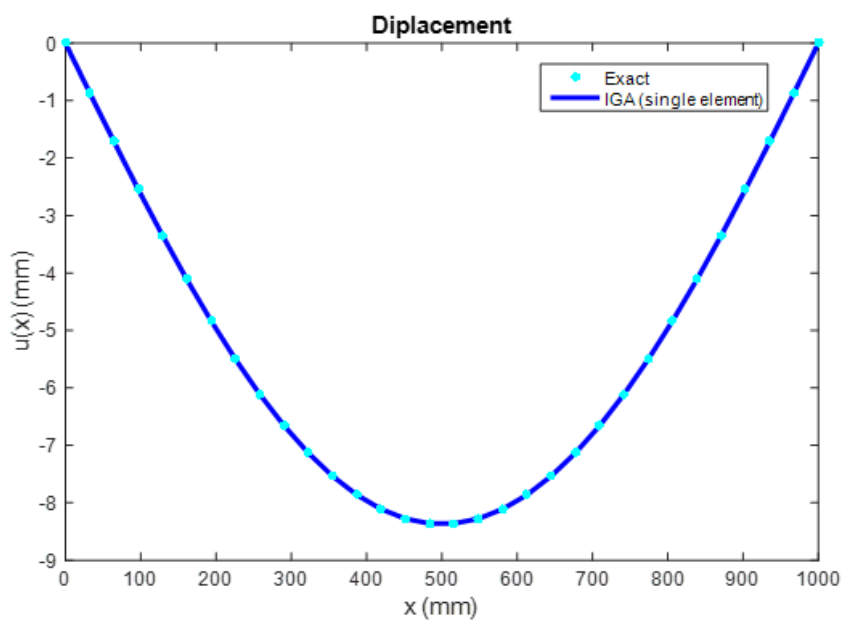
Figure 4.11 Displacement results comparison for single element IGA with fourth order and exact solution

88

After obtaining the displacement values with rotation free formulation, in order to get stress values through the beam length, rotation and stress values should be calculated via taking the derivatives of displacement with respect to x similar to the classical finite element analysis. Isogeometric analysis rotation and stress results obtained by using either four cubic elements or single quartic element that both give exact analytical solution and they are given in the following figures.
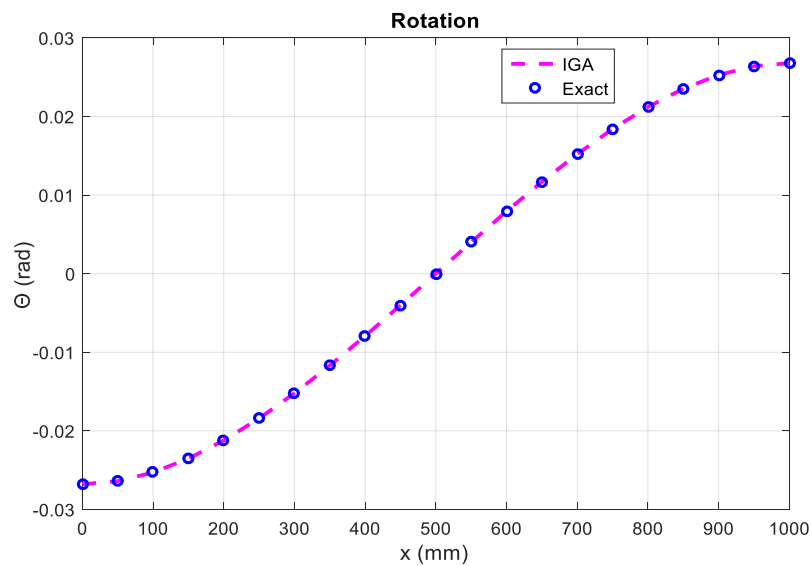
Figure 4.12 Rotation results of Isogeometric Analysis in radians
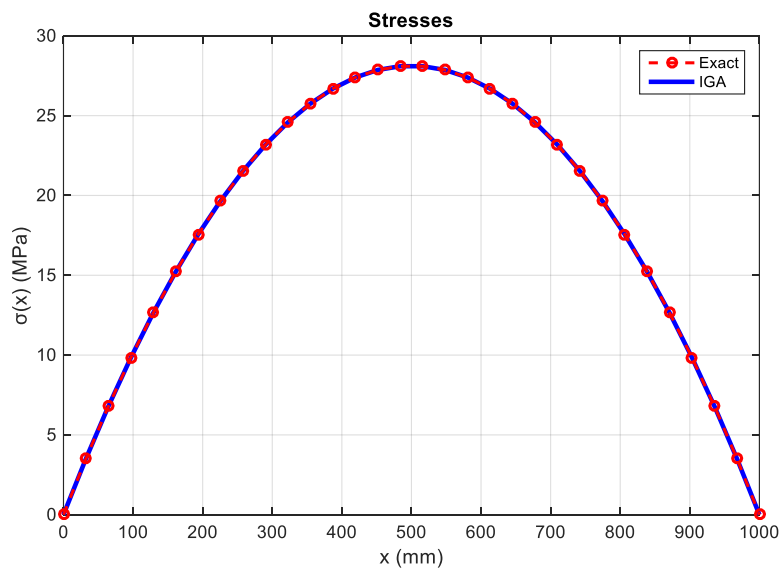
Figure 4.13 Stress results of Isogeometric Analysis in MPas

4.2 2D Isogeometric Analysis

In this section, Kirchhoff plate under uniformly distributed force and infinite plate with circular hole are investigated by isogeometric analysis. Same problems are also solved with finite element method approach by using commercial FEA software package Abaqus. At the end, isogeometric analysis results, if exists analytical results and FEM results are compared.

4.2.1 Kirchhoff Plate Bending

For an isotropic Kirchhoff plate under uniformly distributed force, strong form plate bending equation can be written as follows

$$\frac{\partial^4 w}{dx^4} + 2\frac{\partial^4 w}{dx^2 dy^2} + \frac{\partial^4 w}{dy^4} = \frac{q}{D} \tag{4.62}$$

In this formulation, q is used to denote distributed force, w is deflection of the plane in transverse direction and D represents bending stiffness;

$$D = \frac{Eh^3}{12(1 - v^2)} \tag{4.63}$$

where E, v and h are modulus of elasticity, Poisson's ratio and the plate thickness respectively. Strains and stresses of Kirchhoff plate bending problem can be found with the following formulas,

$$\boldsymbol{\varepsilon} = -z\boldsymbol{L}w = -z\begin{bmatrix} \partial^2/\partial x^2 \\ \partial^2/\partial y^2 \\ 2\partial^2/\partial x \partial y \end{bmatrix} w \tag{4.64}$$

$$\boldsymbol{\sigma} = \boldsymbol{C}\boldsymbol{\varepsilon} \tag{4.65}$$

where $\boldsymbol{C}$ matrix forms constitutive relation and constructed by material properties.

$$\boldsymbol{C} = D \begin{bmatrix} 1 & v & 0 \\ v & 1 & 0 \\ 0 & 0 & (1-v)/2 \end{bmatrix} \tag{4.66}$$

After the application of Galerkin's method, element stiffness matrix can be obtained as,

$$\boldsymbol{K}_{ji} = \int_{\Omega} \boldsymbol{B}_j^T \boldsymbol{C} \boldsymbol{B}_i d\Omega \tag{4.67}$$

where

$$\boldsymbol{B}_i = \begin{bmatrix} -\dfrac{\partial^2 N_i}{\partial x^2} \\[2mm] -\dfrac{\partial^2 N_i}{\partial y^2} \\[2mm] -2\dfrac{\partial^2 N_i}{\partial x \partial y} \end{bmatrix} \tag{4.68}$$

Force vector can be calculated by using following equation

$$\boldsymbol{F}_i = \int_{\Omega} q N_i d\Omega \tag{4.69}$$

An important advantage of isogeometric analysis in bending problems is its rotation free formulation for deformation calculation due to high order continuity of NURBS as in the case of beam bending problem. Consequently, in this analysis of Kirchhoff plate by IGA, only transverse degrees of freedoms are assigned to control points.

Problem case which is a square plate under the action of uniformly distributed pressure of 10 kPa is demonstrated in Figure 4.14. All edges of the plate are fixed. The dimensions and material properties of the plate are given in Table 4.5.

Table 4.5 Parameters of the Kirchhoff plate problem

Elastic Modulus (E) [GPa]	200
Poisson's Ratio (v)	0.3
Length x width x thickness (a x b x t) [mm]	1000 x 1000 x 10
Uniform pressure (q) [kPa]	10
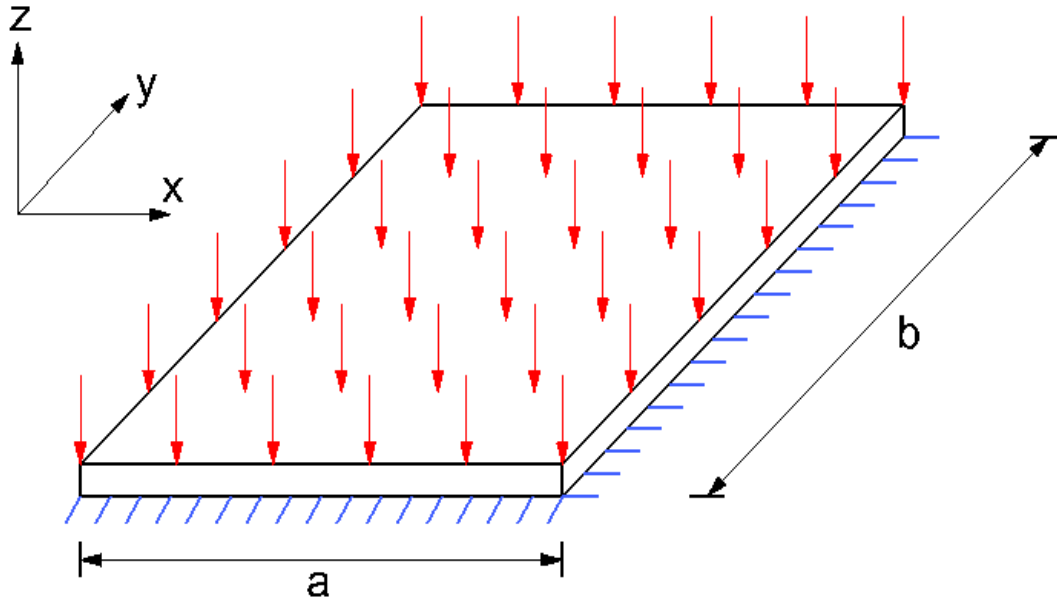
Figure 4.14 Representation of Kirchhoff plate problem

In IGA, firstly linear element with knot vectors $\Xi = [0\ 0\ 1\ 1]$ and $\Theta = [0\ 0\ 1\ 1]$ has been used where Ξ represents element coordinates in parametric space along ξ direction while Θ gives parametric coordinates of elements in η directions that they correspond to x and y-directions in physical space respectively. These initial knot vectors were refined to increase the number of the elements and finally the geometry was modeled by using 18 control points and 16 elements in both x and y directions. These points were obtained after conducting one order elevation and four times knot insertion. At the end following knot vectors were obtained.

$$\Xi = \begin{bmatrix} 0\ 0\ 0\ 0.0625\ 0.0125\ 0.1875\ 0.25\ 0.3125\ 0.3750\ 0.4375\ 0.5 \\ 0.5625\ 0.6250\ 0.6875\ 0.75\ 0.8125\ 0.8750\ 0.9375\ 1\ 1\ 1 \end{bmatrix}$$

$$\Theta = \begin{bmatrix} 0\ 0\ 0\ 0.0625\ 0.0125\ 0.1875\ 0.25\ 0.3125\ 0.3750\ 0.4375\ 0.5 \\ 0.5625\ 0.6250\ 0.6875\ 0.75\ 0.8125\ 0.8750\ 0.9375\ 1\ 1\ 1 \end{bmatrix}$$

At the end, control mesh of the geometry can be created as given in Figure 4.15.
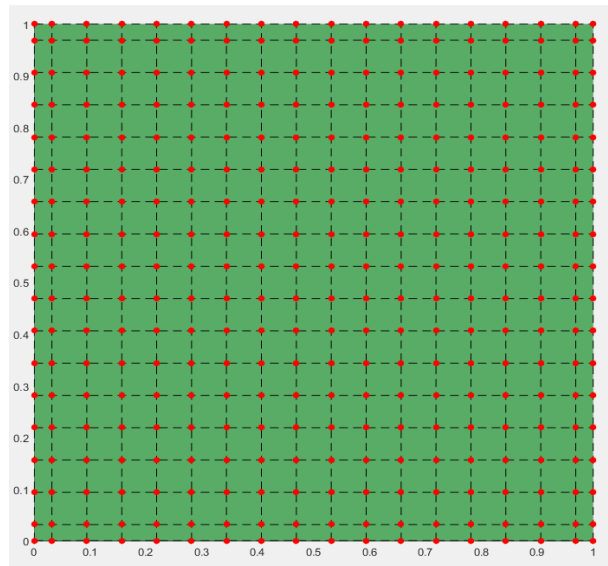
Figure 4.15 Control mesh of Kirchhoff plate

In order to give clamped boundary condition to edges of the plate, control points on the edges and the control points next to them were fixed since tangency of that region depends on two neighbor points as stated in [81]. The mentioned clamped boundary condition is shown in Figure 4.16.
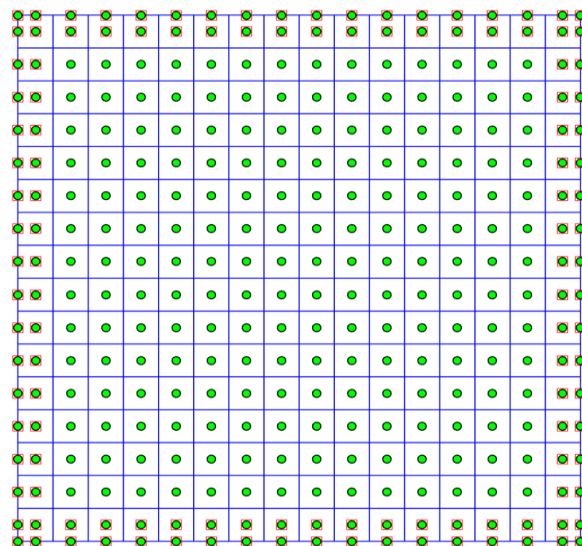
Figure 4.16 Clamped boundary condition representation

Here, green points are control points and control points enclosed with red squares are fixed points. Blue grid is given to indicate element boundaries.

After creating the geometry and applying boundary conditions, problem was solved to obtain transverse displacements. A sensitivity analysis was conducted to observe the effect of element number on the results. Solution has started with the usage of 16 elements. Accurate results were obtained by utilization of 256 elements.
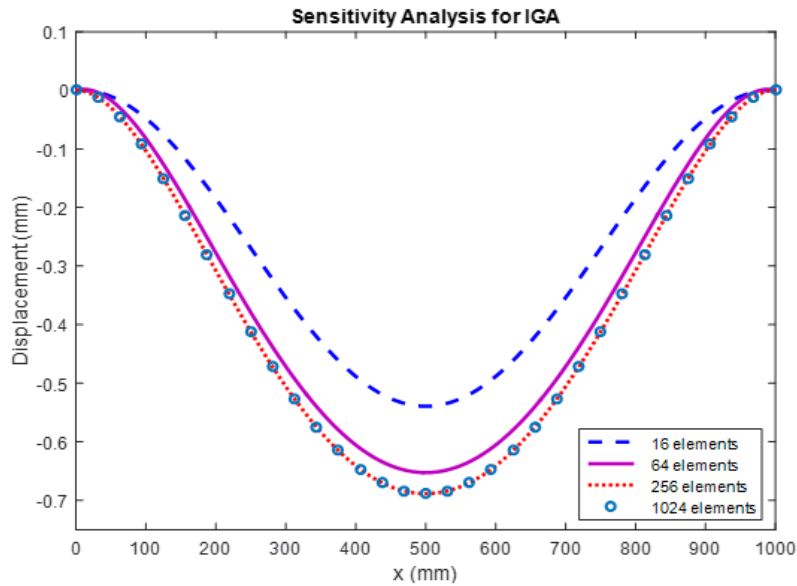
Figure 4.17 Effect of element number on the IGA result

Deformation and equivalent stress results of the plate are given in Figures 4.18 and 4.19.
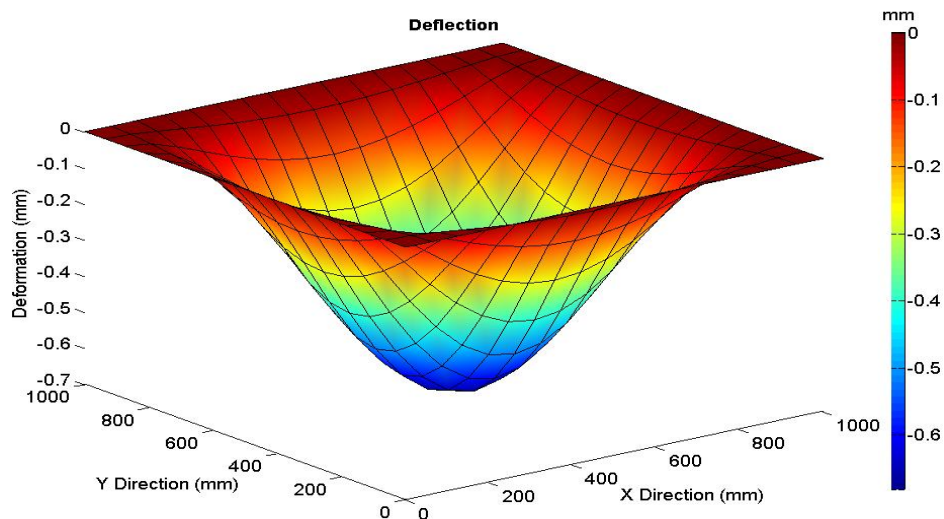
Figure 4.18 IGA displacement results of the Kirchhoff plate problem in meters

94
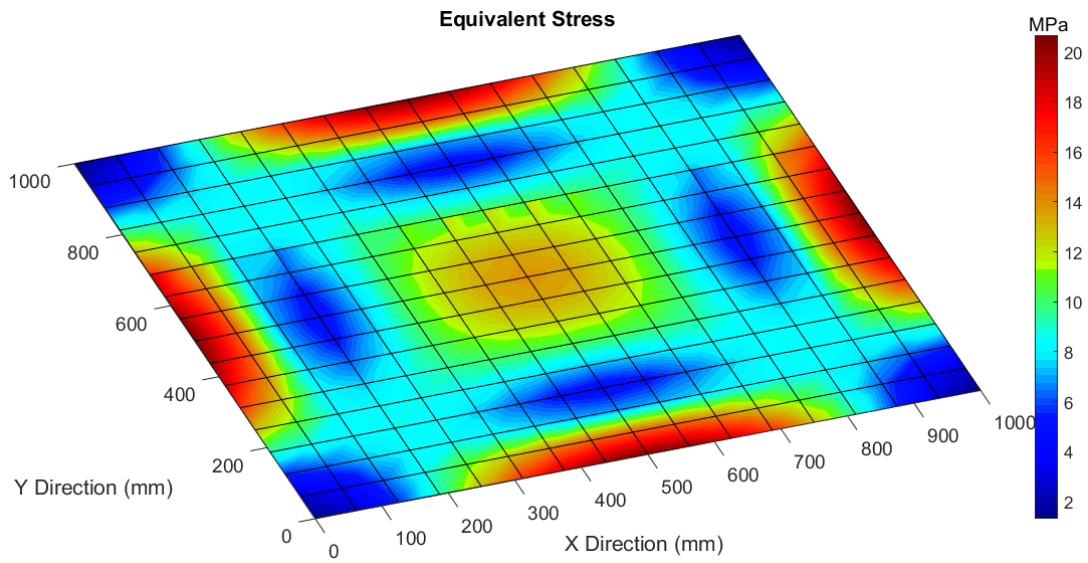
Figure 4.19 IGA equivalent stress results of the Kirchhoff plate problem in MPa

Maximum deflection was obtained at the mid-section of the plate with the value of -0.6885 mm. Maximum stress values were captured at the clamped edges of the plate as 20.54 MPa. For this analysis, 256 elements were used. Analysis lasted for 2.6 seconds. Same analysis was also conducted by using Abaqus FEA program. A sensitivity analysis was also conducted for FEA beginning with the usage of 256 elements. Accurate results were obtained with 729 elements.
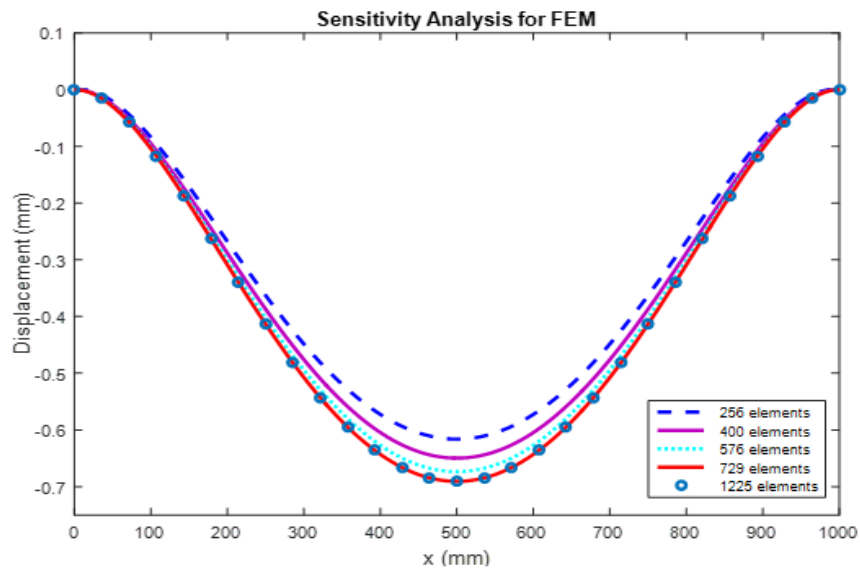
Figure 4.20 Effect of element number on the FEA result

Displacement and stress results obtained using finite element analysis are shared in Figures 4.21 and 4.22.
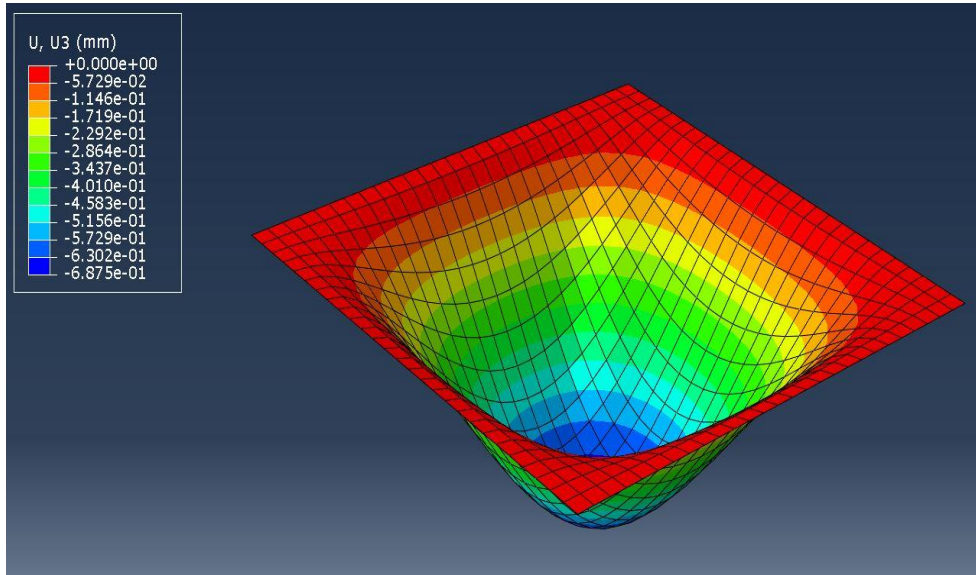
Figure 4.21 Abaqus displacement results for the Kirchhoff plate problem
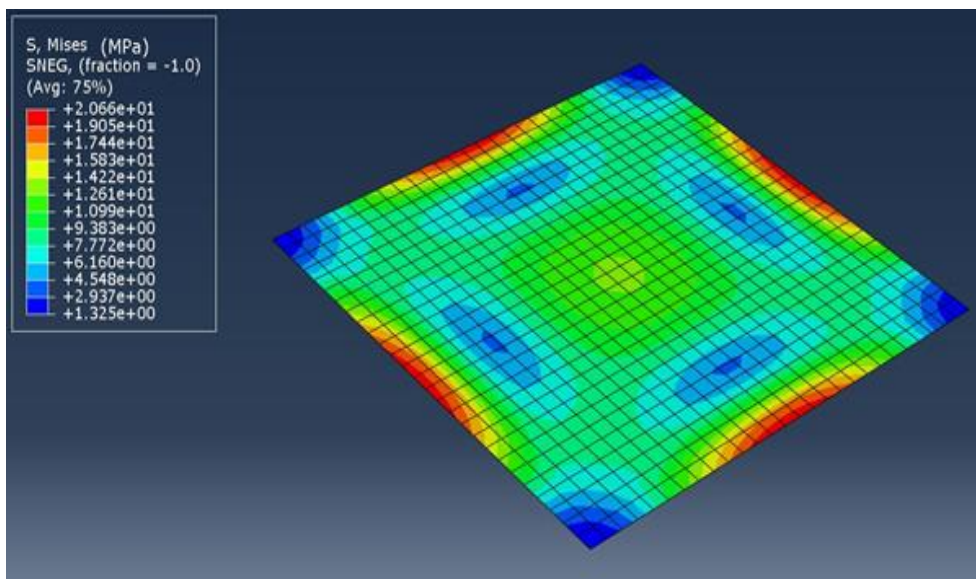
Figure 4.22 Abaqus equivalent stress results for the Kirchhoff plate problem

As can be seen from the Figure 4.21, maximum deflection is again obtained at the mid-region of the plate with the value of -0.6875 mm. Maximum equivalent stresses are observed at the clamped edges with the value of 20.66 MPa. Therefore, FEA

results are close to results of IGA. However, in finite element analysis 729 elements were used to obtain results and analysis continued through 14.3 seconds despite the usage of linear elements. The main reason lies behind this time difference is computational efficiency of isogeometric analysis and its rotation free nature.

4.2.2 Infinite Plate with a Circular Hole

In this two dimensional linear elasticity problem, an infinite plate with circular hole under constant in-plane tension is introduced. Problem is demonstrated in Figure 4.23 as a quarter model by taking advantage of symmetry. T_x (N/mm^2) is used to denote traction applied at the edges of plate. R (mm) is the radius of the hole and L (mm) is the edge length of the finite quarter plate. Moreover, $E = 100\ GPa$ and $v = 0.3$.
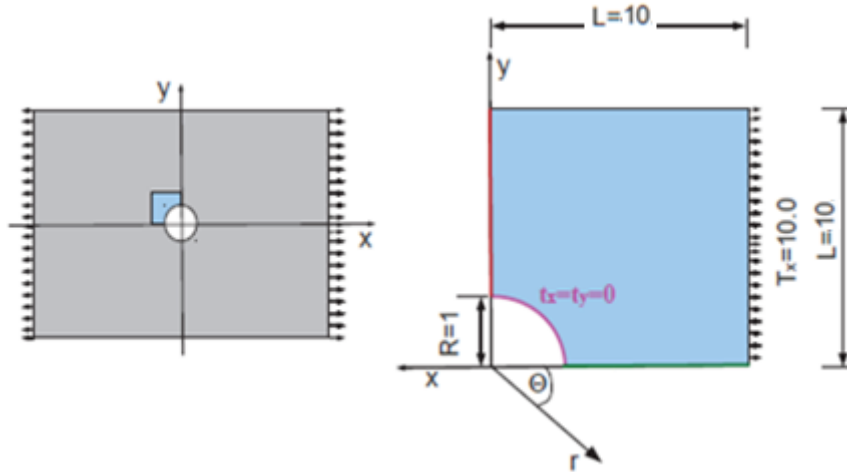
Figure 4.23 Infinite plate with a circular hole under constant tension

This problem has exact analytical solution given below [82].

$$\sigma_{rr}(r,\theta) = \frac{T_x}{2}\left(1 - \frac{R^2}{r^2}\right) + \frac{T_x}{2}\left(1 - 4\frac{R^2}{r^2} + 3\frac{R^4}{r^4}\right)\cos2\theta,$$

$$\sigma_{\theta\theta}(r,\theta) = \frac{T_x}{2}\left(1 + \frac{R^2}{r^2}\right) - \frac{T_x}{2}\left(1 + 3\frac{R^4}{r^4}\right)\cos2\theta, \tag{4.70}$$

$$\sigma_{r\theta}(r,\theta) = -\frac{T_x}{2}\left(1 + 2\frac{R^2}{r^2} - 3\frac{R^4}{r^4}\right)\sin2\theta,$$

In this problem accurate geometry has been defined by IGA instead of approximated geometry defined in the case of FEA due to the hole boundary. In order to represent the circular hole, at least quadratic order basis functions should be used. By utilizing only two elements, quarter geometry can be exactly created.

These two element coarsest mesh structure can be constructed by using following knot vectors

$$\Xi = \{0\ 0\ 0\ 0.5\ 1\ 1\ 1\} \ \& \ \mathcal{H} = \{0\ 0\ 0\ 1\ 1\ 1\}$$

By using given knot vectors, the obtained control mesh and physical mesh are given in Figure 4.24.

(a) Physical Mesh (b) Control Mesh

(c) Control Points and Physical Mesh
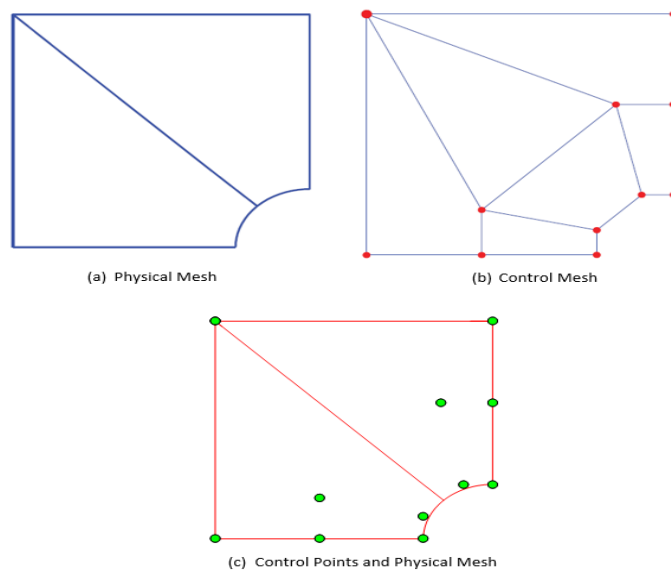
Figure 4.24 Two element mesh and exact representation of geometry

In Figure 4.24, non-interpolatory nature of the IGA element boundaries can be better seen. Therefore, control mesh and physical mesh differs from each other. Control points and their weights used to construct these two element mesh is shared at Table 4.6. Although the discretization of the geometry has begun with 2 elements, they are not enough to get accurate results. Three knot insertion processes were practiced to get finer mesh. After these refinements element number was increased to 128 and number of control points has become 180.

Table 4.6 Control Points used to construct 2 element mesh

	X Coordinate	Y Coordinate	Weights
Point 1	-1	0	1
Point 2	-1	0.4142	0.8536
Point 3	- 0.4142	1	0.8536
Point 4	0	1	1
Point 5	-2.5	0	1
Point 6	-2.5	0.75	1
Point 7	-0.75	2.5	1
Point 8	0	2.5	1
Point 9	-4	0	1
Point 10	-4	4	1
Point 11	-4	4	1
Point 12	0	4	1

Plate under the effect of 10 MPa experiences quite small deformations in x and y directions as given in the Figure 4.25. Using analytical solutions, the hoop stress value for $\theta/2$ will be $3T_x$ around the hole, and stress concentration will be exactly three. The stress concentration and overall stress results of isogeometric analysis are consistent with analytical results as given in Figure 4.26.
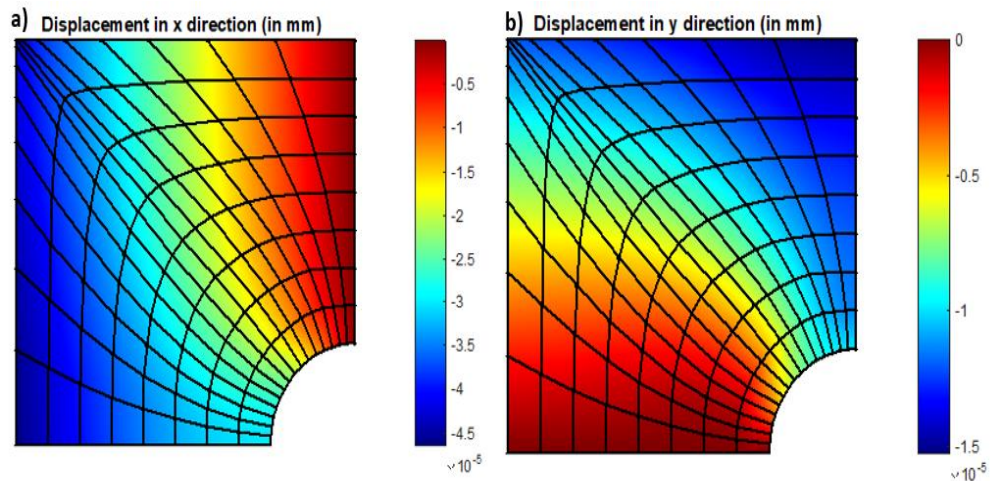
Figure 4.25 Displacement of the plate a) along x direction
and b) along y direction

When the coordinates of the points of deformed shape were compared with result of the exact solution, a good matching between the results was obtained as given in

Figure 4.27. Additionally, same analysis was conducted by using Abaqus FEA package to observe the finite element method performance on the same problem. Normal stress in x and y directions and shear stress results of this analysis is also shared in Figure 4.28.
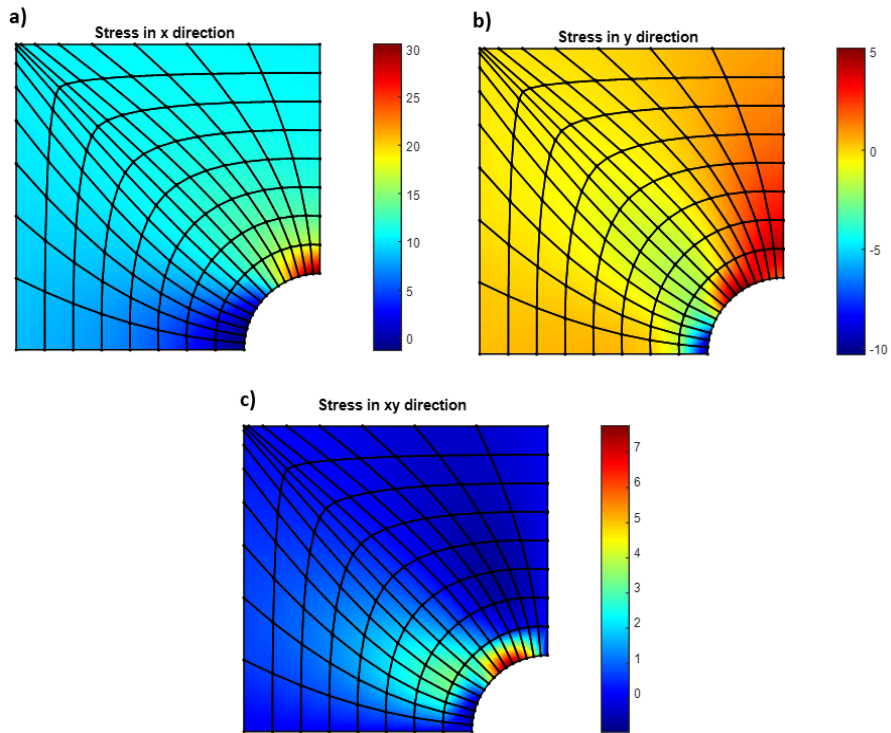
Figure 4.26 IGA stress results a) Normal stress x direction b) Normal stress in y direction c) Shear stress
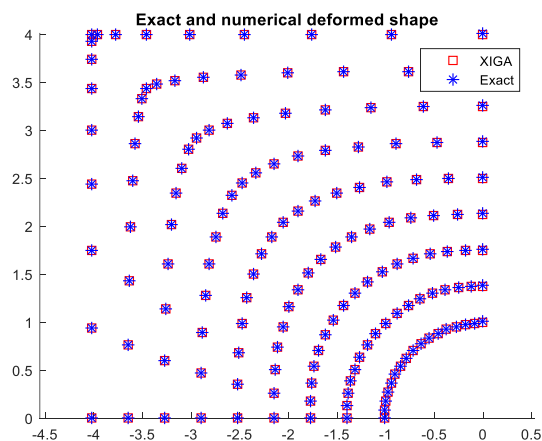
Figure 4.27 Comparison of exact deformed shape and deformed shape obtained by IGA
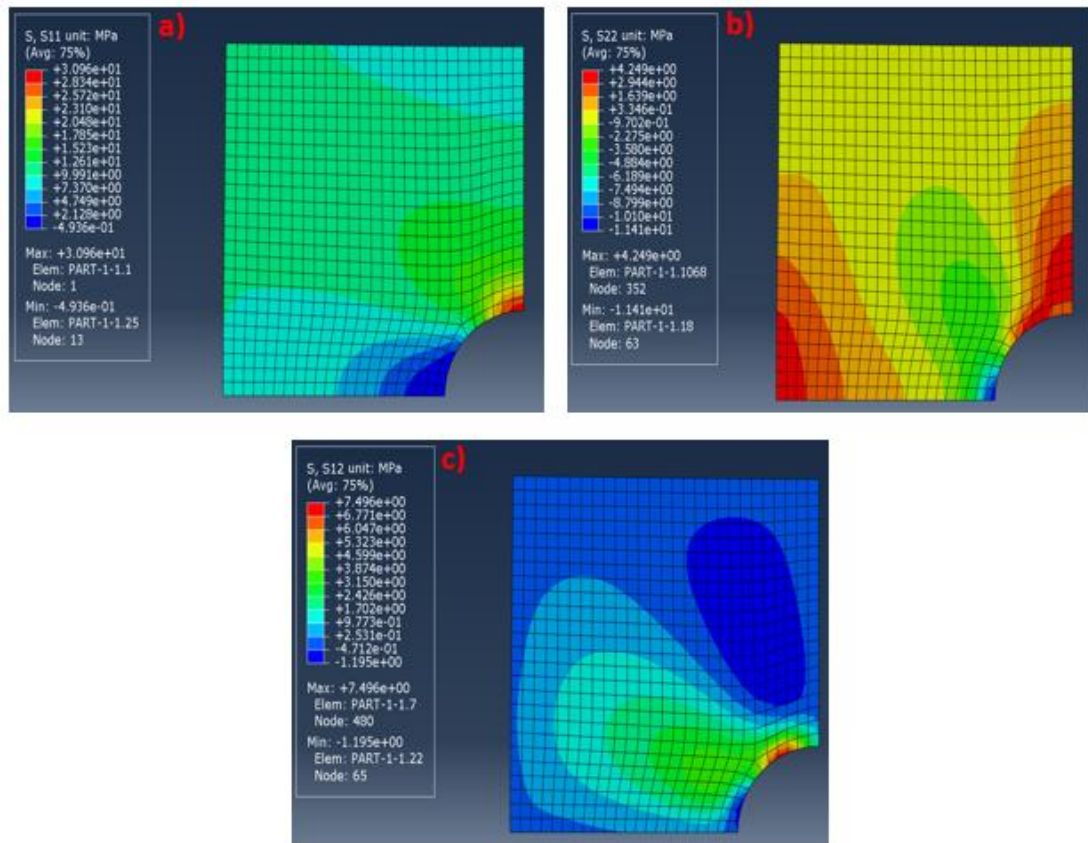
Figure 4.28 IGA stress results a) Normal stress x direction b) Normal stress in y direction c) Shear stress

Figures clearly state the consistency between IGA and FEA results. In order to run isogeometric analysis in Matlab, only 128 elements were used while in Abaqus 650 elements have been generated in pre-processing phase. Additionally, Matlab has finished its computation in 6.1 seconds. On the other hand, finite element analysis conducted using Abaqus lasted for 19.6 seconds.

4.3 3D Isogeometric Analysis

As a 3D example of isogeometric analysis, a pinched cylinder problem has been considered.

In pinched cylinder problem, two concentrated forces which are equal in magnitude but acting in opposite directions at the mid-section of the cylinder were used. Fixed

boundary conditions are defined at both ends of the cylinder. Due to these constraints highly localized deformations are obtained at the points of applied concentrated forces. Only one eight of the geometry was modeled by using the symmetry conditions. Under defined conditions, cubic NURBS elements were used through all directions for discretization in order to eliminate shear locking problem. Problem geometry and necessary parameters were shared in Figure 4.29.
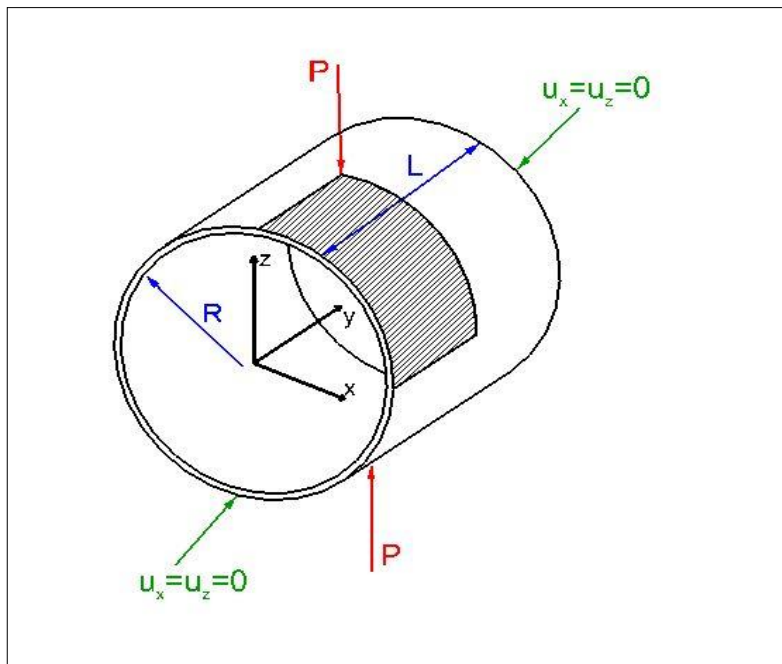
Figure 4.29 Pinched cylinder problem description

Table 4.7 Parameters for pinched cylinder problem

Elastic Modulus (*E*) [GPa]	3000
Dimensions (*L* x *R* x *thickness*) [mm]	600 x 300 x 3
Poisson's Ratio (*v*)	0.3
Force [*N*]	1

Displacement and stress results of isogeometric analysis are given in Figure 4.30 and Figure 4.31 respectively. Displacement value at the application point of force was found as $1.8276(10^{-5})$ mm at the end of IGA. Total displacement result is given as $1.8248(10^{-5})$ mm in the study of Belytschko et al. [83]. Analysis was performed by

using Matlab and the results were viewed through "Paraview" software which is commonly used for post-processing visualization purpose as a free source. In order to obtain these results five knot insertion refinements were applied and at the end 512 cubic elements were utilized for analysis.
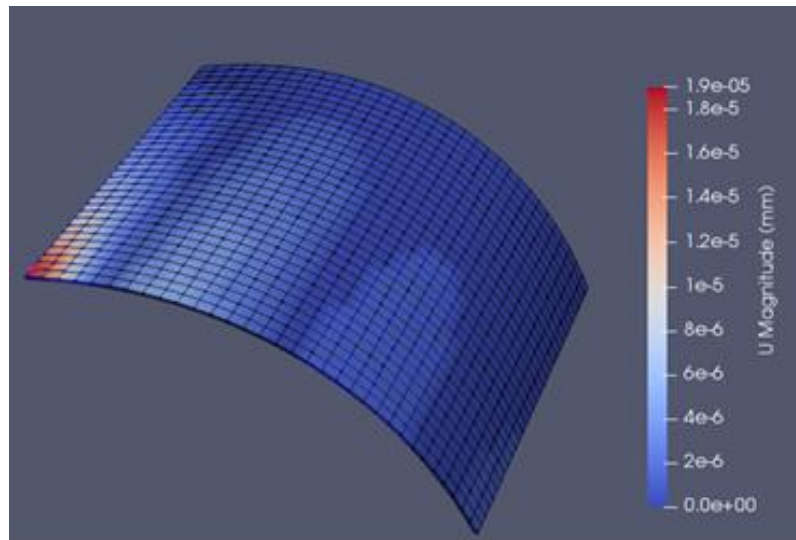
Figure 4.30 Total displacement results for pinched cylinder problem
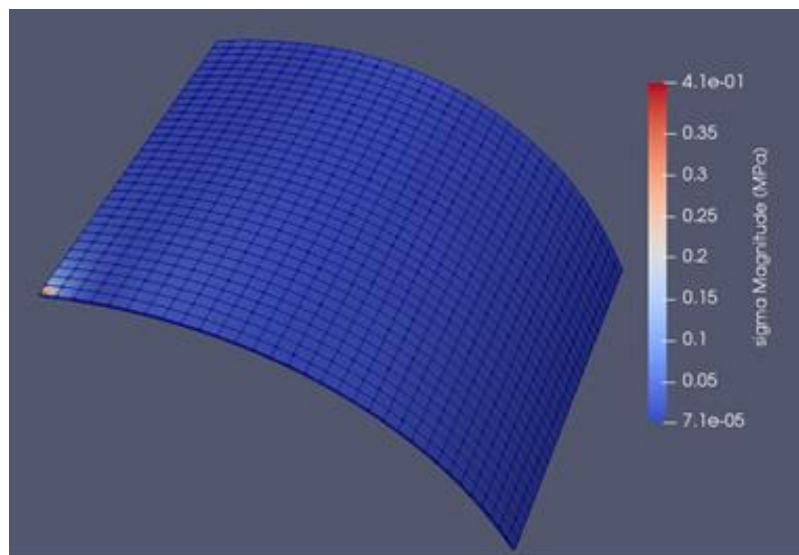
Figure 4.31 Total stress results for pinched cylinder problem

Same problem was solved also by using Abaqus. In order to obtain accurate results 2242 quadratic S8R, 8-node doubly curved thick shell, reduced integration elements were used. Results of this analysis is given in Figure 4.32 and Figure 4.33. Computation time for isogeometric analysis was 27.4 seconds while it is 34.6 seconds for finite element analysis.
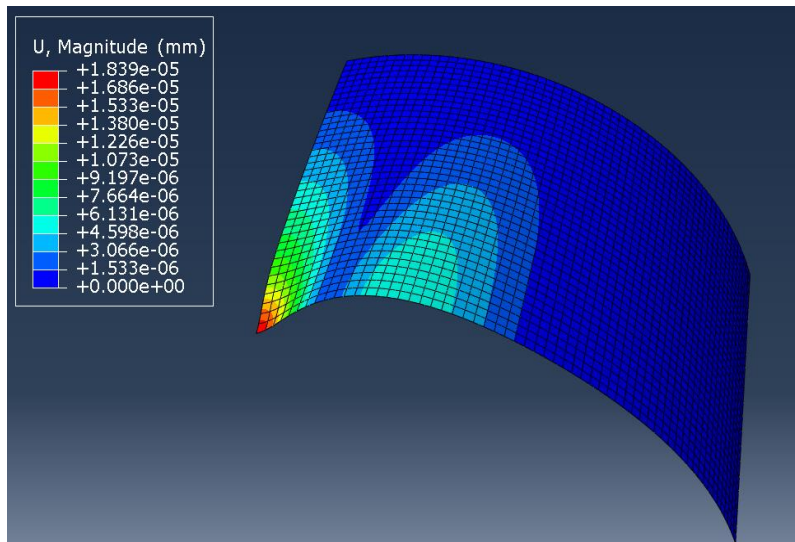
Figure 4.32 Total displacement results for pinched cylinder in Abaqus
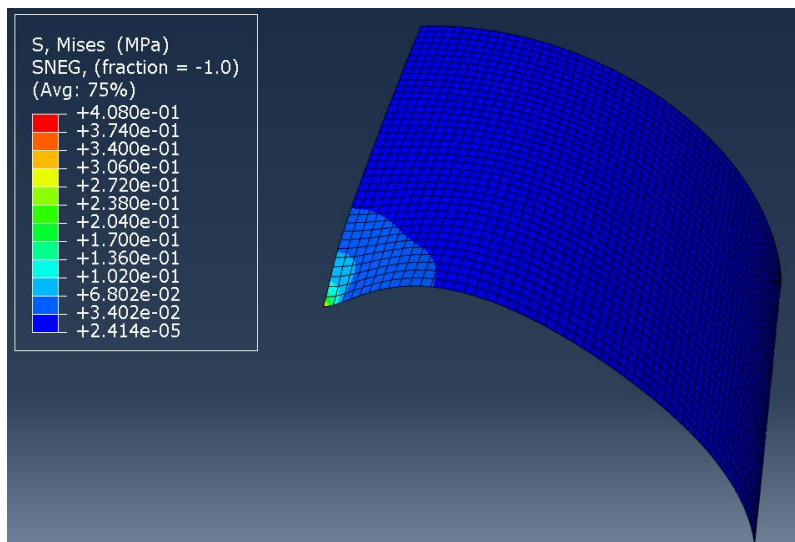
Figure 4.33 Total stress results for pinched cylinder problem in Abaqus

CHAPTER 5

APPLICATION OF ISOGEOMETRIC ANALYSIS TO PLASTICITY PROBLEMS

In this chapter, isogeometric analysis is applied to some plasticity problems which are; uniaxial loading, v-die bending and deep drawing. Materials are modeled as elastic-plastic material. Moreover, von Mises yield criterion and isotropic hardening are used. For solution process, a commercial finite element program LS-DYNA is used since its library has isogeometric shell elements. Finally, IGA results are compared with classical finite element analysis results which are conducted by using another software Abaqus.

5.1 Uniaxial Loading

5.1.1 Experiment

In order to determine anisotropic properties of materials, test sheets were produced along rolling direction (0°), diagonal direction (45°) and transverse direction (90°) of the material. Two different material types which are AISI 304 stainless steel and AA 2024 T3 aluminum were used in the experiments. For each direction and material type five parts were produced and hence totally thirty parts were employed during experiments in order to increase the reliability of the results. Dimensions of the parts are given in Figure 5.1 and some of the parts are shared in Figure 5.2. The part length, thickness and width dimensions were taken as 180 mm, 2mm and 20 mm respectively. However, at both ends of the parts additional parts with 30 mm length were spot welded to specimen to increase the thickness of the regions where machine jaws will grip. All specimens were cut by laser cutting machine and levelling performed on them to remove burrs. Directions of the specimen were drawn on them and all samples were numerated.
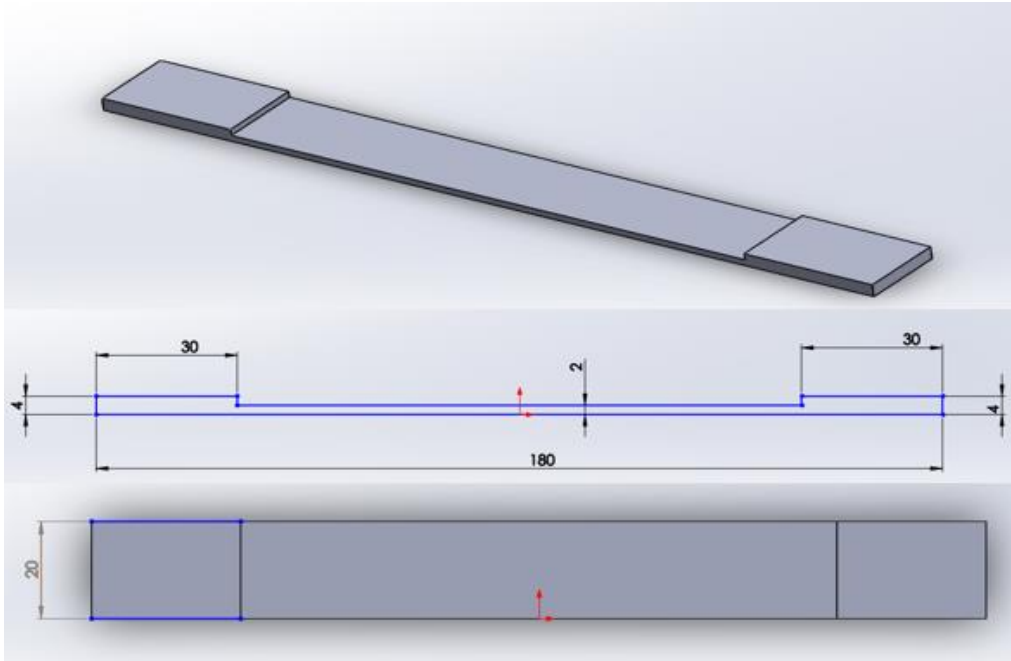
Figure 5.1 Tensile test specimen dimensions

Figure 5.2 Representation of test specimens before tests

Tension of the parts were performed by using Lloyd LR100K test machine that is able to apply maximum 100 kN tensile force.

Figure 5.3 Lloyd LR100K tension test machine

During the application of tensile loading, force and extension values were collected. Tests were continued until failure of the samples. Demonstrations of the failed specimens are shared in Figure 5.4.
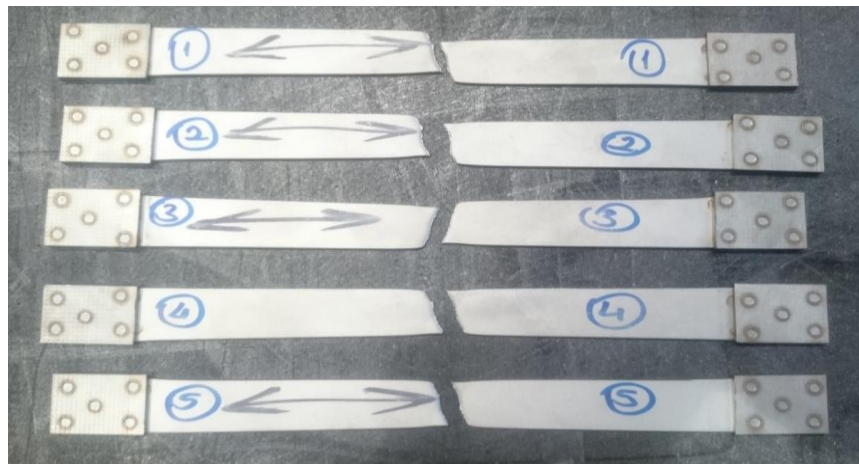
Figure 5.4 Representation of AISI 304 failed samples after tests

Mechanical properties; elastic modulus, Poisson's ratio, yield strength and ultimate tensile strength of materials obtained from the uniaxial loading process are given in Table 5.1.

Table 5.1 Mechanical properties of AISI 304 stainless steel and AA 2024 T3 aluminum

Mechanical Properties						
Material	AISI 304 Stainless Steel			AA 2024 T3 Aluminum		
Direction	0°	45°	90°	0°	45°	90°
Yield Strength (MPa)	277	265	272	335	328	330
Ultimate Tensile Strength (MPa)	675	630	653	466	441	455
Elastic Modulus (GPa)	193.8	187.4	191.3	74.3	73.1	73.5
Poisson's Ratio	0.29	0.27	0.29	0.33	0.33	0.33
Anisotropy (Lankford) Coefficient	0.94	1.39	0.88	0.73	0.96	0.81

True stress and strain graphs of the materials are given in Figure 5.5 and Figure 5.6 for AISI 304 stainless steel and AA 2024 T3 aluminum respectively.
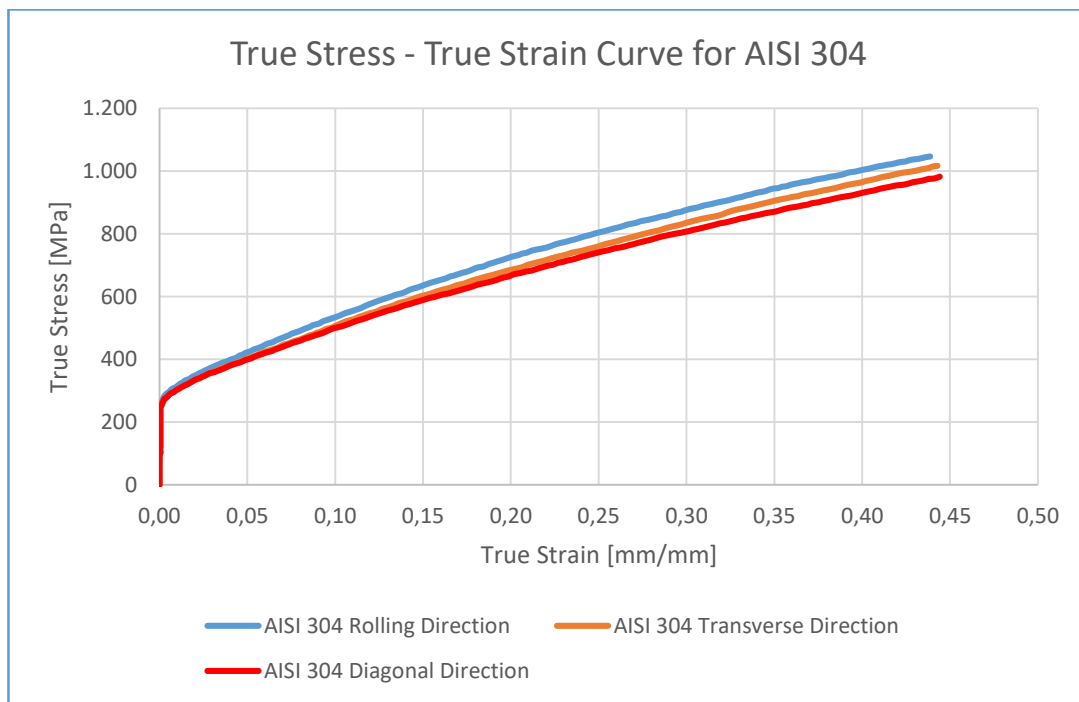
Figure 5.5 True stress versus true strain curve for AISI 304 stainless steel

Stress versus strain curves are close to each other for all directions of the AISI 304 material. Highest stress values were obtained in rolling direction for the same strain state. Transverse direction follows the rolling direction in terms of stress magnitude. Lowest stress amount is seen for diagonal direction.

108
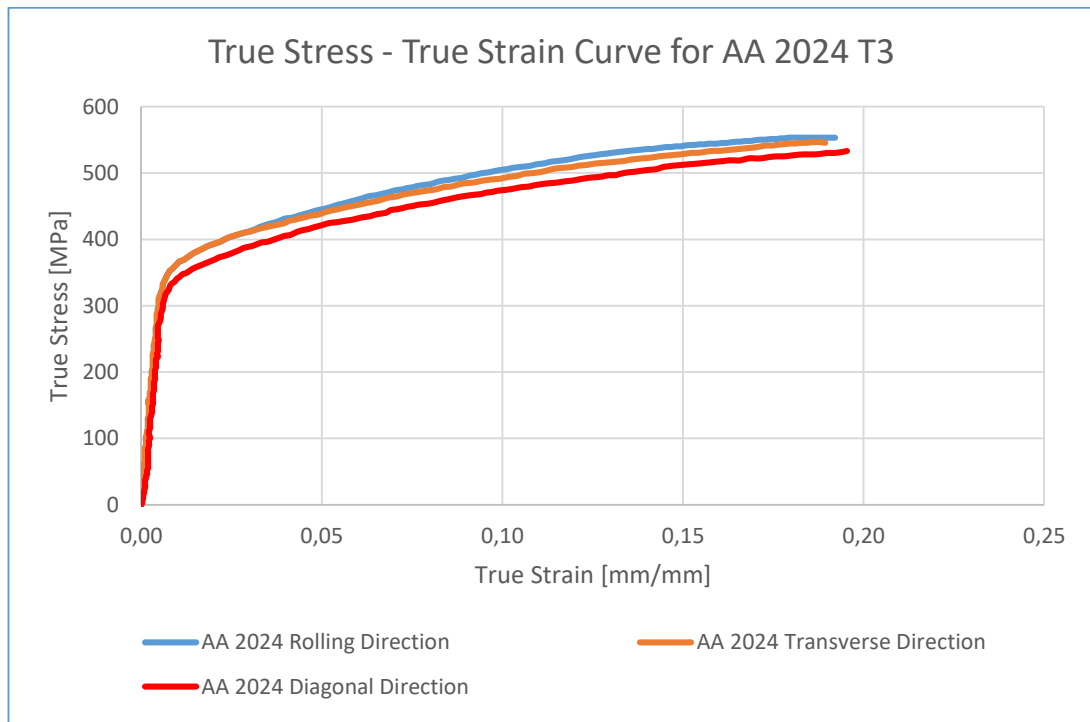
Figure 5.6 True stress versus true strain curve for AA 2024 T3 aluminum

Stress-strain curve for the aluminum 2024 T3 material showed also similar trend. Stress values are again greatest for rolling direction. Between the two remaining directions, transverse direction has greater stress values than diagonal direction.

5.1.2 Analyses

5.1.2.1 Finite Element Analysis

In this part, finite element analysis was used to simulate the tension of a sheet plate. Part has been modeled by using the dimensions given in Figure 5.1. For meshing of the part, 900 linear S4R shell elements were used. Material density, elastic modulus, Poisson's ratio was defined for elastic properties. Stress strain curve values were entered to define plastic behavior of materials. Data required to define AISI 304 stress-strain curve was taken from the study of A. Andrade-Campos et al. [84] and data for AA 2024 T3 was obtained from the study [85]. For boundary conditions, one end of the part was fixed while the other end of the material was pulled with a 25.4 mm/min velocity. The demonstration of necking for rolling direction of AISI 304 and chosen

element at middle of necking region to draw stress-strain curve is given in Figure 5.7. Stress-strain curve drawn by utilizing finite element analysis for this element is given in Figure 5.8.
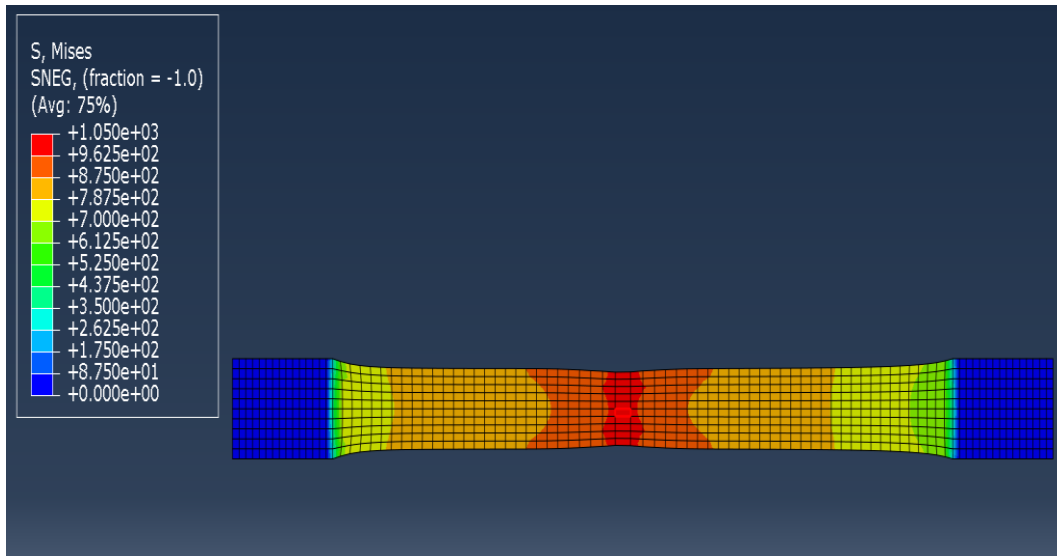
Figure 5.7 Total stress for FEA tensile test for AISI 304 rolling direction in MPa
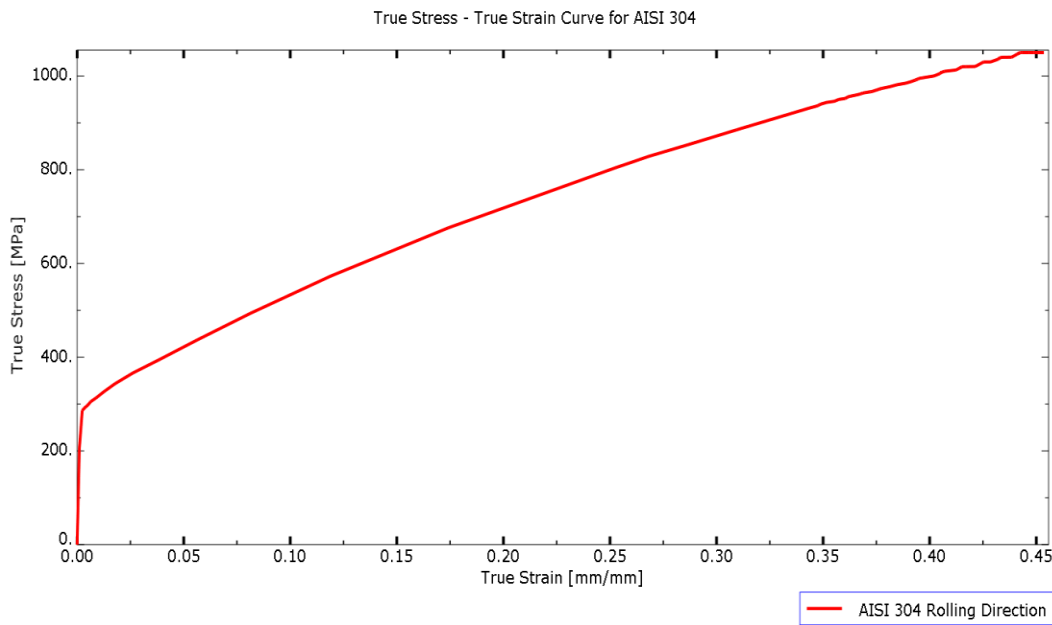
Figure 5.8 True stress versus true strain graph drawn for AISI 304 rolling direction using FEA results

5.1.2.2   Isogeometric Analysis

For the isogeometric analysis stage, part dimensions, material model and forming velocity values were taken same as the experiment and finite element analysis parameters. Material type of the part was defined as an elastic-plastic material by using "Piecewise Linear Plasticity" command of LS-DYNA. Throughout this study, all elements were defined using one patch. In order to numerically model the part, 836 elements have been used. The element type defined as Element_Shell_NURBS_Patch with quadratic order. By using this element type, a rectangular grid of control points was created and a NURBS surface was generated. This grid consisted of NPR times NPS control points where NPR and NPS are the number of control points in local r and s directions, correspond to longitudinal and transverse directions respectively. Necessary basis functions are defined through two knot vectors:

1- Knot-Vector in r-direction with length NPR + PR + 1 and
2- Knot-Vector in s-direction with length NPS + PS + 1

where PR and PS are the order of elements in r and s directions. Weight of the control points can also be specified during IGA meshing, otherwise, program automatically assign unity value for all control points which creates a B-Spline surface. Another point that should be noted is creation of additional element type called as interpolation shell elements for result visualization. Results are given by using these interpolation elements instead of shell NURBS patch elements.

After the analysis, one element was chosen at the mid-section of necking region to get stress-strain curve. The demonstration of necking for the rolling direction analysis of AISI 304 is given in Figure 5.9. Moreover, stress-strain curve drawn for selected element is given in Figure 5.10.

5.1.3   Comparison of the Results

By observing the results for AISI 304 in the rolling direction it is seen that isogeometric analysis and finite element analysis results are close to each other and
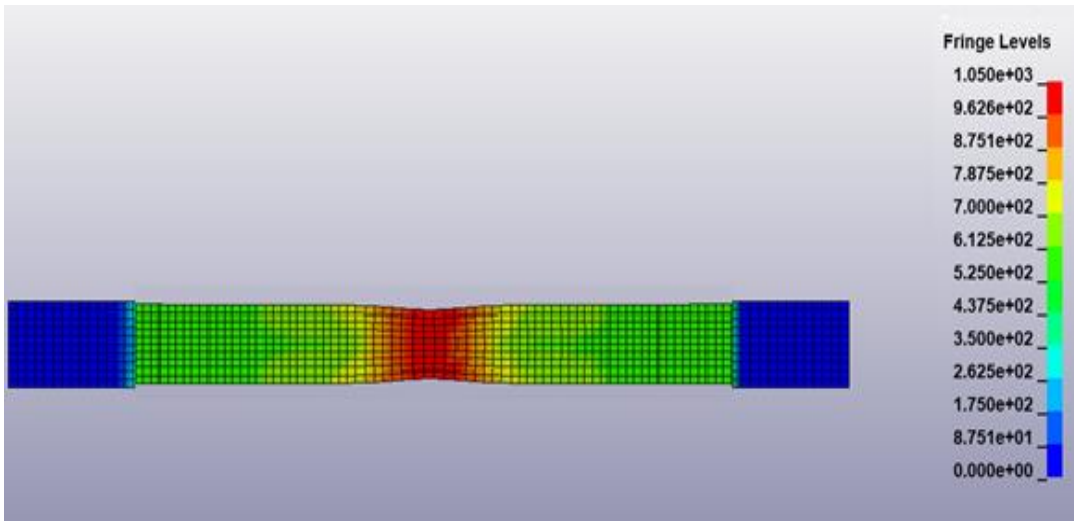
Figure 5.9 Total Stress for IGA tensile test for AISI 304 rolling direction in MPa
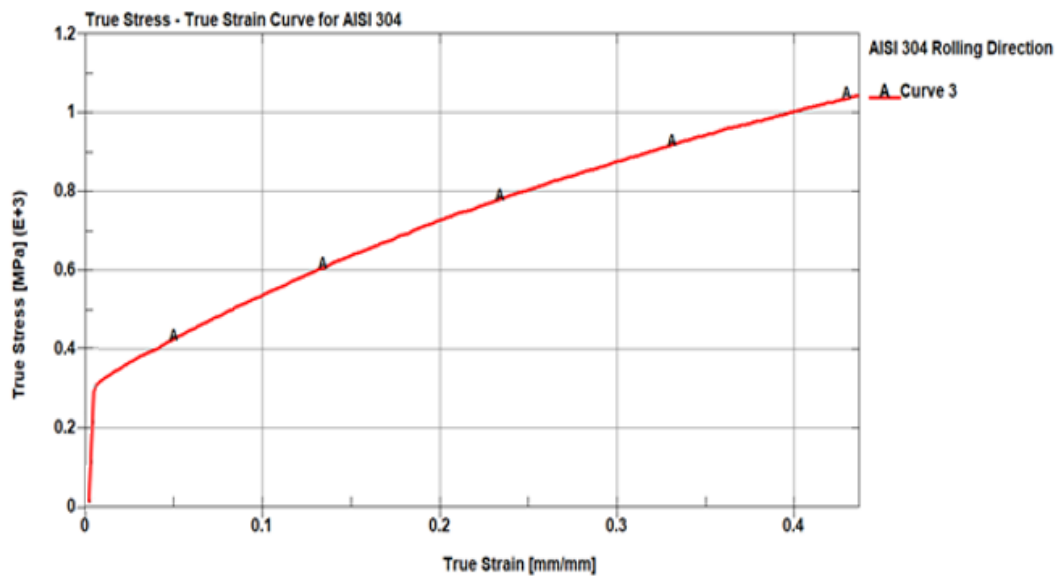
Figure 5.10 True stress versus true strain graph drawn for AISI 304 rolling direction using IGA results

compatible with stress-strain curves obtained from the experiments. Computational times of both methods were near to each other for this quasi-static analysis. In addition to the rolling direction, analyses were also performed for $45°$ and $90°$ directions of AISI 304 and for $0°$, $45°$ and $90°$ directions of AA 2024 T3. For all cases, analyses results and experiment results overlapped. Comparison of these results which belongs to AISI 304 rolling direction is given in Figure 5.11.

112

True Stress - True Strain Curve for AISI 304 0° Direction
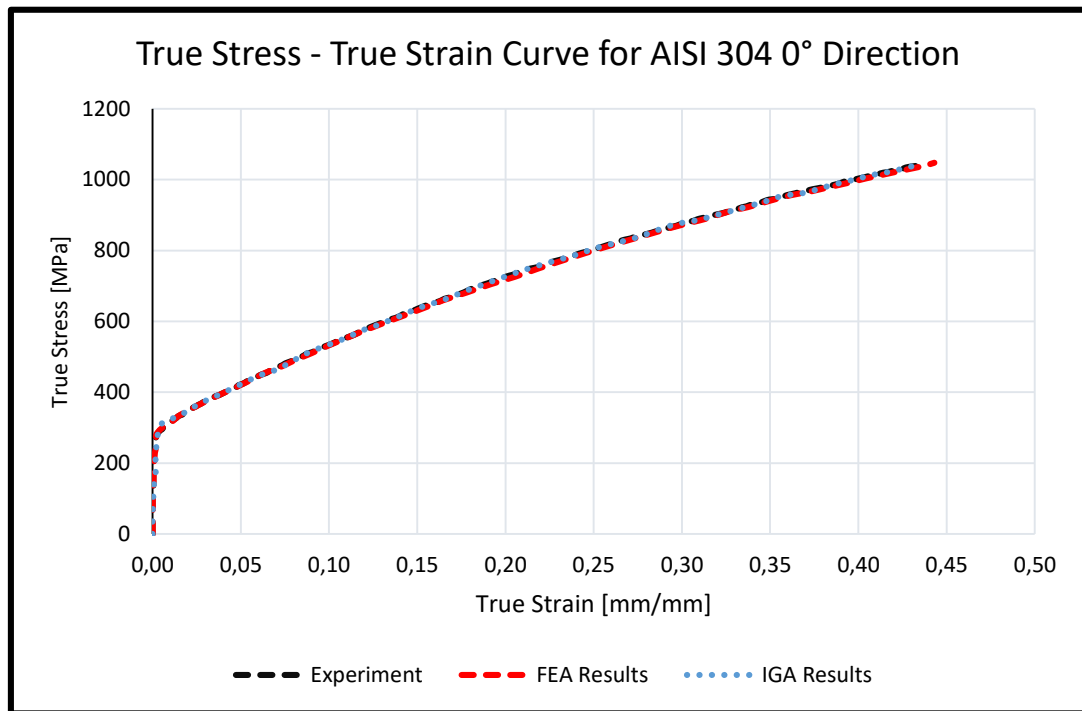
Figure 5.11 Comparison of experiment, IGA and FEA results for AISI 304 rolling direction

5.2 V-Die Bending

5.2.1 V-Die Bending Experiment

V-Die bending tests were conducted by using CNC controlled "Baykal APHS 26090" hydraulic bending press that can apply 900 kN bending load. Machine is shown in Figure 5.12. Two kinds of materials were chosen as specimen materials which are AA 2024 T3 aluminum and AISI 304 stainless steel. Dimensions of the samples were taken as 100 mm length x 40 mm depth. The thickness of the blank was 1 mm for both kinds of materials. Specimens were cut by laser cutting process along rolling direction, 45° from rolling direction and along transverse directions as given in Figure 5.13. Three specimens for each direction of different material types were produced and hence totally 18 specimens were used.

Figure 5.12 Hydraulic bending press used during experiments

Before the application begins, grease was applied on blank, die and punch to decrease friction between tools and workpiece. During the experiments, the utmost attention has been paid to reducing the factors that affect the experiment results such as dirt, dust and heat etc. Punch and die representations are given in Figure 5.14 and their dimensions are given in Figure 5.15.
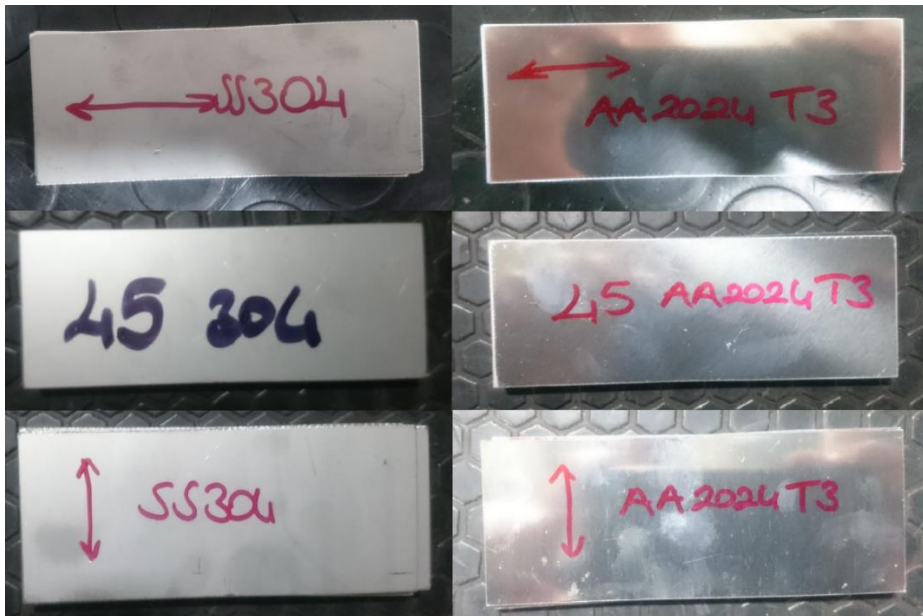
Figure 5.13 Test specimens AISI 304 and AA 2024 in three different directions
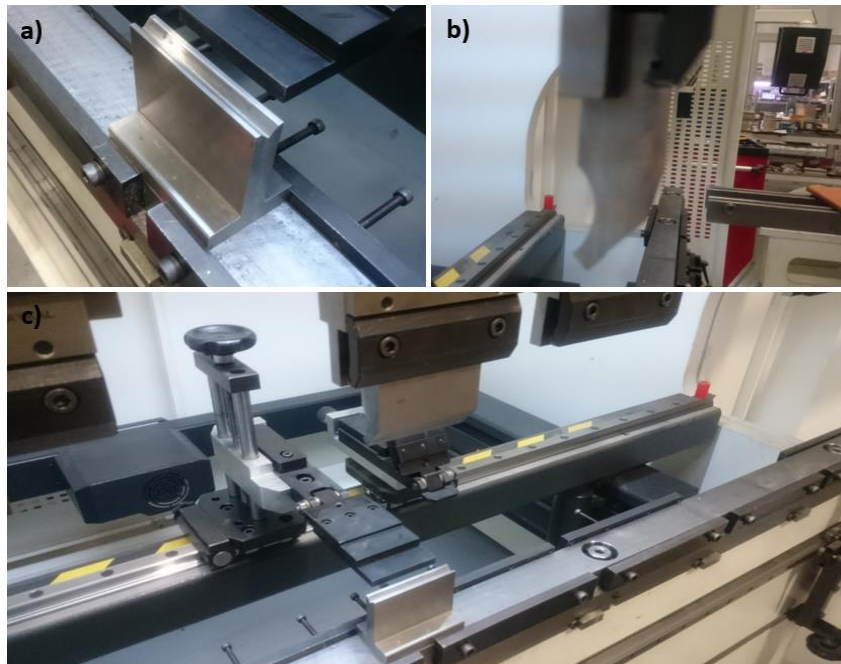
Figure 5.14 Representation of punch and die a) Die b) Punch c) Die and punch together
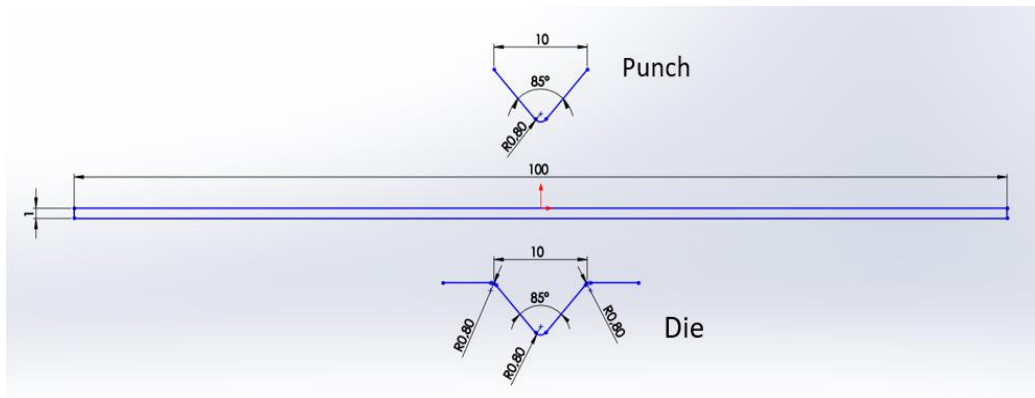
Figure 5.15 Die and punch dimensions

Experiments were performed for three different bending angles: 90°, 120° and 135° as given in Figure 5.16. Punch stroke required to give specified bend angles were automatically calculated by CNC hydraulic machine as; 4 mm, 2,58 mm and 1,95 mm. Although, AISI 304 steel could be bent in all selected angles, aluminum has cracked for 90°. The failed figure of the aluminum is given in Figure 5.17. After bending operations have finished, bent angle of each part was measured by using a profile projector with 0.01° resolution. Results are given in Table 5.2.

Figure 5.16 Specimens after bending operation
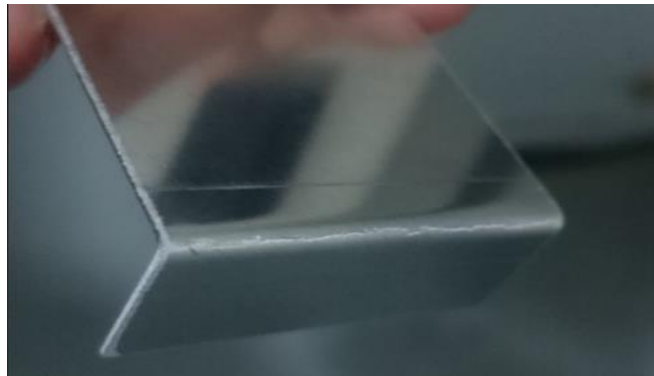
Figure 5.17 AA 2024 T3 failure for 90° bent angle

From the experiments, some conclusions can be drawn as listed below.

- For the same bending angle AISI 304 has greater spring-back than AA 2024 T3 material.
- As bending angle increases, spring-back amount decreases for both kinds of materials.
- Spring-back amount is greater for rolling direction due to the fact that material yield strength is greater in this direction.

Table 5.2 V-Die bending experiments

Bending Angle	Material	Specimen 1	Specimen 2	Specimen 3	Average Degree	Spring-back
90°	AISI 304 (0°)	93.34°	93.16°	93.45°	93.32°	3.32°
120°	AISI 304 (0°)	122.85°	122.54°	122.88°	122.76°	2.76°
135°	AISI 304 (0°)	137.07°	137.42°	137.64°	137.38°	2.38°
90°	AISI 304 (45°)	92.45°	92.21°	93.06°	92.57°	2.57°
120°	AISI 304 (45°)	122.08°	122.13°	122.00°	122.07°	2.07°
135°	AISI 304 (45°)	136.59°	136.94°	136.91°	136.81°	1.81°
90°	AISI 304 (90°)	93.12°	93.05°	92.96°	93.04°	3.04°
120°	AISI 304 (90°)	122.28°	122.39°	122.28°	122.32°	2.32°
135°	AISI 304 (90°)	137.82°	137.04°	136.53°	137.13°	2.13°
120°	AA 2024 (0°)	121.89°	121.63°	121.82°	121.78°	1.78°
135°	AA 2024 (0°)	136.50°	136.84°	136.49°	136.61°	1.61°
120°	AA 2024 (45°)	121.61°	121.40°	121.27°	121.43°	1.43°
135°	AA 2024 (45°)	136.16°	136.42°	136.30°	136.29°	1.29°
120°	AA 2024 (90°)	122.00°	121.38°	121,57°	121.65°	1.65°
135°	AA 2024 (90°)	136.12°	136.86°	136.72°	136.57°	1.57°

5.2.2 V-Die Bending Analyses

5.2.2.1 Finite Element Analysis

The first of the v-die bending analyses was finite element method application. The models have been created by taking the dimensions given in Figure 5.15. Created models and their assembly are given in Figure 5.18. AISI 304 stainless steel and

aluminum 2024 temper 3 materials were defined by using their stress versus plastic strain values. Additionally, anisotropy coefficients of materials were also introduced to software. In order to simulate three different bending angle, three different punch displacements were given to program as obtained via experiments. Coefficient of friction between steel tools and steel blank was taken as 0.144 while for aluminum blank it is taken as 0.162. [86]
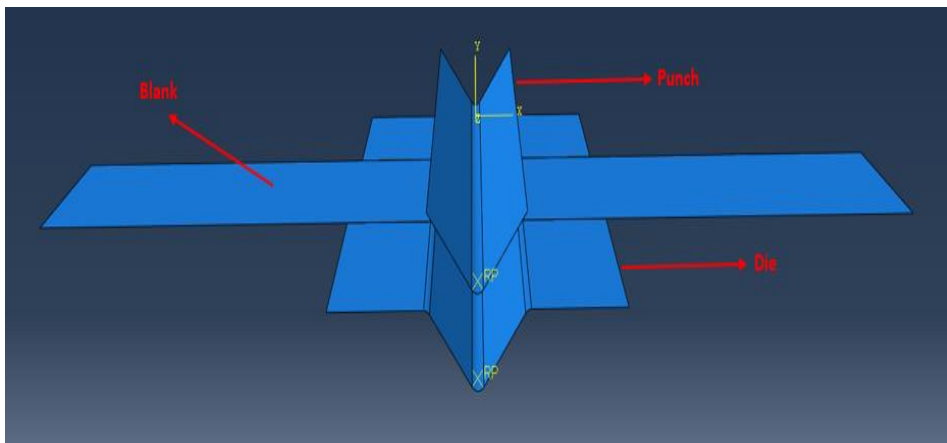
Figure 5.18 Assembled model of v-die bending process

Symmetry boundary conditions have not been used in these analyses to see the whole model. Fixed boundary condition was defined for die and only one direction of the motion of punch which is towards the piece has been left as free.

The punch and die were defined as discrete rigid bodies while blank was created as a deformable part. In order to numerically model punch and die; 720 and 1860 R3D4 (4-node 3-D bilinear rigid quadrilateral) discrete rigid elements were used, respectively. On the other hand, for meshing of blank part, 1947 linear S4R reduced integration, hourglass controlled shell elements were used. This element number for blank was attained after applying a sensitivity analysis and beyond these element numbers, no difference was observed on the analysis results. Regions of the blank that is in contact with punch and die were finely meshed. Coarse mesh was assigned for other regions. Meshed parts were represented in Figure 5.19.
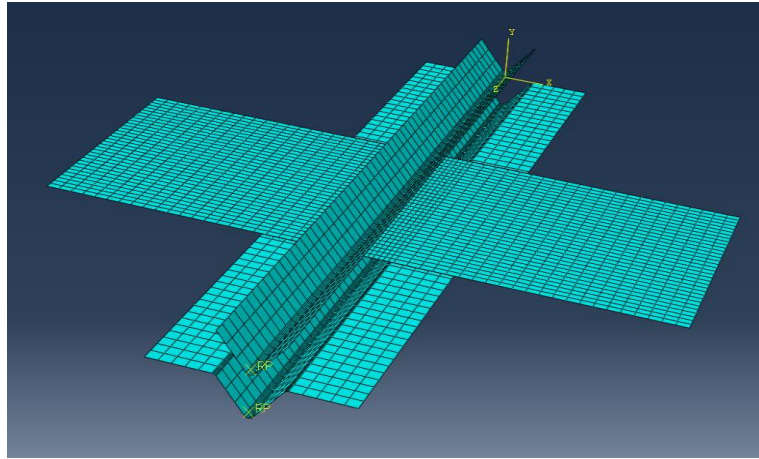
Figure 5.19 Meshed assembly of the v-die bending process

Analysis results were evaluated in terms of bending angles of parts. The demonstration of bent AISI 304 part for 90° is given in Figure 5.20 and U2 represents upward displacement in mm. Moreover, the stress distribution is shown in Figure 5.21. A geometric approach has been used to accurately measure bending angle. Total of four points were selected, two from each side of the part. The coordinates of these points were taken from analysis program and two lines were drawn for each point group. Finally, angle between these lines has been measured. Selected points for drawing mentioned lines corresponds to nodes 97,110,151 and 164 respectively and represented in Figure 5.21. The coordinates of these points are given in Table 5.3.
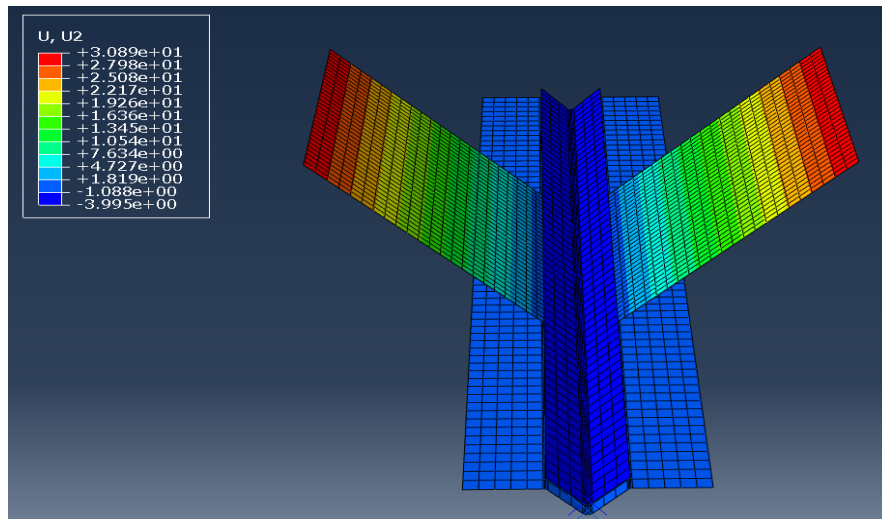
Figure 5.20 90° bent AISI 304 specimen
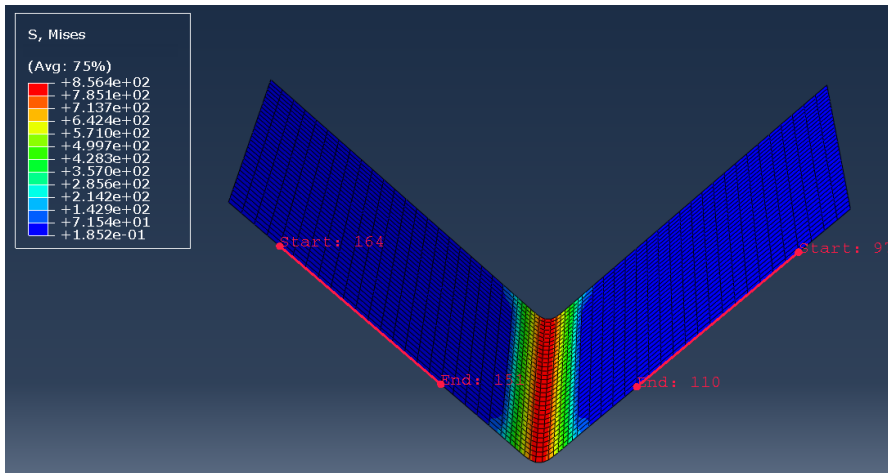
Figure 5.21 Selected nodes/points and total stress scale in MPa

Table 5.3 Coordinates of selected points for FEA spring-back measurement

Point	Corresponding Node	X Coordinate	Y Coordinate
1	97	3.00349e+001	2.57223e+001
2	110	1.16545e+001	7.33061e+000
3	151	-1.16529e+001	7.33249e+000
4	164	-3.00282e+001	2.57283e+001

Line 1 passes through points 1 & 2 (nodes 97 & 110) and Line 2 passes through points 3 & 4 (nodes 151 & 164). Representations of the lines and angle measurement between these lines is shown in Figure 5.22.
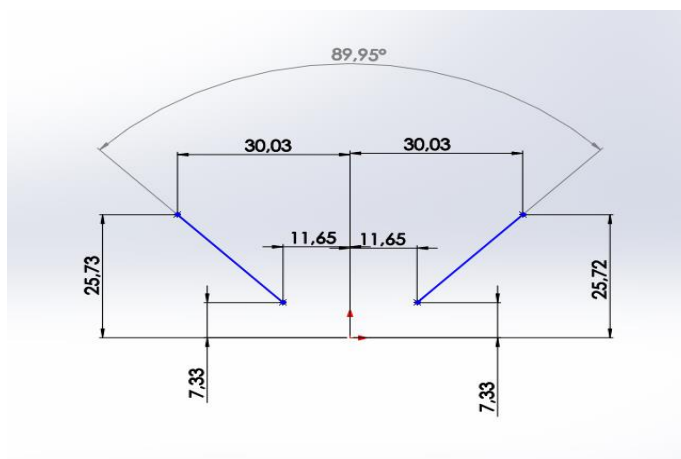
Figure 5.22 Bending angle measurement

120

Finally, after bending simulation with FEA, 89.95° bend angle was obtained which has only 0.05 degree deviation from 90° bending. For the rest of the bending operations same procedure was followed for angle calculation and 90,120 and 135 degrees obtained as results of analyses. Therefore, entered punch stroke values were evaluated as correct for desired bending angles.

Important point for bending analysis is the spring-back consideration. After the bending operation, pieces undergo some amount of spring-back and this is generally dealt with by manufacturers with trial and error productions. However, this method causes consumptions of both time and material. On the other hand, this spring-back phenomenon can be analyzed through simulations for arranging punch motion and other parameters accordingly to obtain desired shape. At this point, the importance of correct analysis of spring-back amount comes into prominence. Therefore, after the first stage bending analysis, second stage analysis was conducted as a spring-back analysis. Spring-back analysis was carried out by importing deformed shape of the previously conducted bending analysis to new analysis as initial model without applying any loads. Analysis duration was defined to program and during this time elastic deformation was waited to be retrieved. Although explicit dynamic analysis was used for bending analysis it cannot be used for spring-back analysis since the objective is to obtain a static spring-back solution, free from dynamic oscillations. Therefore, static analysis was run for spring-back analysis. Result of the analysis is given in Figure 5.23 in terms of displacement along longitudinal direction in mm.

As can be seen from spring-back analysis results, ends of the part experiences nearly 1.46 mm displacement along longitudinal direction in opposite directions and due to this displacement bent angle increases. Final angle between the two sides of the part was calculated again using previously mentioned approach. After this application, final angle was found as 95°. These analyses were conducted for other material types for defined bending angles. However, in the name of clarity their results have been tabulated at Table 5.4 and not given with figures.
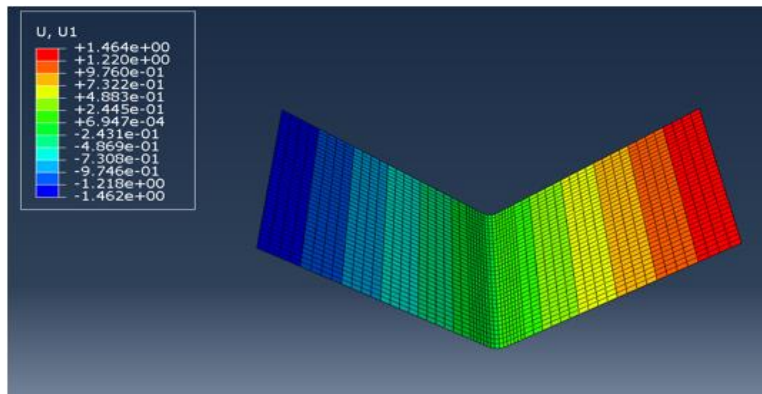
Figure 5.23 Spring-back analysis of the deformed part

Table 5.4 Bending angle and spring-back results obtained by FEA

Bending Angle	Material	Bending Analysis Result	Spring-back Analysis Result	Spring-back	Error (%)
90°	AISI 304 (0°)	89.95°	94.99°	5.04°	51.81
120°	AISI 304 (0°)	120.06°	123.72°	3.66°	32.61
135°	AISI 304 (0°)	135.14°	138.25°	3.11°	30.67
90°	AISI 304 (45°)	90.27°	94.71°	4.44°	72.76
120°	AISI 304 (45°)	120.12°	123.49°	3.37°	62.80
135°	AISI 304 (45°)	135.50 °	138.39°	2.89°	59.67
90°	AISI 304 (90°)	90.04°	94.73°	4.68°	53.95
120°	AISI 304 (90°)	119.82°	122.98°	3.16°	36.20
135°	AISI 304 (90°)	135.31 °	138.06°	2.75°	29.11
120°	AA 2024 (0°)	120.26°	122.51°	2.25°	26.40
135°	AA 2024 (0°)	134.88°	136.84°	1.96°	21.58
120°	AA 2024 (45°)	120.32°	122.23°	1.91°	33.57
135°	AA 2024 (45°)	135.24°	136.91°	1.67°	29.46
120°	AA 2024 (90°)	119.93°	121.96 °	2.03°	23.03
135°	AA 2024 (90°)	135.16°	137.05°	1.89°	20.38

5.2.2.2   Isogeometric Analysis

Every parameter of the isogeometric analysis; tool dimensions, blank dimensions, material models, punch strokes and friction coefficient values were taken same as experiment and finite element analysis parameters. As in the FEA, the punch and die

were defined as discrete rigid bodies and blank was defined as deformable part. In order to eliminate the effect of punch and die element sizes, they were taken as same with sizes used for finite element analysis. Therefore, punch and die were modeled by using 720 and 1860 elements respectively. Rigid material property (Mat_Rigid) has been assigned to these elements. For these parts, element formulation is defined as Belytschko-Tsay shell element that based on Reissner-Mindlin theory. On the other hand, blank has been modeled by using one NURBS patch which was discretized uniformly into 1219 elements by using Element_Shell_NURBS_Patch element type which is defined for isogeometric analysis. This element number has been determined by applying a sensitivity analysis as given in Figure 5.28. Order of the NURBS elements used for blank was chosen to be cubic.
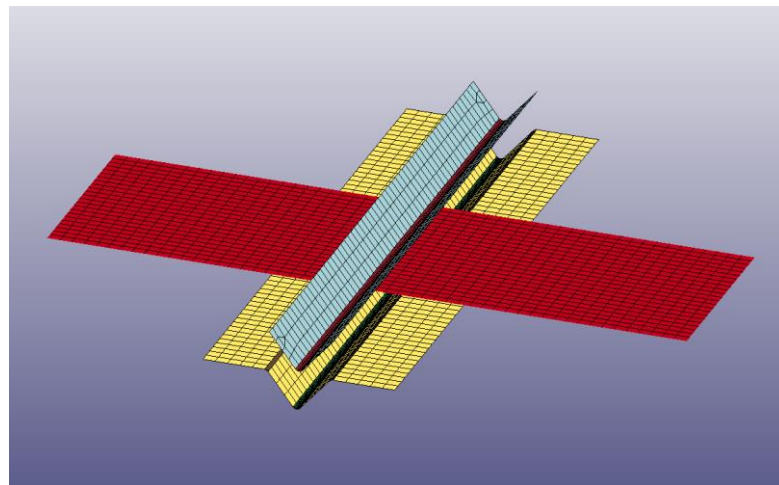
Figure 5.24 Meshed representation of v-die bending assembly at LS-DYNA

As in the finite element analysis case, analysis results were evaluated according to final bending angle. For this purpose, again previously mentioned geometric approach was used. Analysis stages were divided into two parts. First one was performed to evaluate first bending angle and the second one was carried out to get angle after spring-back. The demonstration of bent AISI 304 part for 90° is given in Figure 5.25. Selected points on the part to draw lines for angle measurement are also shown in Figure 5.26.
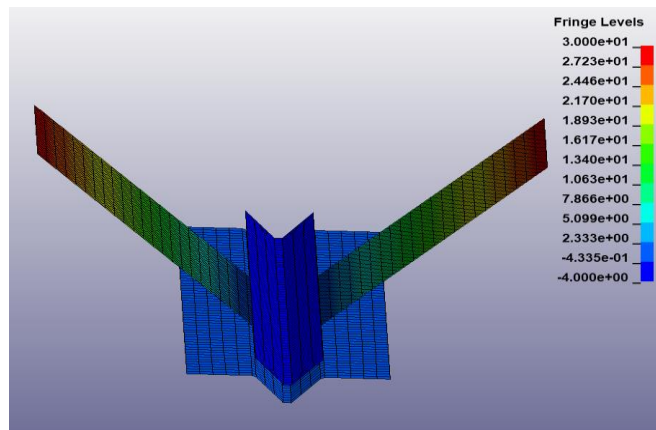
Figure 5.25 90° bent AISI 304 specimen and displacement scale
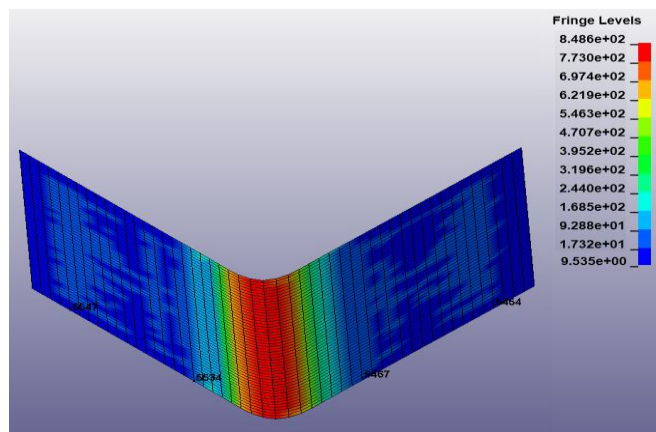
Figure 5.26 Selected nodes/points and total stress scale in MPa

After obtaining the 90° bent shape with first stage analysis, spring-back analysis has been conducted as a second stage analysis. Spring-back amounts were determined by using the same angle measurement procedure and selected points for this aim are represented in Figure 5.27 which also shows displacement amounts experienced by part during spring-back. Coordinates of selected points are also shared in Table 5.5.

Table 5.5 Coordinates of selected points for IGA spring-back measurement

Point	Corresponding Node	X Coordinate	Y Coordinate
1	107	-34.8153	28.6508
2	83	-12.5511	7.60674
3	1444	13.478	8.4813
4	1421	34.8236	28.6395
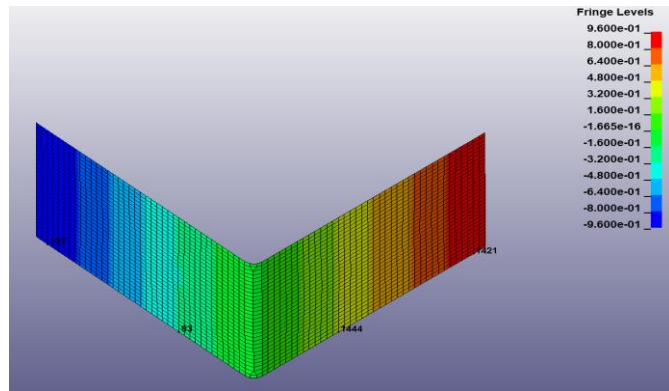
Figure 5.27 Total Displacement result of spring-back analysis

The spring-back amount was found for 90° bending of AISI 304 steel for rolling direction as 3.11°. This process has been repeated for all material and bending angle combinations. Results are tabulated in the Table 5.6.

Table 5.6 Bending angle and spring-back results obtained by Isogeometric Analysis

Bending Angle	Material	Bending Analysis Result	Spring-back Analysis Result	Spring-back	Error (%)
90°	AISI 304 (0°)	90.07 °	93.18°	3.11°	6.32
120°	AISI 304 (0°)	119.96°	122.62°	2.66°	3.62
135°	AISI 304 (0°)	135.10 °	137.55°	2.45°	2.94
90°	AISI 304 (45°)	90.12°	92.91°	2.79°	8.56
120°	AISI 304 (45°)	120.05 °	122.26°	2.21°	6.76
135°	AISI 304 (45°)	135.11 °	137.03°	1.92°	6.08
90°	AISI 304 (90°)	90.17°	93.39°	3.22°	5.91
120°	AISI 304 (90°)	120.02°	122.43°	2.41°	3.88
135°	AISI 304 (90°)	134.94 °	137.15°	2.21°	3.76
120°	AA 2024 (0°)	120.14°	122.05°	1.91°	7.30
135°	AA 2024 (0°)	135.27°	136.99°	1.72°	6.83
120°	AA 2024 (45°)	120.06°	121.61°	1.55°	8.39
135°	AA 2024 (45°)	135.22°	136.61°	1.39°	7.72
120°	AA 2024 (90°)	120.15°	121.91 °	1.76°	6.67
135°	AA 2024 (90°)	134.97°	136.64°	1.67°	6.37

5.2.3 Comparison of the V-Die Bending Results

By examining the results of the experiment and analyses it can be said that, isogeometric analysis is by far more successful than finite element analysis in estimating spring-back amounts. The error values for isogeometric analyses are relatively low. As a general trend, analyses methods better evaluate the spring-back for higher bending angles and for rolling and transverse directions. In addition to more accurate results, isogeometric analysis method also decreases the run time of analyses and required element numbers. Sensitivity analyses conducted to obtain minimum required element number to get accurate results are given in Figure 5.28. In these sensitivity analyses, errors were taken from spring-back error values of AISI 304 along 90°.
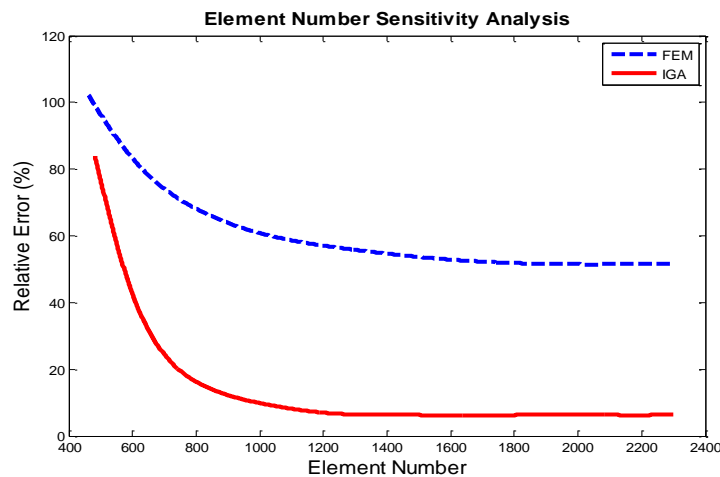
Figure 5.28 Element number sensitivity analysis for AISI 304 along rolling direction for 90° bending

In order to evaluate computation times given in Table 5.7 correctly, it is useful to know computer properties. Analyses were performed on a computer with system specifications as follows, 8 cores with Intel Core i7-6700HQ 2.6 GHz processor.

Table 5.7 Equivalent stress and plastic strain values for both FEA and IGA with computation time

Material	Bending Angle	Max Von-Mises Stress FEA (MPa)	Max. Plastic Strain FEA (mm/mm)	Max. Von-Mises Stress IGA (MPa)	Max. Plastic Strain IGA (mm/mm)	Total Comp.Time FEA (min.)	Total Comp.Time IGA (min.)	Relative Time Saving (%)
AISI 304 (0°)	90°	856.4	0.289	848.6	0.276	79	54	31.6
AISI 304 (0°)	120°	819.0	0.262	811.7	0.257	48	35	27.1
AISI 304 (0°)	135°	788.9	0.227	773.0	0.214	41	26	36.6
AISI 304 (45°)	90°	812.7	0.309	803.1	0.297	83	51	38.6
AISI 304 (45°)	120°	768.2	0.268	762.4	0.254	46	33	28.3
AISI 304 (45°)	135°	741.6	0.257	734.6	0.248	40	25	37.5
AISI 304 (90°)	90°	851.6	0.371	844.9	0.363	78	53	32.1
AISI 304 (90°)	120°	816.1	0.306	807.4	0.295	48	36	25.0
AISI 304 (90°)	135°	782.8	0.277	770.2	0.268	40	22	45.0
AA 2024 (0°)	120°	550.3	0.186	542.8	0.173	35	25	28.6
AA 2024 (0°)	135°	524.6	0.177	519.4	0.171	26	19	26.9
AA 2024 (45°)	120°	532.0	0.192	523.3	0.184	37	24	35.1
AA 2024 (45°)	135°	509.7	0.179	502.0	0.167	28	18	35.7
AA 2024 (90°)	120°	547.4	0.188	541.9	0.179	35	27	22.9
AA 2024 (90°)	135°	520.1	0.164	514.6	0.155	23	18	21.7

5.3 Deep Drawing

In this part, square deep drawing process is introduced by investigating some of the process parameters and results.

5.3.1 Square Deep Drawing Experiment

The experimental results were taken from the study of Danckert, Joachim [86]. Experiment in the Danckert's study had been performed as a part of an international benchmark presented at the NUMISHEET 1993 conference. Properties of the mild steel used in this study has been given in Table 5.8. The stress-plastic strain relation of the material is given by the Swift law:

$$\sigma = 565.32(0.007117 + \varepsilon_p)^{0.2589} \tag{5.1}$$

For this square deep drawing process, geometries and dimensions of the used die and punch set are given in Figure 5.29. Dimensions of the blank was given as 150x150 mm width and depth while its thickness has been taken as 0.75 mm. In the paper, the friction coefficient is defined as $\mu = 0.144$ for steel to steel contact case where punch, die and blank holder materials are also specified as tool-steel AISI A2 material hardened to 60 HRc. In the tests; 15 and 40 mm punch travels had been utilized. During the process, nearly 19.5 kN blank holder force was used for both 15 mm and 40 mm punch travels.

Table 5.8 Properties of mild steel material

Direction	Yield Strength (MPa)	Tensile Strength (MPa)	E (GPa)	v	n	r	ρ (g/cm^3)
0°	167.0	308.5			0.238	1.79	
45°	176.5	316.0	206	0.3	0.239	1.51	7.8
90°	172.5	305.0			0.222	2.27	
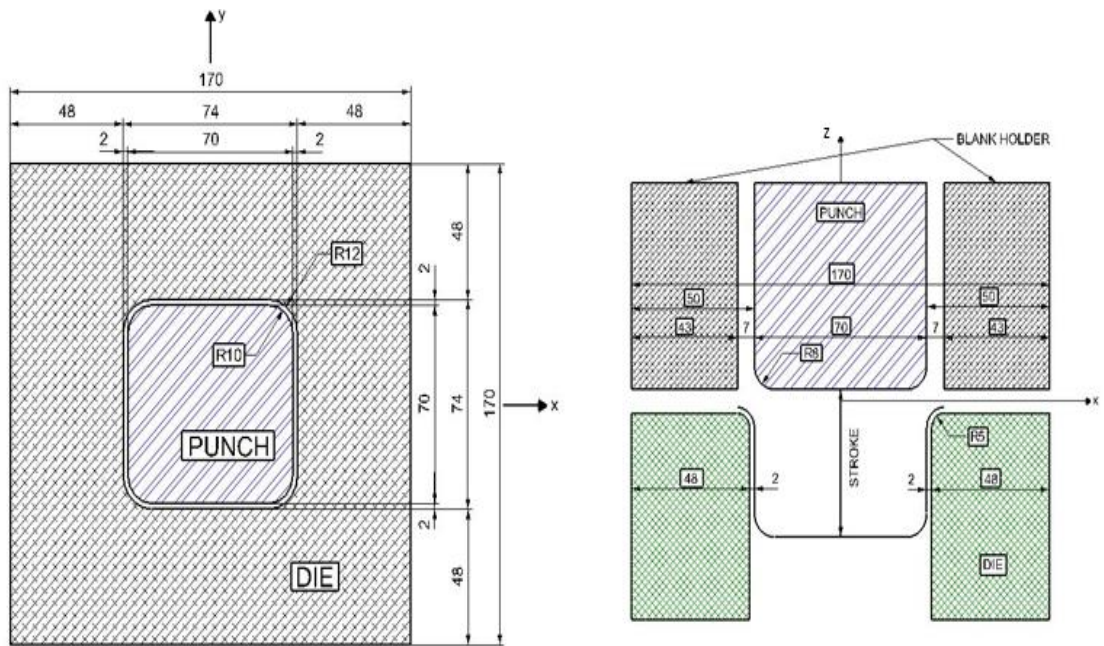
Figure 5.29 Schematic illustration of the deep-drawing tool for the square deep drawing [86]

The thickness strains are given in the directions named as OA, OB and OC directions and shared through Figure 5.31 and Figure 5.33.
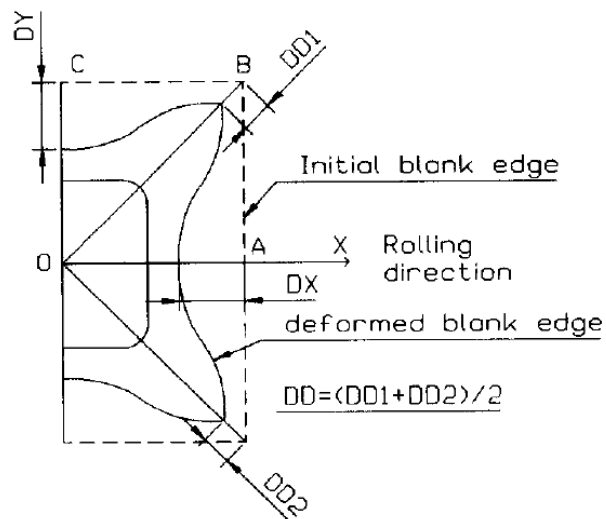
Figure 5.30 Strain calculation directions [86]
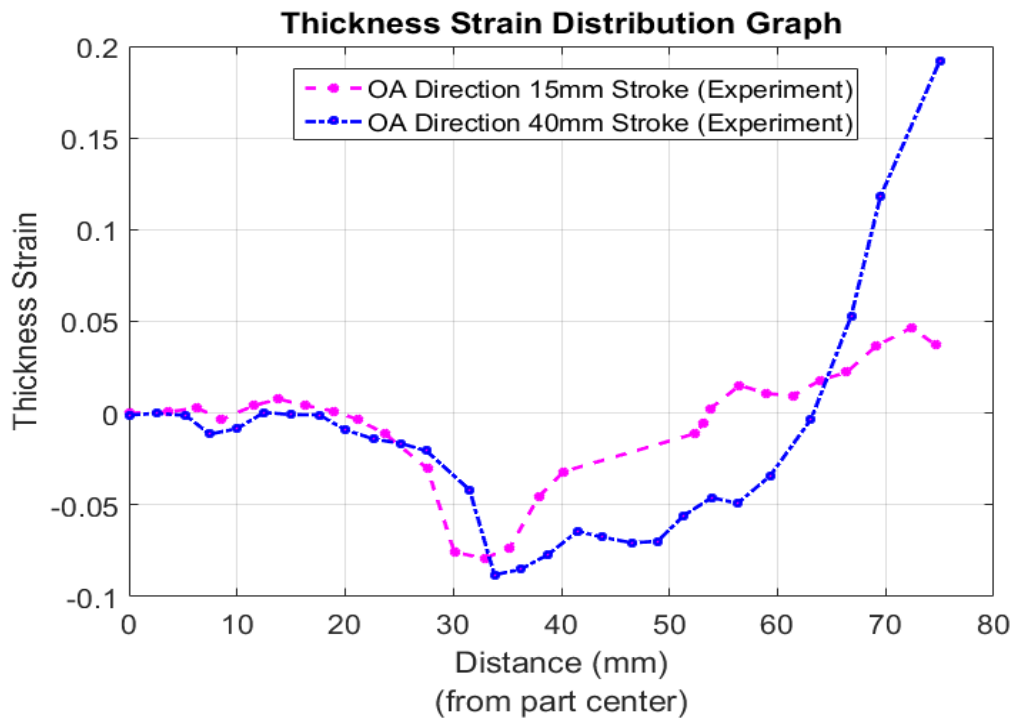
Figure 5.31 Thickness strain distributions along OA direction for 15 mm and 40 mm punch strokes constructed during the experiment
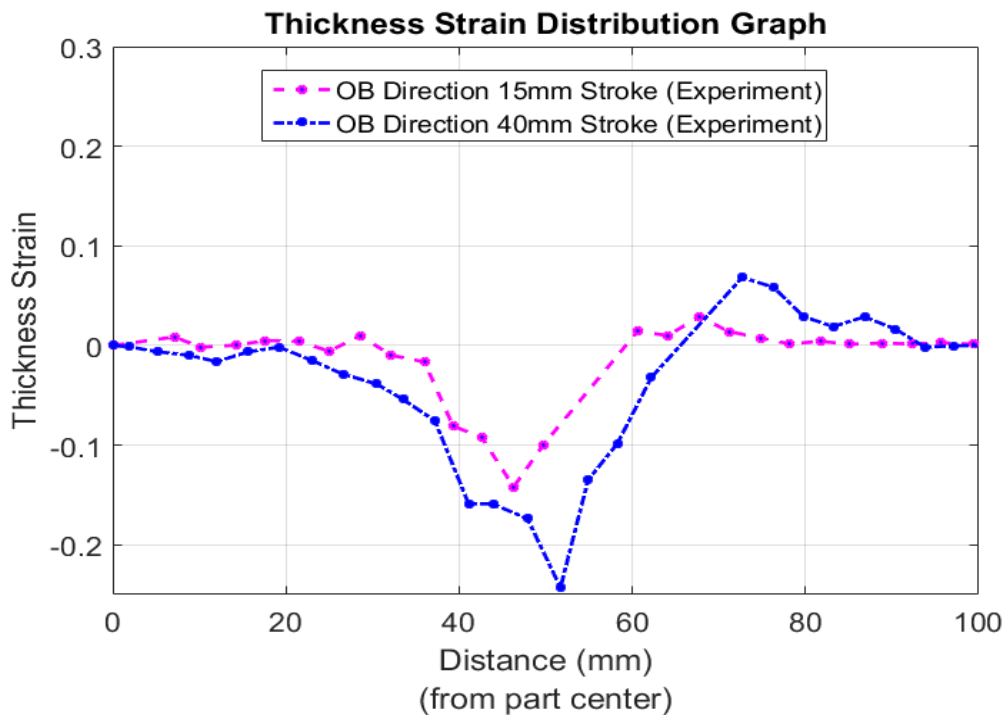
Figure 5.32 Thickness strain distributions along OB direction for 15 mm and 40 mm punch strokes constructed during the experiment
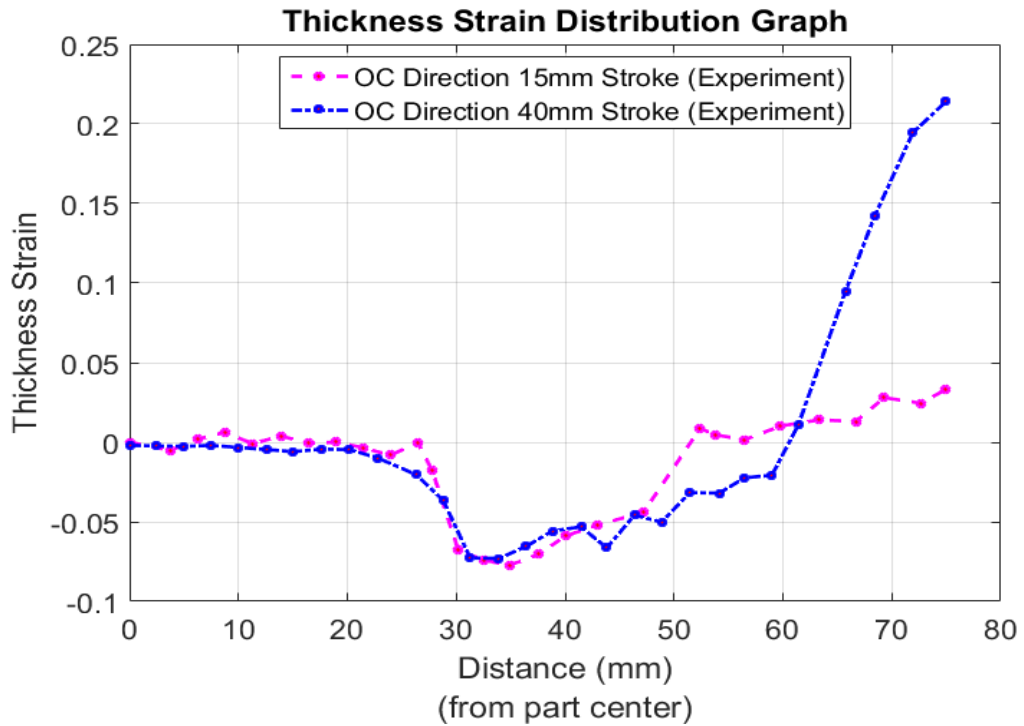
Figure 5.33 Thickness strain distributions along OC direction for 15 mm and 40 mm punch strokes constructed during the experiment

5.3.2   Square Deep Drawing Analyses

In this part of the study, analyses were performed to simulate same square deep drawing process given in previous experiment section with the same dimensions, material, punch stroke, blank-holder force and friction coefficients. Classical finite element method approach and isogeometric analysis approach were used as two different numerical techniques during these analyses.

5.3.2.1 Finite Element Analysis

While conducting finite element analysis, the material has been modeled as elasto-plastic material by using properties obtained from Table 5.8 and from formula 5.1. Two different punch strokes were investigated as 15 mm and 40 mm. Only quarter of the components was modeled. The representation of assembled and exploded models are shown in Figure 5.34.
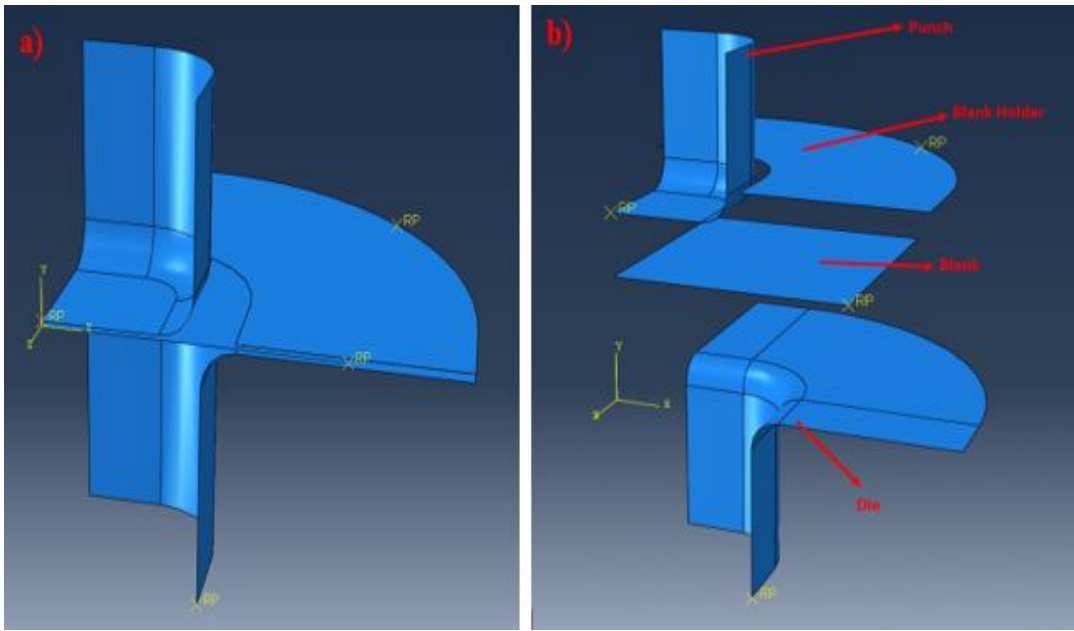
Figure 5.34 a) Assembled view and b) Exploded view of model for square deep drawing analysis

As previously used in experiment phase, 19.5 kN blank holder force was applied onto blank. Coefficient of friction between parts was taken as 0.144 to represent steel to steel lubricated static contact as mentioned in [86].

The punch, die and blank holder were defined as discrete rigid bodies. The blank was defined as deformable part. In order to numerically model punch, die and blank holder; 2628, 1116 and 828 R3D4 (4-node 3-D bilinear rigid quadrilateral) discrete rigid elements were used, respectively. On the other hand, for meshing of blank, 1156 S4R reduced integration, hourglass controlled shell elements were utilized. Meshed parts are represented in Figure 5.35.

After analyses has been carried out, thickness strains were calculated by using deformed thickness and initial thickness values. This procedure was applied for specified OA, OB and OC directions given in Figure 5.30. Demonstrations of these directions on the deformed analysis of 40 mm punch stroke are given in Figure 5.36.
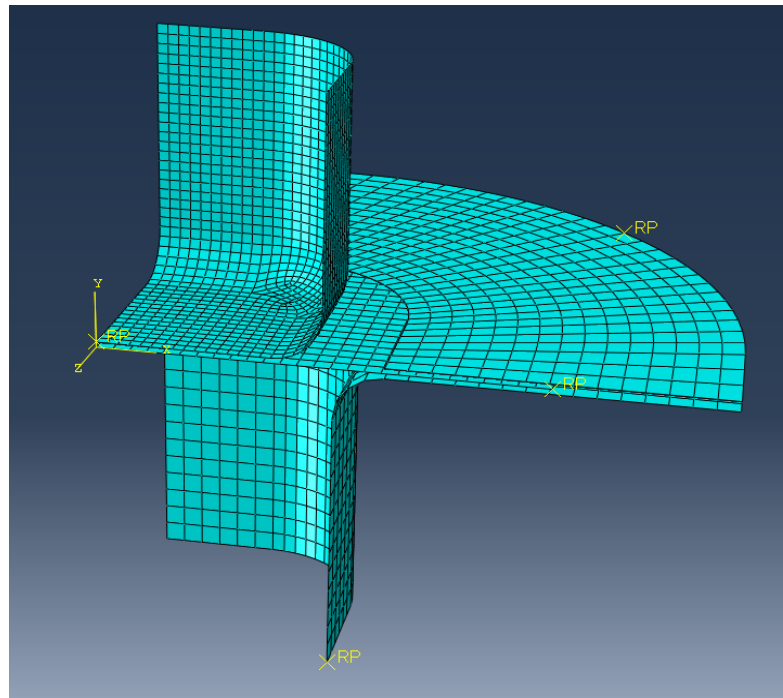
Figure 5.35 Meshed assembly of the square deep drawing process components
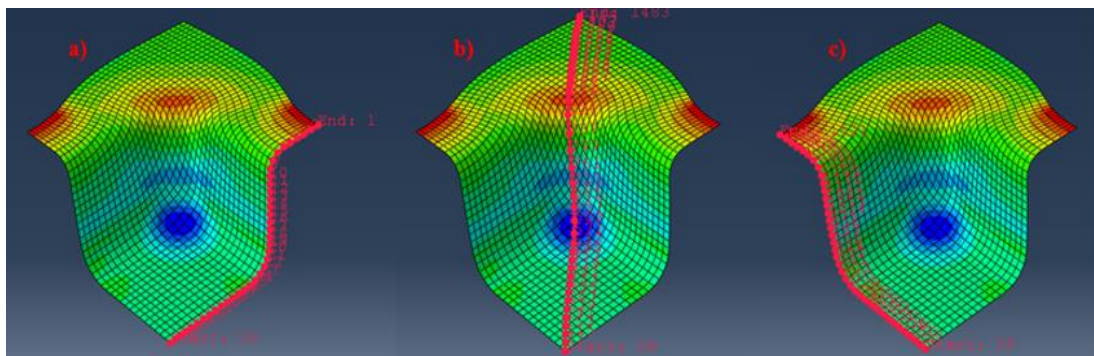
Figure 5.36 Thickness strain calculation directions for FEA on deformed part a) OA
direction b) OB direction and c) OC direction

It has seen that most severe thinning occurred at the bottom corner of the deformed
sheets. region where part interacts with punch radius. On the other hand, maximum
thickening is observed at the midpoints of the flanges indicated by red color. Analysis
results were given in Figure 5.37 and Figure 5.38.
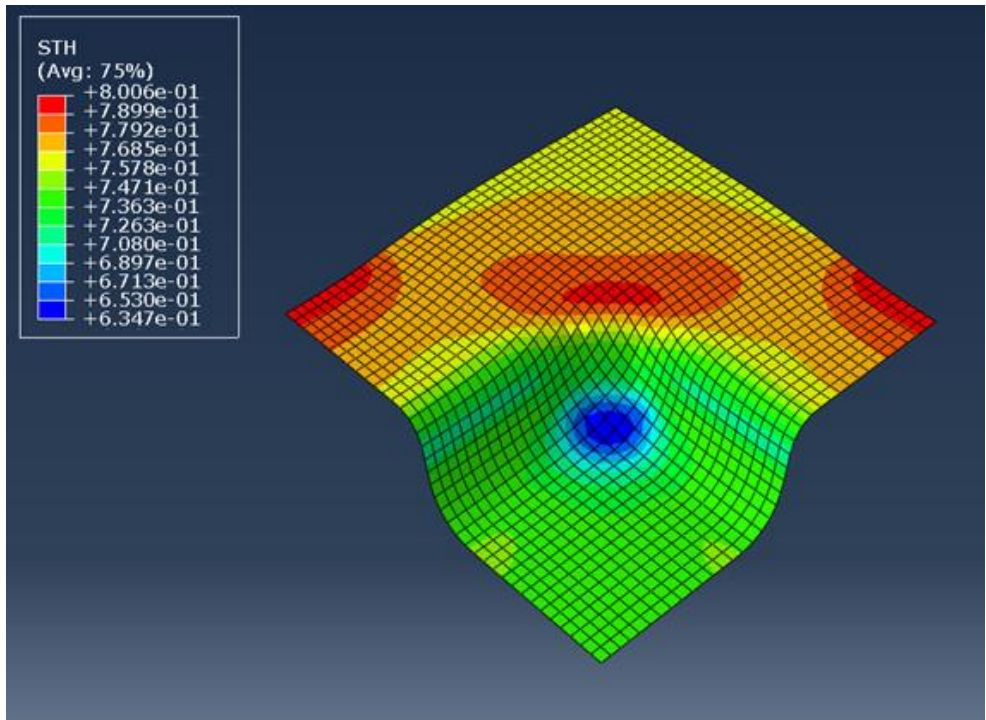
Figure 5.37 15mm deep drawn part and deformed sheet thickness values in mm
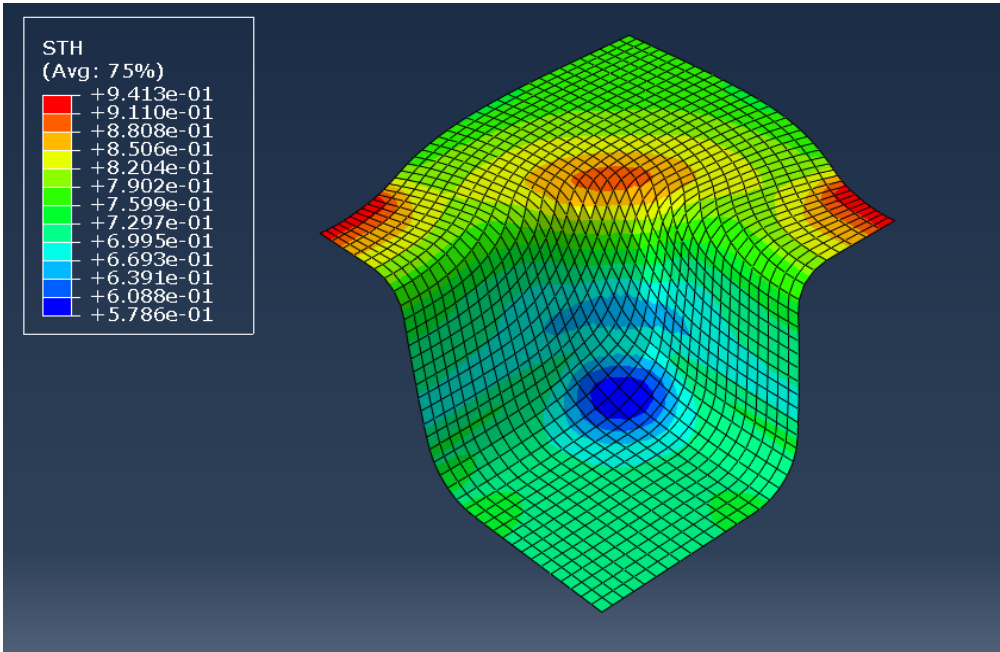
Figure 5.38 40mm deep drawn part and deformed sheet thickness values in mm

Thickness strain values were presented in Figures 5.39-41.
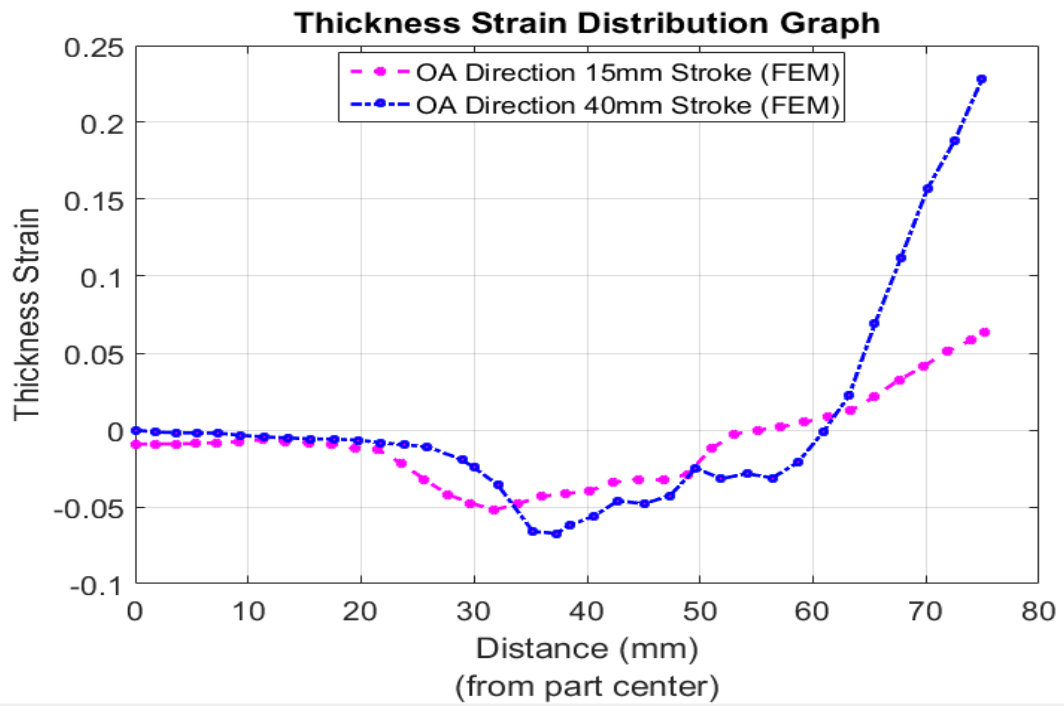
Figure 5.39 Thickness strain distributions along OA direction for 15 mm and 40 mm punch strokes constructed during the FEM
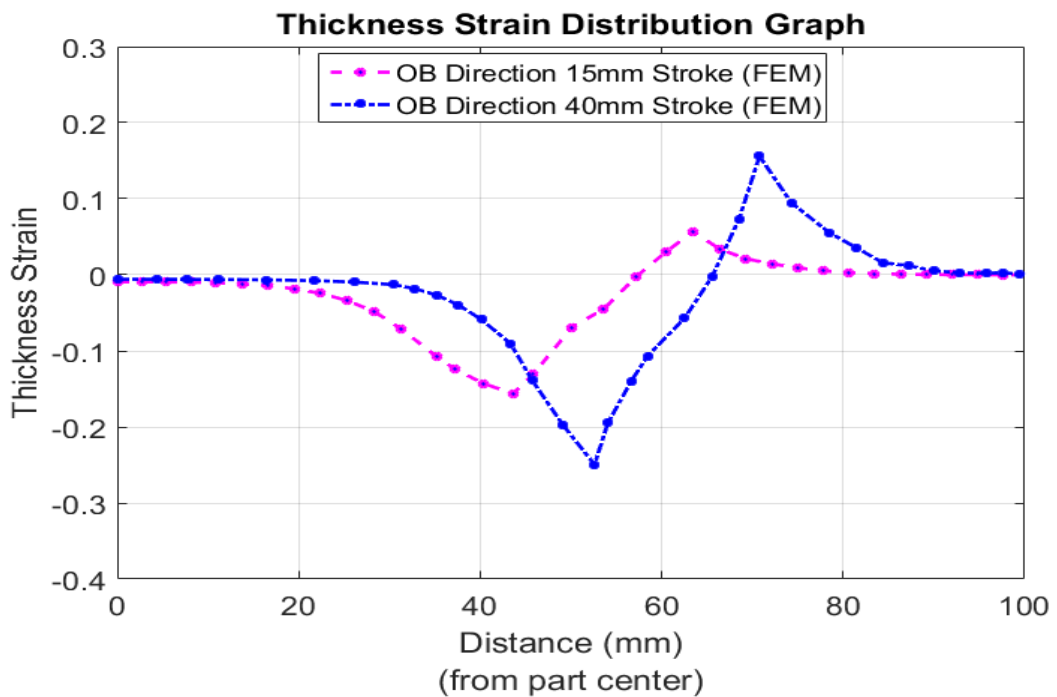
Figure 5.40 Thickness strain distributions along OB direction for 15 mm and 40 mm punch strokes constructed during the FEM
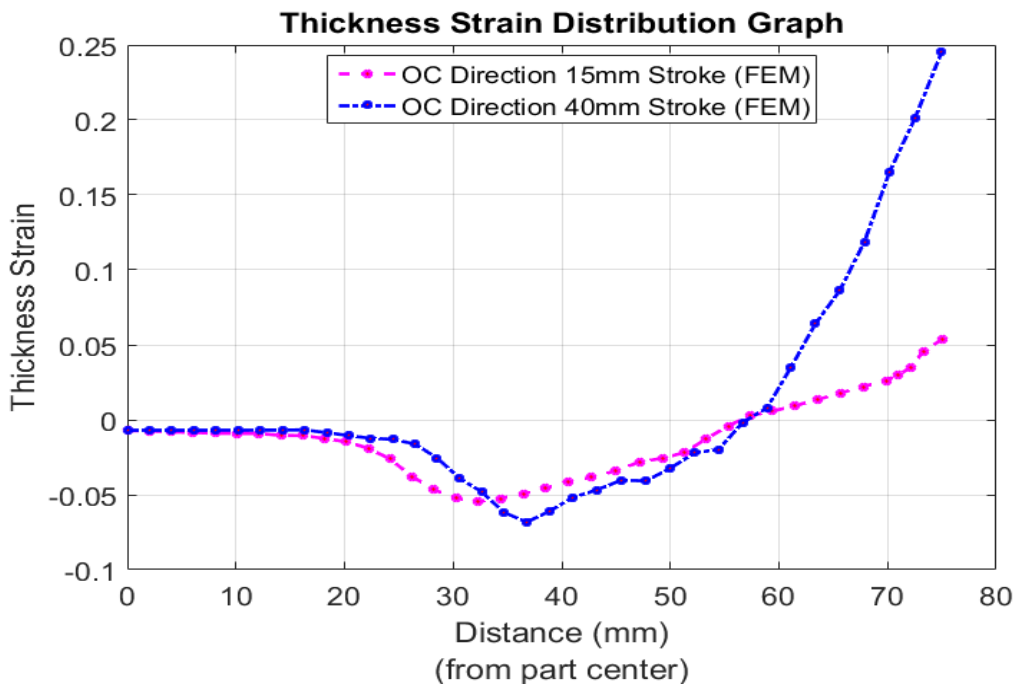
Figure 5.41 Thickness strain distributions along OC direction for 15 mm and 40 mm punch strokes constructed during the FEM

5.3.2.2 Isogeometric Analysis

During modeling of the problem, only quarters of the components were considered. The assembled model was given in Figure 5.42. The punch, die and blank holder were defined as discrete rigid bodies. In order to numerically model them, same element numbers with finite element analysis has been used. Therefore, punch, die and blank holder were modeled by using 2628, 1116 and 828 elements respectively. Rigid material property (Mat_Rigid) has been assigned to these elements. For these parts, element formulation was defined as Belytschko-Tsay shell element that based on Reissner-Mindlin theory. On the other hand, blank has been discretized uniformly into 1024 elements. This element number was considered after carrying out a mesh sensitivity analysis. Element type defined as Element_Shell_NURBS_Patch which

136

was chosen for isogeometric analysis. Order of the NURBS blank was taken to be cubic.
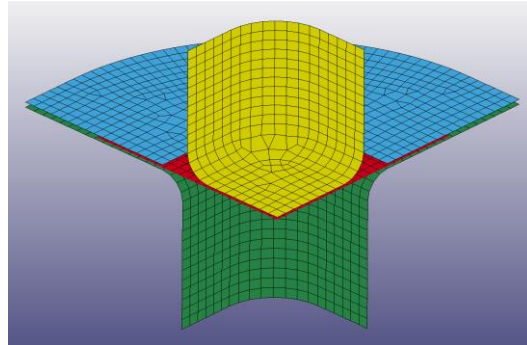
Figure 5.42 Assembled model of Isogeometric Analysis at LS-DYNA

After isogeometric analyses has been carried out, sheet thickness of the material was calculated along specified directions designated as OA, OB and OC in Figure 5.30. Demonstration of these directions on the deformed analysis of 40 mm punch stroke model is also shown in Figure 5.43. Examined sheet thickness values were used to calculate thickness strain distribution along these directions.
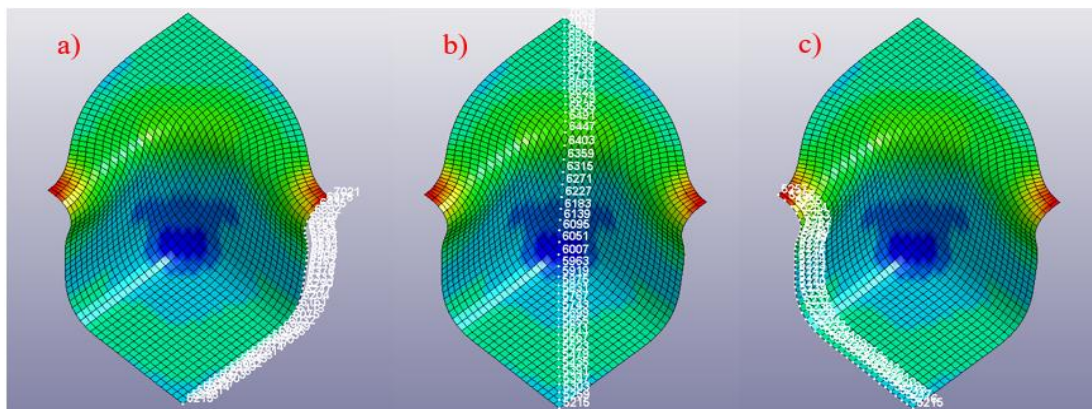
Figure 5.43 Thickness strain calculation directions for IGA on deformed part a) OA direction b) OB direction and c) OC direction

Maximum thinning and thickening were observed at the bottom corner of the cup and at midsection of the flange, respectively, as in the FEA results. Sheet thickness distribution found by using isogeometric analysis are given in Figure 5.44 and Figure 5.45 for 15 and 40 mm punch travel, respectively.
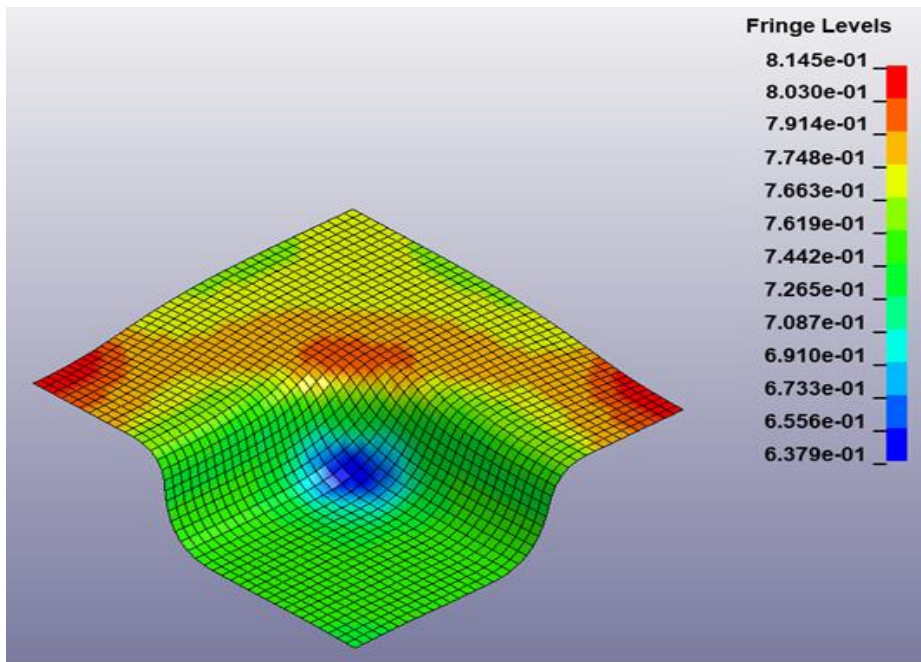
Figure 5.44 Sheet thickness values in mm for 15 mm punch stroke for IGA
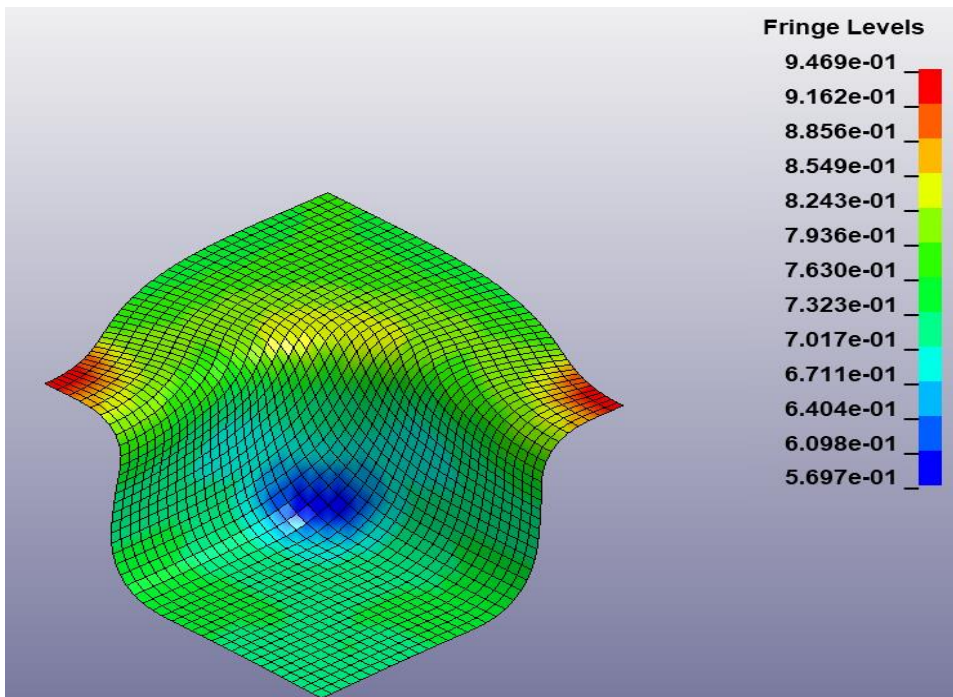
Figure 5.45 Sheet thickness values in mm for 40 mm punch stroke for IGA

Thickness strain distributions along specified directions were calculated and drawn on graphs and shown in Figures 5.46-48.

138
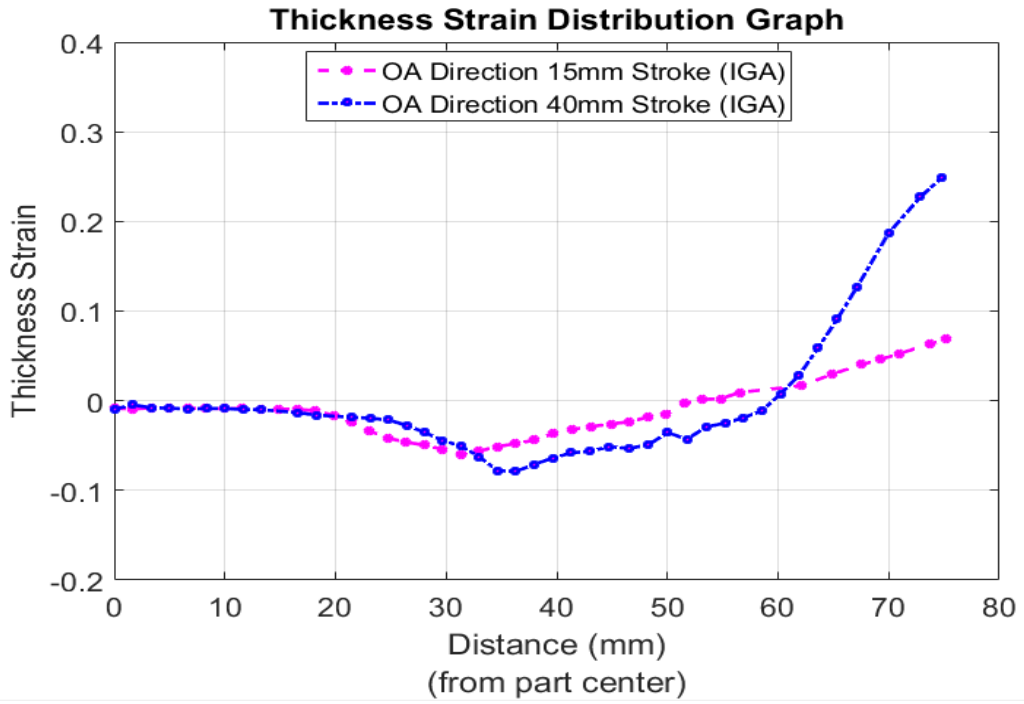
Figure 5.46 Thickness strain distributions along OA direction for 15 mm and 40 mm
punch strokes constructed during the IGA
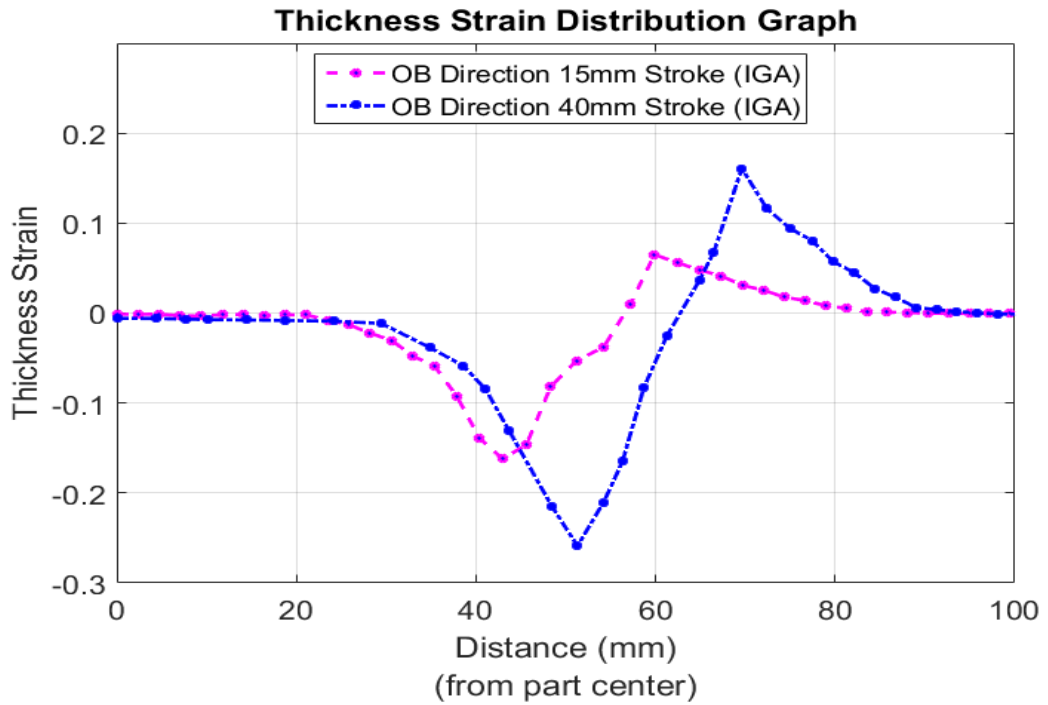
Figure 5.47 Thickness strain distributions along OB direction for 15 mm and 40 mm
punch strokes constructed during the IGA
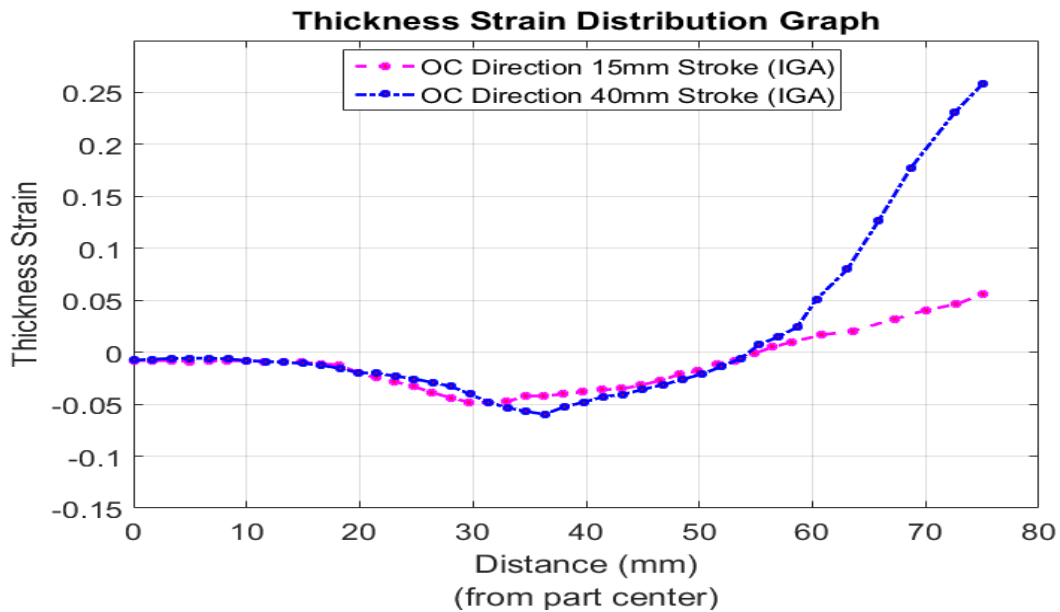
Figure 5.48 Thickness strain distributions along OC direction for 15 mm and 40 mm punch strokes constructed during the IGA

5.3.3 *Comparison of the Square Deep Drawing Results*

Experiment, finite element analysis and isogeometric analysis results were compared along the specified directions OA, OB and OC and given in the Figures 5.49-54.
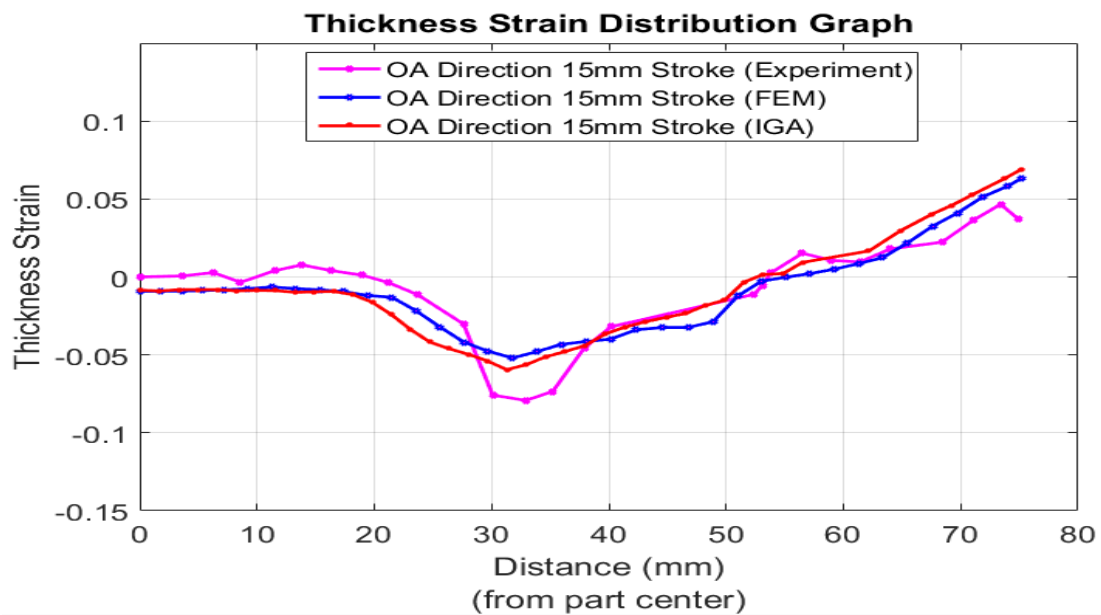
Figure 5.49 Thickness strain comparison along OA direction for 15mm punch stroke
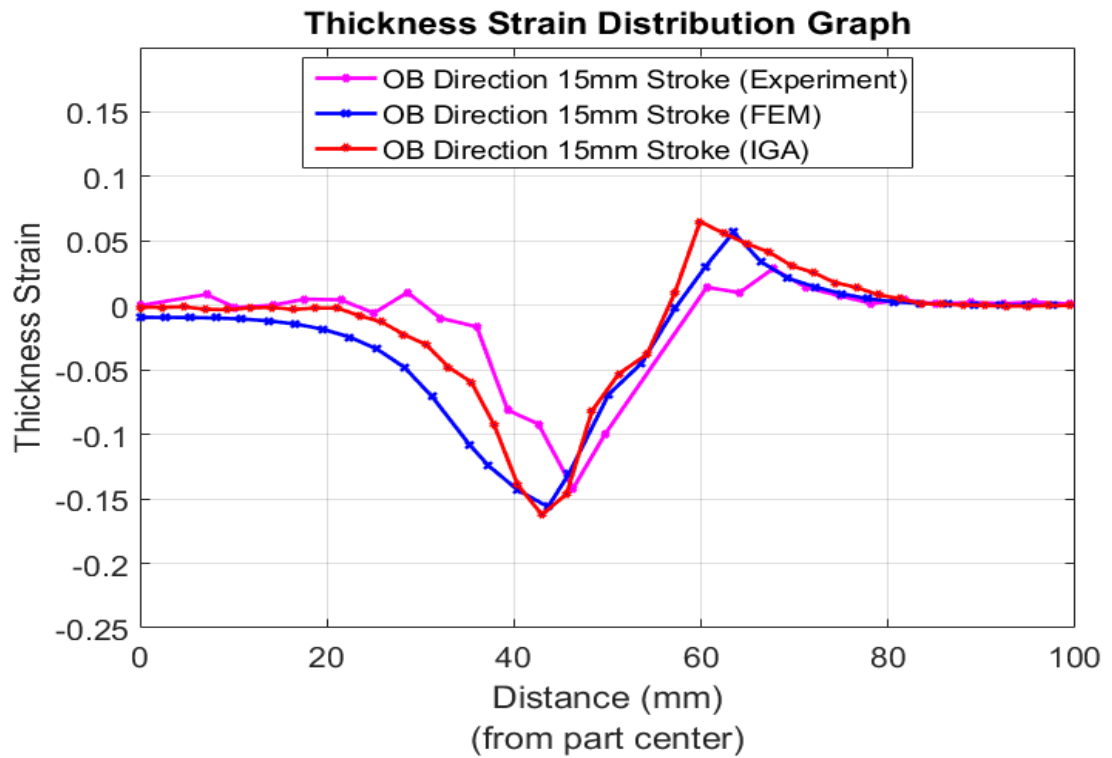
Figure 5.50 Thickness strain comparison along OB direction for 15mm punch stroke
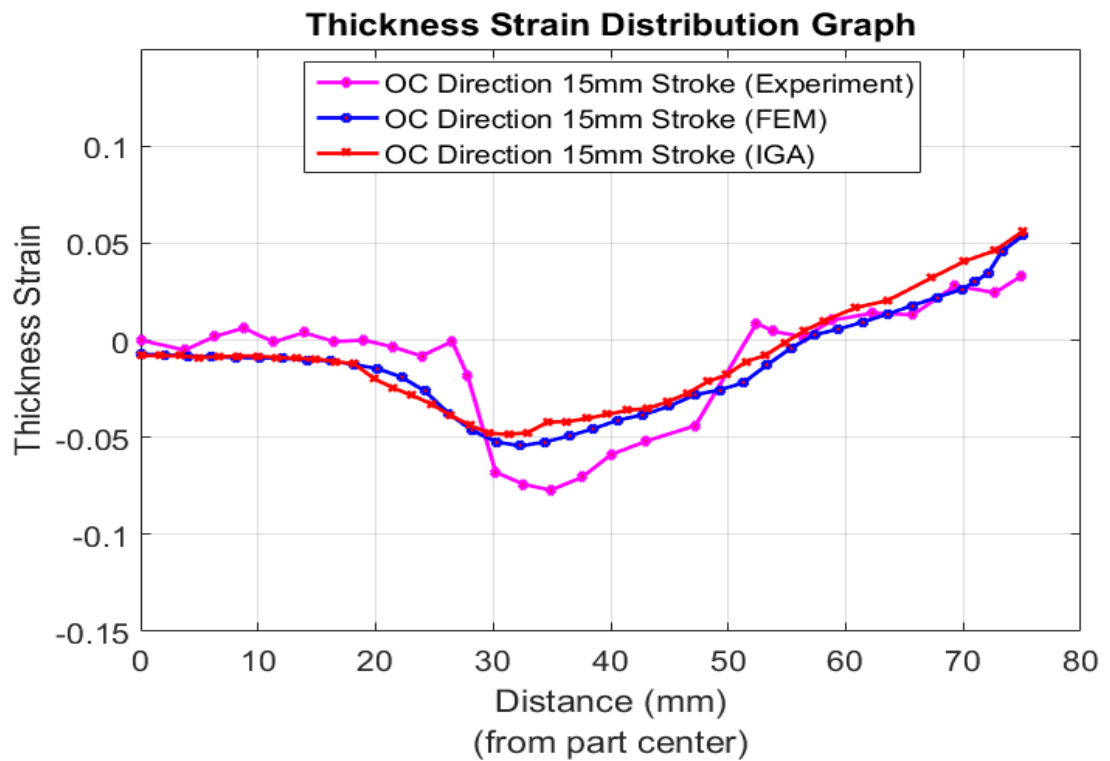
Figure 5.51 Thickness strain comparison along OC direction for 15mm punch stroke
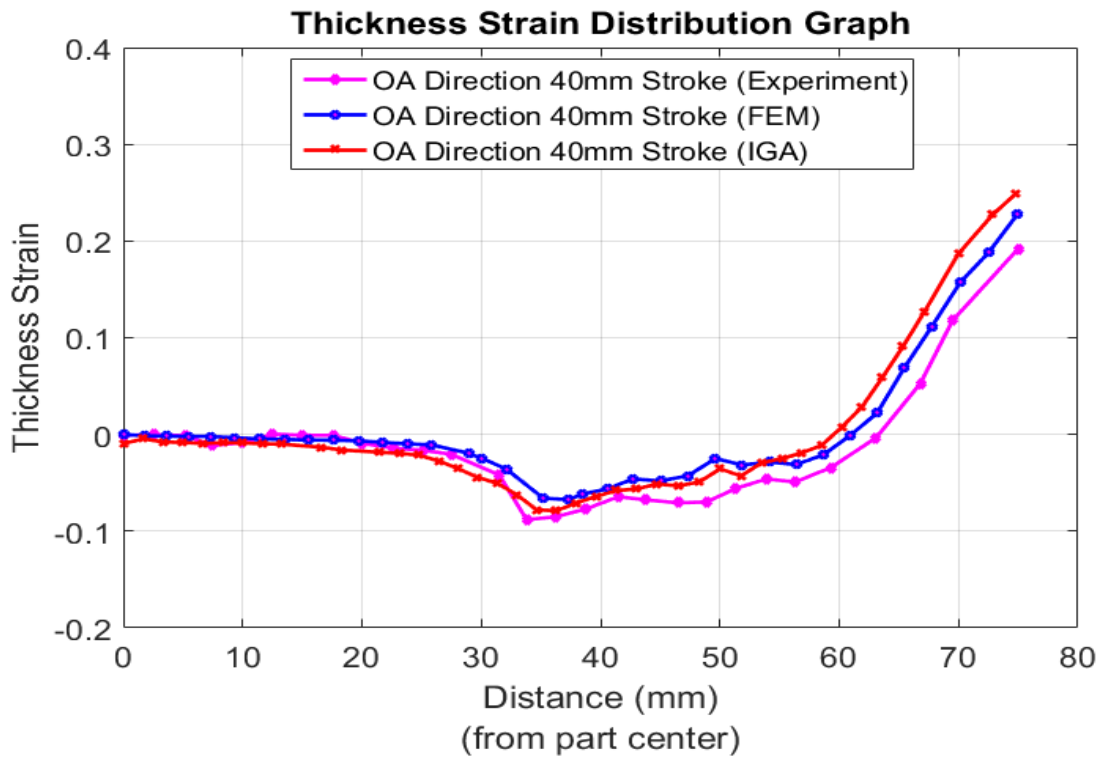
Figure 5.52 Thickness strain comparison along OA direction for 40mm punch stroke
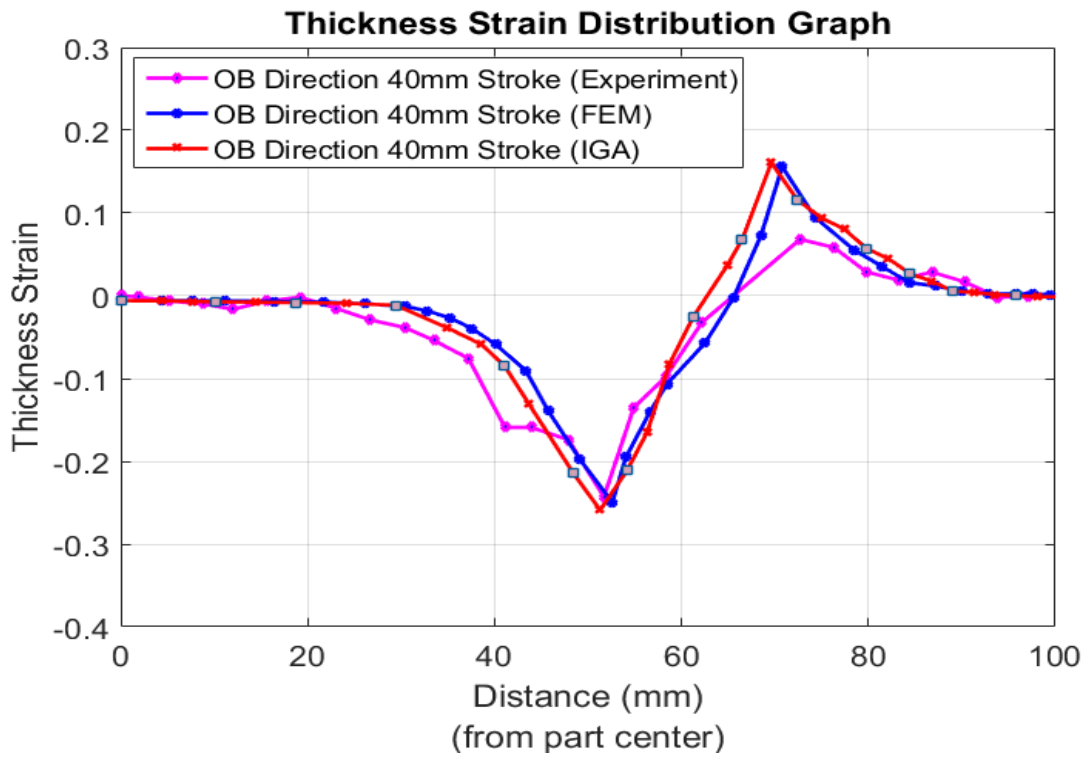
Figure 5.53 Thickness strain comparison along OB direction for 40mm punch stroke
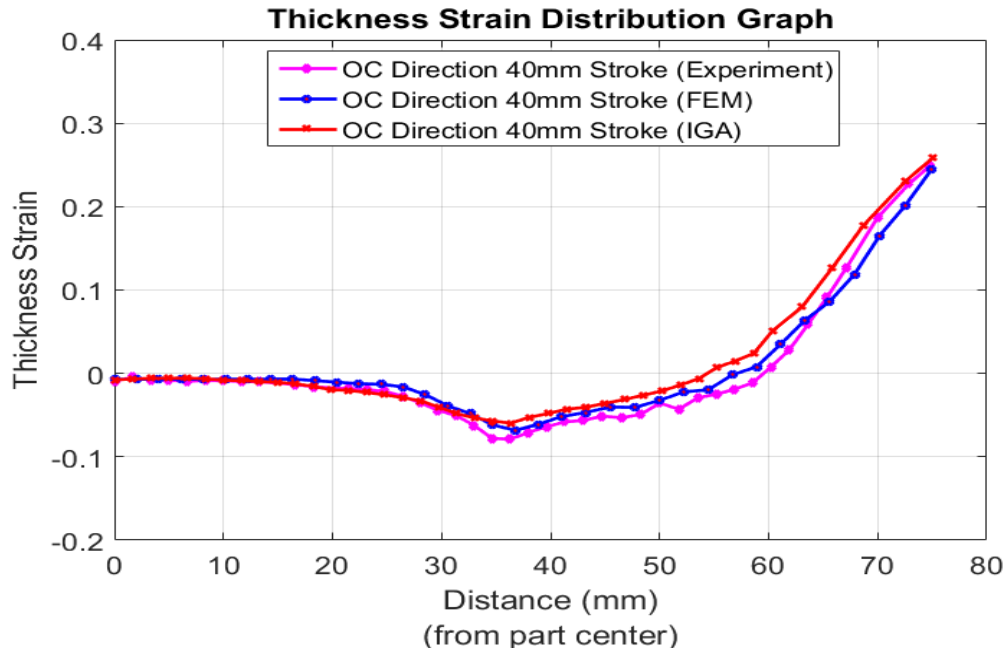
Figure 5.54 Thickness strain comparison along OC direction for 40mm punch stroke

Comparison of the figures shows that isogeometric analysis results show good agreement with the finite element analysis for all cases. The trends of distance versus thickness strain graphs obtained for these two analysis methods are similar. Minimum and maximum values of the thickness strains and the locations of them are very close. Since the results are closer and deviations are very low between FEA and IGA, it is not right to say that one method is better than the other. Moreover, analyses results are highly compatible with the experimental results except for a few points. The results of the analyses differ slightly from the experiment for 15 mm punch stroke in terms of minimum strain amount through OA and OC directions and location of thinnest regions. However, these differences are negligible and they disappear in the experiment made for 40 mm punch stroke. On the other hand, experiment results for 15 mm are fluctuating and this may be the reason of mentioned deviations. For the sake of clarity, the thickest and thinnest locations and thickness strain values at these locations for all cases are tabulated in Table 5.9. Computation times for simulations are also given in this table. Computation time and required element number for accurate results have been reduced with the usage of IGA. Additionally, used number of elements determined by conducting sensitivity analysis is shown in Figure 5.55.

143

Table 5.9 Comparison of Results for FEM and IGA

Method	Punch Stroke (mm)	Direction	The Thinnest Location from the center (mm)	Thickness Strain Value at the Thinnest Location	The Thickest Location from the center (mm)	Thickness Strain Value at the Thickest Location	Computation Time (hours)
Exp.	15	OA	32.9	-0.0792	71.4	0.0466	-
		OB	46.3	-0.1420	67.7	0.0286	-
		OC	34.9	-0.0773	74.9	0.0330	-
	40	OA	33.8	-0.0881	75	0.1910	-
		OB	51.7	-0.2437	72.7	0.0683	-
		OC	31.28	-0.0727	74.97	0.2141	-
FEM	15	OA	31.78	-0.0520	75.22	0.0635	
		OB	43.63	-0.1562	63.45	0.0567	4.2
		OC	32.33	-0.0544	75.1	0.0540	
	40	OA	37.31	-0.0674	74.98	0.2285	
		OB	52.60	-0.2496	70.78	0.1559	6.9
		OC	36.78	-0.0683	74.96	0.2451	
IGA	15	OA	31.29	-0.0595	75.16	0.0690	
		OB	42.97	-0.1622	59.88	0.0649	2.6
		OC	31.35	-0.0480	75.04	0.0560	
	40	OA	34.63	-0.0779	74.82	0.2491	
		OB	51.3	-0.2589	69.61	0.1608	3.8
		OC	36.34	-0.0597	75.05	0.2584	
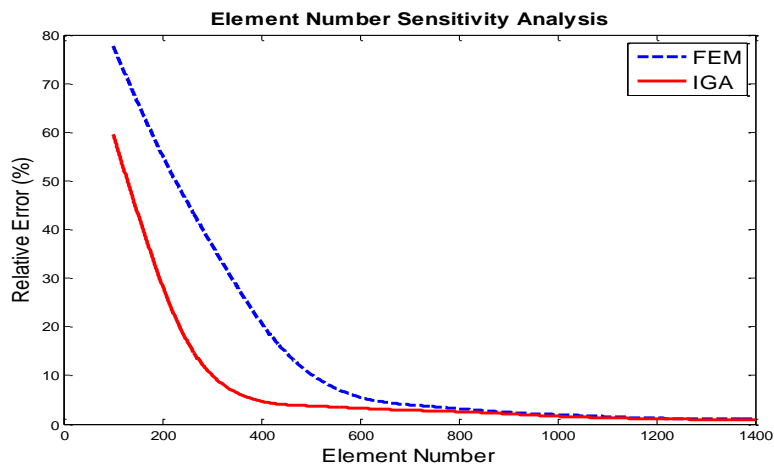
Figure 5.55 Element number sensitivity analysis for AISI 304 along rolling direction for 90° bending

CHAPTER 6

CONCLUSIONS AND FUTURE WORK

In this thesis, a novel numerical analysis method named as isogeometric analysis which is based on usage of NURBS basis functions was introduced. Its theoretical background and advantages over standard finite element method have been studied by investigating different case studies through code that has been developed for 2D analyses. In addition to having many similarities with finite element analysis, isogeometric analysis brought many superiorities into analysis as listed below;

- Using high order NURBS basis functions which may have C^1 and higher continuity instead of employing C^0 continuous classical Lagrange polynomials as basis functions enables more accurate results with less element number of elements especially for beam, plate and shell like structures that require higher continuity.

- In IGA, exact geometry can be represented by utilizing coarse mesh structure. This prevents unnecessary mesh refinements for geometrical representation. Thus, refinement techniques only used for the solution accuracy.

- In isogeometric analysis, mesh refinement is simply handled by reindexing the parametric space without interacting with the geometry contrary to refinement strategies of finite element method that require interaction with the CAD system at each stage.

- Getting higher order basis functions and refinement of basis is easy due to the recursive nature of the NURBS. Moreover, this recursive nature is very convenient for code algorithms.

Further, isogeometric analysis has been verified by structural analysis of linear elasticity problems. Conclusions drawn from these applications stated in the following items:

145

- IGA application on 1D bar problem showed that, first order basis functions are sufficient to accurately solve this problem. However, for first order NURBS basis functions are identical to finite element basis functions. Therefore, solving such problems with isogeometric analysis method does not provide a great advantage but still enables the user to reach correct result.

- In bending of Euler-Bernoulli beam application, IGA provided a great advantage for the solution process which is rotation free formulation. Due to the higher order continuity obtained by NURBS basis functions, this beam problem was solved for deformation by just using transverse degrees of freedom. Additionally, IGA has found the exact result by using single element for quartic order. Computation time has also decreased to nearly half with the usage of isogeometric analysis. However, for cubic order usage both FEM and IGA gave the accurate results with four elements. But for less element number in cubic order comparison FEM gives better results.

- Similarly, Kirchhoff plate bending problem is solved easily with IGA. The rotation free formulation was used for the solution. At the end, less elements were used and time required for the solution has decreased about 80 percent.

- For the 2D investigation, a plane stress problem which is a part of the infinite plate with circular hole was examined. Whole geometry was modeled by using only two elements including the circular hole region. However, with the concern for accuracy, mesh was refined to 128 elements. The main focus was to see the stress concentration around the hole and this was achieved with the mentioned number of elements. On the other hand, to obtain same result with FEA, 650 elements were used.

- Final application of isogeometric analysis on elasticity problems was a pinched cylinder problem which is a 3D problem. IGA has showed its efficiency for this problem as well with utilizing less number of elements and less time to get results.

Isogeometric analysis was also applied to metal forming problems which are the most significant contribution of this research. Uniaxial tension of a sheet, v-die bending and square deep drawing problems were examined as case studies. Two types of materials were used as AISI 304 steel and AA2024 T3 aluminum. For v-die bending, different bending angles were applied and springback results of the process were evaluated. For square deep drawing process, different punch strokes were conducted and thickness strain distributions were analyzed. Conclusions are given below:

- Before the application of forming problems, a simple case which is uniaxial tension of a sheet was studied to see the isogeometric analysis performance in predicting material beahvior. For this case, IGA has given same stress-strain curves as experiment for AISI 304 steel and AA2024 T3 aluminum. Isogeometric analysis and finite element analysis worked in a similar manner.

- Isogeometric analysis is better than FEA in predicting the springback results of v-die bending process. Moreover, isogeometric analysis usage contributed to the reduction of the analysis time.

- For square deep drawing case, IGA results have good agreement with both FEA and experiment results. It is successful in predicting thinning and thickening amounts and their locations on the part. Additionally, using isogeometric analysis decreases computation time dramatically.

As future works;

- Effects of the basis function order, continuity and refinement techniques can be investigated in detail by devoting more time for sensitivity analysis.

- Isogeometric analysis can be applied to non-linear elasticity problems.

- Different forming processes on parts with several materials can be examined as plasticity applications. More complex geometries with various sheet thickness values can be used to find the geometry and thickness effect.

- Particular yield and hardening laws can be implemented into forming analyses to see their consistency with isogeometric analysis.

- In order to eliminate the main disadvantage of IGA which is global refinement, T-Splines and its basis functions should be adapted to isogeometric analysis to get local refinement.

- Multi-patch isogeometric analysis can be constructed especially in order to solve fracture mechanics problems.

- Isogeometric analysis can be compared with finite element analysis that based on basis functions with order higher than quadratic and cubic.

REFERENCES

[1]   J. A. Cottrell, T. J. Hughes and Y. Bazilevs, Isogeometric Analysis: Toward Integration of CAD and FEA, Wiley, 2009.

[2]   T. J. Hughes, J. A. Cottrell and Y. Bazilevs, "Isogeometric analysis: CAD, finite elements, NURBS, exact geometry and mesh refinement," Computer Methods in Applied Mechanics and Engineering, pp. 194(39-41):4135-4195, 2005.

[3]   I. E. Sutherland, "Sketchpad, a Man-Machine Graphical Communication System," (Doctoral Dissertation), 1963.

[4]   P. Bézier, "How Renault uses numerical control for car body design and tooling," in Soc. Automotive Engineers' Congress, Detroit, MI, USA, (1968).

[5]   R. Echter, Isogeometric Analysis of Shells (Unpublished doctoral dissertation), Universität Stuttgart, 2013.

[6]   D. E. Weisberg, The Engineering Design Revolution CAD History, Princeton University Press, 2008.

[7]   R. F. Riesenfeld, Applications of B-spline Approximation to Geometric Problems of Computer-Aided Design (Unpublished Doctoral Dissertation), NY,USA: Syracuse University, Syracuse, 1973.

[8]   K. J. Versprille, Computer-Aided Design Applications of the Rational B-Spline (Doctoral Dissertation), NY,USA: Syracuse University, Syracuse, 1975.

[9]   R.Courant, "Variational methods for the solution of problems of equilibrium and vibrations," Bulletin of American Mathematical Society, vol. 49, pp. 1-23, 1943.

[10]   R. Clough, "The Finite Element Method, in Plane Stress Analysis," in Proc. 2nd A.S.C.E. Conf: on Electronic Comp., Pittsburgh, PA, (1960) .

[11]   "MSC Software," [Online]. Available: https://en.wikipedia.org. [Accessed 06 07 2017].

[12]   A. Hrennikoff, "Solution of problems of elasticity by the framework method," Journal of applied mechanics, vol. 8.4, p. 169–175, 1941.

[13]   A. Hrennikoff, "Framework Method and its Technique for Solving Plane Stress Problems," ETH Zürich, Rämistrasse 101, 1949.

[14]   R. Courant, "Variational methods for the solution of problems of equilibrium and vibration," Bulletin of the American Mathematical Society, vol. 49, pp. 1-23, 1943.

[15]   I. Ergatoudis, B. M. Irons and O. C. Zienkiewicz, "Curved, isoparametric, quadrilateral elements for finite element analysis," Int. Journal of Solid Structures, vol. 4, pp. 31-42, 1968.

[16]   S. Arabshahi, D. C. Barton and N. K. Shaw, "Steps Towards CAD-FEA Integration," Engineering with Computers, vol. 9, pp. 17-26, 1993.

[17]   C. Gontier and C. Vollmer, "A Large displacement analysis of a beam using a CAD geometric definition," Computers & Structures, vol. 57, pp. 981-989, 1995.

[18]   P. Kagan, A. Fıscher and P. Z. Bar-Yoseph, "New B-Spline Finite Element Approach for Geometrical Design and Mechanical Analysis," International Journal for Numerical Methods in Engineering, vol. 41, pp. 435-458, 1998.

[19]   P. Kagan and A. Fischer, "Integrated mechanically based CAE system using B-Spline finite elements," Computer-Aided Design, vol. 32, pp. 539-552, 2000.

[20]   G. Zhang, R. Alberdi and K. Khandelwal, "Analysis of three-dimensional curved beams using isogeometric," Engineering Structures, vol. 117, pp. 560-574, 2016.

[21]   I. N. Tsiptsis and E. J. Sapountzakis, "Generalized warping and distortional analysis of curved beams with isogeometric methods," Computers and Structures, vol. 191, pp. 33-50, 2017.

[22]   M. B. B. P. R. W. K.-U. B. A.M. Bauer∗, A. M. Bauer, M. Breitenberger, B. Philipp, R. Wüchner and K. U. Bletzinger, "Nonlinear isogeometric spatial Bernoulli beam," Computer Methods in Applied Mechanics and Engineering, vol. 303, pp. 101-127, 2016.

[23]   D. J. Benson, Y. Bazilevs, M. C. Hsu and T. J. Hughes, "Isogeometric shell analysis: The Reissner–Mindlin shell," Computer Methods in Applied Mechanics and Engineering, vol. 199, pp. 276-289, 2010.

[24]   D. J. Benson, Y. Bazilevs, M. C. Hsu and T. J. Hughes, "A large deformation, rotation-free, isogeometric shell," Computer Methods in Applied Mechanics and Engineering, vol. 200, pp. 1367-1378, 2011.

[25]   N. Nguyen-Thanh, N. Valizadeh, N. M. Nguyen, H. Nguyen-Xuan, X. Zhuange, P. Areias, G. Zi, Y. Bazilevs, L. De Lorenzisa and T. Rabczukb, "An extended isogeometric thin shell analysis based on Kirchhoff–Love theory," Computer Methods in Applied Mechanics Engineering, vol. 284, pp. 265-291, 2015.

[26]   X. Wang, X. Zhu and P. Hu, "Isogeometric finite element method for buckling analysis of generally laminated composite beams with different

boundary conditions," International Journal of Mechanical Sciences, vol. 104, pp. 190-199, 2015.

[27]   L. Anh-Tuan, N.-I. Kim and L. Jaehong, "Bending and buckling of general laminated curved beams using NURBS-based isogeometric analysis," European Journal of Mechanics A/Solids, vol. 54, pp. 218-231, 2015.

[28]   A. Gupta and A. Ghosh, "Bending analysis of laminated and sandwich composite reissner-mindlin plates using nurbs-based isogeometric approach," in 11th International Symposium on Plasticity and Impact Mechanics, Implast 2016, 2017.

[29]   H. Kapoor and R. K. Kapania, "Geometrically nonlinear NURBS isogeometric finite element analysis of laminated composite plates," Composite Structures, vol. 94, p. 3434–3447, 2012.

[30]   Y. Urthaler and J. N. Reddy, "A mixed finite element for the nonlinear bending analysis of laminated composite plates based on FSDT," Mechanics of Advanced Material and Structures, vol. 15, pp. 335-354, 2008.

[31]   L. V. Tran, L. Jaehong, H. Nguyen-Van, H. Nguyen-Xuan and M. AbdelWahab, "Geometrically nonlinear isogeometric analysis of laminated composite plates based on higher-order shear deformation theory," International Journal of Non-Linear Mechanics, Vols. 42-52, p. 72, 2015.

[32]   I. Temizer, P. Wriggers and T. J. Hughes, "Contact treatment in isogeometric analysis with NURBS," Computer Methods in Applied Mechanics and Engineering, vol. 200, pp. 1100-1112, 2011.

[33]   L. Jia, "Geometric basis and formulation for frictionless contact," Computer Methods in Applied Mechanics and Engineering, vol. 200, pp. 726-741, 2011.

[34]   I. Temizer, P. Wriggers and T. J. Hughes, "Three-Dimensional Mortar-Based frictional contact treatment in isogeometric analysis with NURBS," Computer Methods in Applied Mechanics and Engineering, vol. 209, pp. 115-128, 2012.

[35]   T. P. W. a. G. Z. L. De Lorenzis, L. De Lorenzis, I. Temizer, P. Wriggers and G. Zavarise, "A large deformation frictional contact formulation using NURBS-bases isogeometric analysis," International Journal for Numerical Methods in Engineering, vol. 87, pp. 1278-1300, 2011.

[36]   M. E. Matzen, T. Cichosz and M. Bischo, "A point to segment contact formulation for isogeometric, NURBS based finite elements," Computer Methods in Applied Mechanics and Engineering, vol. 255, pp. 27-39, 2013.

[37]   W. A. Wall, M. A. Frenzel and C. Cyron, "Isogeometric structural shape optimization," Computer Methods in Applied Mechanics and Engineering, vol. 197, pp. 2976-2988, 2008.

[38]   N. D. Manh, A. Evgrafov, A. R. Gersborg and J. Gravesen, "Isogeometric shape optimization of vibrating membranes.," Computer Methods in Applied Mechanics and Engineering, vol. 200, pp. 1343-1353, 2011.

[39]   X. Qian, "Full analytical sensitivities in NURBS based isogeometric shape optimization," Computer Methods in Applied Mechanics and Engineering, vol. 199, pp. 2059-2071, 2010.

[40]   A. P. Nagy, M. M. Abdalla and Z. Gürdal, "Isogeometric sizing and shape optimisation of beam structures," Computer Methods in Applied Mechanics and Engineering, vol. 199, pp. 1216-1230, 2010.

[41]   T. Le-Manh and L. Jaehong, "Stacking sequence optimization for maximum strengths of laminated composite plates using genetic algorithm and isogeometric analysis," Composite Structures, vol. 116, pp. 357-363, 2014.

[42] J. A. Cottrell, A. Reali, Y. Bazilevs and T. J. Hughes, "Isogeometric analysis of structural vibrations," Computer Methods in Applied Mechanics and Engineering, vol. 195, pp. 5257-5296, 2006.

[43] T. J. Hughes, A. Reali and G. Sangalli, "Duality and unified analysis of discrete approximations in structural dynamics and wave propagation: Comparison of p-method finite elements with k-method NURBS," Computer Methods in Applied Mechanics and Engineering, vol. 197, pp. 4104-4124, 2008.

[44] H. C. Thai, H. Nguyen-Xuan, N. Nguyen-Thanh, T.-H. Le, T. Nguyen-Thoi and T. Rabczuk, "Static, free vibration and buckling analysis of laminated composite Reissner-Mindlin plates using NURBS-based isogeometric approach," International Journal for Numerical Methods in Engineering, vol. 91, 2012.

[45] D. Wang, W. Liu and H. Zhang, "Novel higher order mass matrices for isogeometric structural vibration analysis," Computer Methods in Applied Mechanics and Engineering, 2013.

[46] H. Gomez, T. J. Hughes, X. Nogueira and V. M. Calo, "Isogeometric analysis of the isothermal Navier-Stokes-Korteweg equations," Computer Methods in Applied Mechanics and Engineering, vol. 199, pp. 1828-1840, 2010.

[47] P. N. Nielsen, A. R. Gersborg, J. Gravesen and N. L. Pedersen, "Discretizations in isogeometric analysis of Navier-Stokes flow," Computer Methods in Applied Mechanics and Engineering, vol. 200, pp. 3242-3253, 2011.

[48] B. Bastl, M. Brandner, J. Egermaier, K. Michálková and E. Turnerová, "Isogeometric analysis for turbulent flow," Mathematics and Computers in Simulation, 2016.

[49] J. Bulling, V. John and P. Knobloch, "Isogeometric analysis for flows around a cylinder," Applied Mathematics Letters, vol. 63, pp. 65-70, 2017.

[50] M. N. Nguyen and T. Q. Bui, "Isogeometric analysis for unsaturated flow problems," Computers and Geotechnics, vol. 62, pp. 257-267, 2014.

[51] Y. Bazilevs, V. M. Calo, T. J. Hughes and Y. Zhang, "Isogeometric fluid-structure interaction: theory, algorithms, and computations.," Computational Mechanics, vol. 43, no. 43:3{37, 2008., pp. 3-37, 2008.

[52] Y. Bazilevs, J. R. Gohean, T. J. Hughes and R. D. Mose, "Patient-specific isogeometric fluid-structure interaction analysis of thoracic aortic blood flow due to implantation of Jarvik 2000 left ventricular assist device," Computer Methods in Applied Mechanics and Engineering, vol. 198, pp. 3534-3550, 2009.

[53] Z. Kacprzyka and K. Ostapska-Luczkowsk, "Isogeometric Analysis as a New FEM Formulation - Simple Problems of Steady State Thermal Analysis," in XXIII R-S-P seminar, Theoretical Foundation of Civil Engineering, 2014.

[54] M. Yoon, H. Seung-Hyun and C. Seonho, "Isogeometric shape design optimization of heat conduction problems," Internati onal Journ alofHeat and Mass Transfer, vol. 62, no. Transfer 62(2013)272–285, pp. 272-285, 2013.

[55] L. V. Tran, C. H. Thai and H. Nguyen-Xuan, "An isogeometric finite element formulation for thermal buckling analysisof functionally graded plates," Finite Elements in Analysis and Design, vol. 73, pp. 65-76, 2013.

[56] H. Bayesteh, A. Afshar and S. Mohammdi, "Thermo-mechanical fracture study of inhomogeneous cracked solids by the extended isogeometric analysis method," European Journal of Mechanics - A/Solids, vol. 51, pp. 123-139, 2015.

[57]   H. Wu, W. Ye and W. Jiang, "Isogeometric finite element analysis of interior acoustic problems," Applied Acoustics, vol. 100, pp. 63-73, 2015.

[58]   L. Coox, O. Atak, D. Vandepitte and W. Desmet, "An isogeometric indirect boundary element method for solving acoustic problems in open-boundary domains," Computer Methods in Applied Mechanics and Engineering, vol. 316, pp. 186-208, 2017.

[59]   M. Dinachandra and S. Raju, "Isogeometric Analysis for Acoustic Fluid-Structure Interaction Problems," International Journal of Mechanical Sciences, Vols. 131-132, pp. 8-25, 2017.

[60]   M. Kästner, P. Metsch and R. d. Borst, "Isogeometric analysis of the Cahn-Hilliard equation – a convergence study," Journal of Computational Physics, vol. 305, pp. 360-371, 2016.

[61]   C. V. Verhoosel, M. A. Scott, T. J. Hughes and R. d. Borst, "An isogeometric analysis approach to gradient damage models," International Journal for Numerical Methods in Engineering, vol. 86, pp. 115-134, 2011.

[62]   P. Fischer, M. Klassen, J. Mergheim, P. Steinmann and R. Müller, "Isogeometric analysis of 2D gradient elasticity," Computational Mechanics, vol. 47, pp. 325-334, 2010.

[63]   Y. P. Gong, C. Y. Dong and Y. Bai, "Evaluation of nearly singular integrals in isogeometric boundary element method," Engineering Analysis with Boundary Elements, vol. 75, pp. 21-35, 2017.

[64]   A. -V. Vuong, C. Heinrich and B. Simeon, "ISOGAT: a 2D tutorial MATLAB code for Isogeometric Analysis," Computer Aided Geometric Design, vol. 27, pp. 644-655, 2010.

[65]   C. d. Falco, A. Reali and R. Vazquez, "GeoPDEs: a research tool for Isogeometric Analysis of PDEs," Advances in Engineering Software, vol. 44, pp. 116-125, 2011.

[66]   L. Dalcin, N. Collier, P. Vignal, A. M. Cortes and V. M. Caloe, "PetIGA: A Framework for High-Performance Isogeometric Analysis," Computer Methods in Applied Mechanics and Engineering, vol. 308, pp. 151-181, 2016.

[67]   L. M. Bernal, V. M. Calo, N. Collier, G. A. Espinosa, F. Fuentes and J. C. Mahecha, "Isogeometric analysis of hyperelastic materials using PetIGA," in International Conference on Computational Science, Barcelona, Spain, 2013.

[68]   S. Khakalo and J. Niiranen, "Isogeometric analysis of higher-order gradient elasticity by user elements of a commercial finite element software," Computer-Aided Design, vol. 82, pp. 154-169, 2017.

[69]   Y. Lai, Y. J. Zhang, L. Liu, X. Weia, E. Fang and J. Lua, "Integrating CAD with Abaqus: A practical isogeometric analysis software platform for industrial applications," Computers and Mathematics with Applications, pp. In Press, Corrected Proof, 2017.

[70]   A. Duval, T. Elguedj, F. Maurin and H. Al-Akhras, "Abaqus user element implementation of NURBS based isogeometric analysis," in 6th European Congress on Computational Methods in Applied Sciences and Engineering, Vienna, Austria, 10-14 September 2012.

[71]   Y. Bazilevs, V. M. Calo, J. A. Cottrell, J. A. Evans, T. J. Hughes, S. Lipton, M. A. Scott and T. W. Sederberg, "Isogeometric analysis using T-splines," Computer Methods in Applied Mechanics and Engineering, vol. 199, pp. 229-263, 2010.

[72]   T. . W. Sederberg, J. Zheng, A. Bakenov and A. Nasri, "T-splines and T-NURCCs," Brigham Young University, 2003.

[73]   T.-K. Uhm and S.-K. Youn, "T-spline finite element method for the analysis of shell structures," International Journal for Numerical Methods in Engineering, vol. 80, pp. 507-536, 2009.

[74]   L. Piegl and W. Tiller, The NURBS Book, Springer, 1997.

[75]   M. Cox, "The numerical evaluation of B-splines, Technical report," National Physics Laboratory DNAC 4, 1971.

[76]   C. De Boor, "On calculation with B-splines," Journal of Approximation Theory, vol. 6, pp. 50-62, 1972.

[77]   S. B. Raknes, Isogeometric Analysis and Degenerated, Trondheim: Norwegian University of Science and Technology, 2011.

[78]   K. A. M. Hansvold, Mesh Generation Techniques for Isogeometric Analysis, Trondheim: Norwegian University of Science and Technology, 2015.

[79]   V. P. Nguyen, R. N. Simpson, S. P. Bordas and T. Rabczuk, "Isogeometric Analysis: A review and computer implementation aspects," Cardiff University, The Parade, Cardiff, 2013.

[80]   T. J. Hughes, A. Reali and G. Sangalli, "Efficient quadrature for NURBS-based isogeometric analysis," Computer Methods in Applied Mechanics and Engineering, vol. 199, pp. 301-313, 2010.

[81]   G. Beer and S. Bordas, Isogeometric Methods for Numerical Simulation, Springer, 2015.

[82]   P. L. Gould, Introduction to Linear Elasticity, Springer, 1999.

[83] T. Belytschko, H. Stolarski, W. K. Liu, N. Carpenter and J. S. Ong, "Stress Projection for Membrane and Shear Locking in Shell Finite Elements," Computer Methods in Applied Mechanics and Engineering, vol. 51, pp. 221-258, 1985.

[84] A. Andrade-Campos, F. Teixeira-Dias, U. Krupp, F. Barlat, F. Rauch and J. J. Gracio, "Effect of Strain Rate, Adiabatic Heating and Phase Transformation Phenomena on the Mechanical Behaviour of Stainless Steel," An International Journal for Experimental Mechanics, vol. 46, pp. 283-297, 2010.

[85] J. D. Seidt and A. Gilat, "Plastic deformation of 2024-T351 aluminum plate over a wide range of loading conditions," International Journal of Solids and Structures, vol. 50, p. 1781–1790, 2013.

[86] J. Danckert, "Experimental Investigation of a Square Cup Deep Drawing Process," Journal of Materials Processing Technology, vol. 50, pp. 375-384, 1995.

[87] E. Kreyszig, Advanced Engineering Mathematics, John Wiley & Sons, 2006.

[88] G. R. Liu and S. S. Quek, The Finite Element Method: A Prcatical Course, Butterworth-Heinemann, 2014.

[89] W. D. Pilkey and D. F. Pilkey, Peterson's Stress Concentration Factors, New Jersey: John Wiley & Sons, Inc., 2008.

[90] J. Lubliner, Plasticity Theory, New York: Macmillan Publishing, 1990.

[91] V. Boljanovic, Sheet Metal Forming Processes and Die Design, South Norwalk: Industrial Press, Inc., 2014.

[92] S. Semiatin, ASM Handbook: Volume 14B: Metal Working: Sheet Forming, Materials Park, Ohio, USA: ASM international, 2006.

[93]   Schuler, Metal forming handbook, Berlin: Spring-Verlag, 1998.

[94]   A. I. O. Zaid, "Deep drawing mechanism, parameters, defects and recent results: state of the art," in 14th International Symposium on Advanced Materials, Islamabad, Pakistan, 2016.

[95]   N. Arab and A. Javadimanesh, "Theoretical and Experimental Analysis of Deep Drawing Cylindrical Cup," Journal of Minerals and Materials Characterization and Engineering, vol. 1, no. 6, pp. 336-342, 2013.

[96]   D. O. Kipp, "matweb," 1996. [Online]. Available: http://www.matweb.com/search/datasheet.aspx?matguid=bd20a4281ae343 0d97cfbebf6904ec50. [Accessed 16 11 2017].

[97]   D. O. Kipp, "matweb," 1996. [Online]. Available: http://www.matweb.com/search/DataSheet.aspx?MatGUID=57483b4d782 940faaf12964a1821fb61. [Accessed 16 11 2017].